F 1503/2

BULETINUL INSTITUTULUI POLITEHNIC DIN IAŞI

F 1503/2
41. v.
'95
L S Z
9 000004 031193

Tomul XLI (XLV)
Fasc. 1-4

Secția II

CHIMIE şi INGINERIE CHIMICĂ

1995

MŰSZAKI INFORMÁCIÓS KÖNYVTÁR 1883 KÖZPONT ORSZÁGOS

BULETINUL INSTITUTULUI POLITEHNIC DIN IAŞI

Tomul XLI (XLV)
Fasc. 1–4

Secţia II
CHIMIE şi INGINERIE CHIMICĂ

1995

EDITORIAL STAFF

Prof. dr. eng. **VITALIE BELOUSOV** (President)
Prof. dr. eng. **PAULICĂ RĂILEANU** (Secretary)
Prof. dr. eng. **EFTIMIE NIŢESCU**
Prof. dr. doc. **ALFRED BRAIER** (Editor)
Prof. dr. eng. **HUGO ROSMAN** (Editor)
Prof. dr. eng. **MIHAIL VOICU** (Head of the Exchange Service)
Prof. dr. **AUREL BEJANCU**
Prof. dr. eng. **VICTOR BULACOVSCHI**
Prof. dr. eng. **DIMITRIE ALEXA**
Prof. dr. eng. **SPIRIDON CREŢU**
Prof. dr. eng. **ADRIAN RADU**
Prof. dr. eng. **ION GIURMA**
Prof. dr. eng. **MIRCEA MATEESCU**

The **Bulletin of the Polytechnic Institute of Jassy** is edited by
the **Technical University "Gh.Asachi"** (the former Polytechnic Institute), Jassy.

TEXredaction:
B. Grigoriu, A. Rotaru
Technical University of Iaşi

BULETINUL INSTITUTULUI POLITEHNIC DIN IAŞI
BULLETIN OF THE POLYTECHNIC INSTITUTE OF JASSY
Tomul XLI (XLV), Fasc. 1–4 1995

Secţia II

CHIMIE ŞI INGINERIE CHIMICĂ

SUMAR

Pag.

DOINA BEJAN şi VIRGIL BĂRBOIU, Caracterizarea pe cale spectrometrică a unor preparate enzimatice cu acţiune proteolitică (engl., rez. rom.) 7

I. ROŞCA, N. FOCA, DANIEL SUTIMAN şi AL. CONSTANTINESCU, Studiul fizico-chimic al catalizatorilor uzaţi, pe bază de V_2O_5, utilizaţi în industria acidului sulfuric (germ., rez. rom.) 15

DANIEL SUTIMAN, ŞT. IVĂŞCAN, I. ROŞCA, IGOR CREŢESCU şi GEORGE GRIGORIU, Coroziunea oţelului nealiat în sistemul etilenglicol–metanol–apă (germ., rez. rom.) 21

SAVEL IFRIM şi ELENA MIHAI, Observaţii asupra destrucţiei termice a unor acizi carboxilici (franc., rez. rom.) 27

I. MĂMĂLIGĂ, RADU Z. TUDOSE şi ECATERINA MERICĂ, Transfer de masă în filme lichide subţiri. III. Influenţa promotorilor de turbulenţă filamentari asupra vitezei de transfer (engl., rez. rom.) 35

OCTAVIAN PETRUŞ şi ILIE SIMINICEANU, Modelarea şi simularea unor biosenzori anticorp–antigen (engl., rez. rom.) 41

ALBIN CZERNICHOWSKI, KHÉLIFA MEGUERNES, EUGEN HNATIUC şi P. ONU, Generatoare de plasmă rece pentru electrochimie şi protecţia mediului (franc., rez. rom.) 51

CAROLINA HAGIU şi RODICA DIACONESCU, Analiza instalaţiei Norsk-hydro de obţinere a nitrofosfaţilor. IV. Procesul tehnologic „Obţinerea îngrăşămintelor N–P şi N–P–K" (franc., rez. rom.) 57

STELIAN PETRESCU, IGOR CREŢESCU şi I. MĂMĂLIGĂ, Concentrarea cristalelor mixte binare prin recristalizare multiplă în echicurent cu salefianţi (engl., rez. rom.) 63

MOULOUD ATTOU, HIROSHI MORIYAMA şi ABDELKRIM AZZOUZ, Studiul prin rezonanţă magnetică nucleară a unor compuşi organofosforici (engl., rez. rom.) 71

SIMION S. PETROVAN, Simularea şi proiectarea asistată de calculator a proceselor de vălţuire şi calandrare a fluidelor care respectă legea puterii (engl., rez. rom.) 79

Pag.

M. RUSU şi DANIELA-LORENA RUSU, Compounduri de polimeri cu pulberi metalice. I. Caracteristici fizico-mecanice (engl., rez. rom.) 89

CORNELIA VASILE, A. STOLERIU, LUCIA ODOCHIAN şi MĂRIOARA LUCHIAN, Reţele semi-interpătrunse pe bază de PVC. IV. Îmbătrânirea şi stabilizarea amestecurilor PVC/NBR cu umplutură (engl., rez. rom.) 95

AURELIAN STANCIU, C. CIOBANU, GH. STOICA şi VICTOR BULACOVSCHI, Poliuretani–polisiloxani reticulaţi (engl., rez. rom.) 107

LIVIU MITITEANU, AUREL DUŢĂ şi VICTOR BULACOVSCHI, Polimerizarea alcalină a acrilamidei (engl., rez. rom.) 115

RECENZII 121

BULETINUL INSTITUTULUI POLITEHNIC DIN IAŞI
BULLETIN OF THE POLYTECHNIC INSTITUTE OF JASSY
Tome XLI (XLV), Fasc. 1–4 1995

Section II

CHEMISTRY and CHEMICAL ENGINEERING

CONTENTS

Pp.

DOINA BEJAN and VIRGIL BĂRBOIU, Characterization of Some Proteolitic Enzyme Preparations by Spectrum Analysis (English, Romanian summary) 7

I. ROŞCA, N. FOCA, DANIEL SUTIMAN und AL. CONSTANTINESCU, Physikalisch-chemisches Studium der auf der Grundlage von V_2O_5 verwendeten Katalysatoren in der Schwefelsäureindustrie (German, Romanian summary) 15

DANIEL SUTIMAN, ŞT. IVĂŞCAN, I. ROŞCA, IGOR CREŢESCU und GEORGE GRIGORIU, Die Korrosion von unlegiertem Stahl in einem Äthylenglykol–Methanol–Wasser-System (German, Romanian summary) 21

SAVEL IFRIM et ELENA MIHAI, Observations sur la destruction thermique de quelques acides carboxyliques (French, Romanian summary) 27

I. MĂMĂLIGĂ, RADU Z. TUDOSE and ECATERINA MERICĂ, Mass Transfer in Thin Liquid Films. III. Influence of the Vertical Wiry Promoters of Turbulence on the Transfer Rate (English, Romanian summary) 35

OCTAVIAN PETRUŞ and ILIE SIMINICEANU, Modelling and Simulation of Antibody–Antigen Biosensors (English, Romanian summary) 41

ALBIN CZERNICHOWSKI, KHÉLIFA MEGUERNES, EUGEN HNATIUC et P. ONU, Générateurs des plasmas froids pour l'électrochimie et la protection de l'environnement (French, Romanian summary) 51

CAROLINA HAGIU et RODICA DIACONESCU, Analyse de l'installation Norsk-hydro d'obtention des nitrophosphates. IV. Le processus technologique „Obtention des engrais N–P et N–P–K" (French, Romanian summary) 57

STELIAN PETRESCU, IGOR CREŢESCU and I. MĂMĂLIGĂ, The Concentration of the Binary Mix Crystals by Multiple Recrystallization in Cocurrent Flow with Salting-out Substances (English, Romanian summary) 63

MOULOUD ATTOU, HIROSHI MORIYAMA and ABDELKRIM AZZOUZ, NMR Study of Some Organophosphorus Compounds (English, Romanian summary) 71

SIMION S. PETROVAN, Computer Aided Simulation and Design of Two-Roll Mixing and Calendering Processes of Power-Low Fluids (English, Romanian summary) 79

	Pp.
M. RUSU and DANIELA-LORENA RUSU, Polymeric Composites with Metallic Powders. I. Physico-Mechanical Characteristics (English, Romanian summary)	89
CORNELIA VASILE, A. STOLERIU, LUCIA ODOCHIAN and MĂRIOARA LUCHIAN, Semi-Interpenetrating Polymer Network Based PVC. IV. Aging and Stabilization of the Filled PVC/NBR Mixtures (English, Romanian summary)	95
AURELIAN STANCIU, C. CIOBANU, GH. STOICA and VICTOR BULACOVSCHI, Crosslinked Polyurethane–Polysiloxanes (English, Romanian summary)	107
LIVIU MITITEANU, AUREL DUŢĂ and VICTOR BULACOVSCHI, Alkaline Polymerization of Acrylamide (English, Romanian summary)	115
BOOK REVIEWS	121

BULETINUL INSTITUTULUI POLITEHNIC DIN IAŞI
Tomul XLI (XLV), Fasc. 1–4, 1995
Secţia II
CHIMIE ŞI INGINERIE CHIMICĂ

D.C. 543.866; 544.6

CHARACTERIZATION OF SOME PROTEOLITIC ENZYME PREPARATIONS BY SPECTRUM ANALYSIS

BY

DOINA BEJAN and VIRGIL BĂRBOIU

1. Introduction

The enzymes may be characterized by the entire gamut of spectrum analyses, ultraviolet (UV), light (VIS) and infrared (IR) molecular absorption spectrometry, Raman spectrometry, spin electronic resonance spectrometry, nuclear magnetic resonance spectrometry (NMR), Mössbauer spectrometry, etc. [1],...,[5].

Information can thus be obtained regarding the conformation, structure, interatomic distances, valence angles, hydrogen and disulphide bonds in the enzyme molecules. In case of metal–enzymes some aspects regarding the type of metal–proteine bond, the position of the metal attachment to the aminoacids in enzyme structure can be made evident. The location and geometry of the active catalytic situs may also elucidated by means of spectral methods. Apart from this, the above mentioned methods can also be applied for the enzyme purity control as well as for their quantitative estimation.

2. Experimental

a) Trypsin (pure), (TR), Hopkin & Williams Ltd., Fine Chemicals, England.

b) Pancreatine (pure), (P), E. Merck, Darmstadt, Germany.

c) Trizim, (TRIZ), pancreas powder obtained by dehydrating the gland with acetone at a low temperature (Institute of Biological Sciences, Bucharest).

d) Proteolitic enzyme preparations obtained from the ox duodenal mucous membrane by the following extraction procedures at low temperature: 1° extraction with distilled water; 2° extraction with isotonic saline solutions, 0.15 M NaCl; 3° extraction with phosphonate buffer solution (pH=7.6), followed by purification by precipitation with acetone in a 1:1 ratio (enzyme extract : acetone), according to literature method [1].

The purified enzyme preparations were dried at the room temperature and finelly ground.

The UV Spectra have been recorded on a Spekord UV-VIS, Carl Zeiss, Jena, Spectrophotometer.

The IR Spectra have been recorded with KBr pellets on a 71-IR Carl Zeiss, Jena, Spectrophotometer.

The ^{1}H-NMR Spectra have been recorded with D_2O solutions on a JNM-C-60 HL type spectrophotometer of 60 MHz at different temperatures (20°C, 50°C) and sensitivities with DSS as a standard.

The determination of particle shape and size by electronic microscopy was made with a transmission electronic microscope of the Tesla-B-3540 type.

The zinc content of the enzyme preparations was estimated by polarographic analysis and atomic absorption spectrometry.

3. Results and Discussion

According to literature [1], [5] the enzymes in the duodenal mucous membrane belong to the class of hydrolases, namely peptide hydrolases. They may be devided into: aminopeptidases (leucineaminopeptidase, a zinc-containing enzyme; aminopeptidases *A* and *B*; aminotripeptidases) and dipeptidases (glycyl-glycin dipeptidase; glycyl-*L*-leucin dipeptidase; glycyl-*L*-prolin dipeptidase (prolidase), a tiol-enzyme; *L*-prolyl-glycyl dipeptidase (prolinase); glycyl-glycin dipeptidase).

Often one or more aminoacids are to be found in the "catalytic situs" (active catalytic center) of the enzyme, such as: seryne, cysteine, histidine, thyrosine, lysine [1], [6]. Thus the seryne for instance is to be found in the active center by the proteolitic enzymes: chemotrypsin, trypsin, carboxypeptidase [1].

In case of the metal–enzymes the metal ion included in the active center takes part to the catalytic action.

The spectral properties of the enzyme preparations are expected to reflect both the molecule assembly as well as the active center involved in the catalytic action.

3.1. Study on UV Spectra

The UV molecular electron absorption spectra recorded for the enzyme preparations *1, 2* and *3* as well as for the standard pancreatic preparation (TRIZ) are given in Fig.1.

All spectra are noticed to show absorption maxima near $\lambda_1 = 270$ nm, $\lambda_2 = 230...240$ nm and $\lambda_3 = 205...207$ nm ($\lambda_3 = 215$ nm for TRIZ). According to literature [1] these bands may be attributed to: thyrosine, tryptophan and, in a lesser extent, phenylalanine residues, aromatic aminoacids ($\lambda = 280$ nm); to the specific absorption characteristic to certain residues of dibasic acids, to the hydrogen bonds and other interactions involved in the conformation preservation ($\lambda = 210...250$ nm); to the absorption of peptide bonds and also to many conformation factors ($\lambda < 210$ nm).

The enzyme molecules may be appreciated to maintain the properties characteristic to the proteines, which confirms the correctness of the treatment applied for their obtaining. The clear peaks in the spectra of samples *1, 2* and *3* are indicative of a higher purity than in case of TRIZIM.

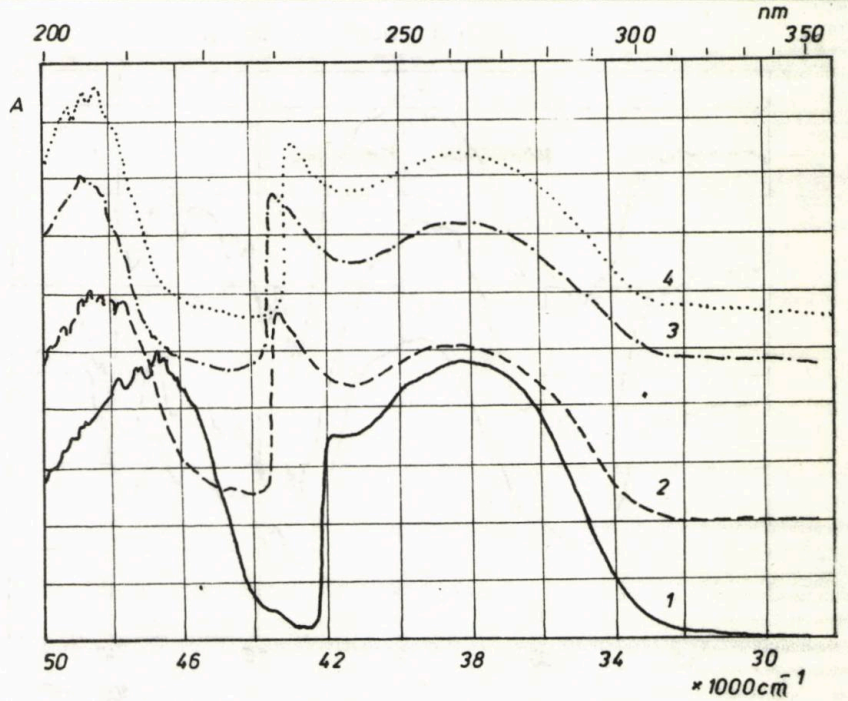

Fig. 1.– UV spectra of: —— TRIZ; - - - sample *1*; ---- sample *2*; ··· sample *3*.

3.2. Study on IR Spectra

The IR Spectra of the enzyme preparations *1, 2* and *3* and those of the standard ones (TR, P and TRIZ) are given in Figs.2 and 3, respectively.

Table 1 lists the principal absorption bands.

Table 1

The Principal Absorption Bands in the IR Spectra

Sample	Characteristic frequencies, [cm^{-1}]								
	$\nu_{C=0}$	Amide *I* ν_{N-H}			Amide *II* ν_{C-N}		ν_{S-H}	ν_{C-OH} phenolic	ν_{C-OH} primary
1	3 100...3 450	1 650	1 660	1 515	–	1 530	2 900	1 240	1 040...1 070
2	3 200...3 400	1 630	1 665	1 510	1 550	1 535	2 920	1 230	1 060
3	3 200...3 400	1 640	1 660	1 510	1 545	1 530	2 910	1 230	1 060
TR	3 200...3 400	1 640	1 665	1 430	1 445	–	2 900	1 200	1 040
P	3 100...3 200 3 200...3 400	1 640	1 665	1 425	1 445	–	2 900	1 260	1 030
TRIZ	3 200...3 300	1 625	1 665	1 520	1 400	–	2 900	1 230	1 060

The polypeptides with random secondary structure are known to show IR ab-

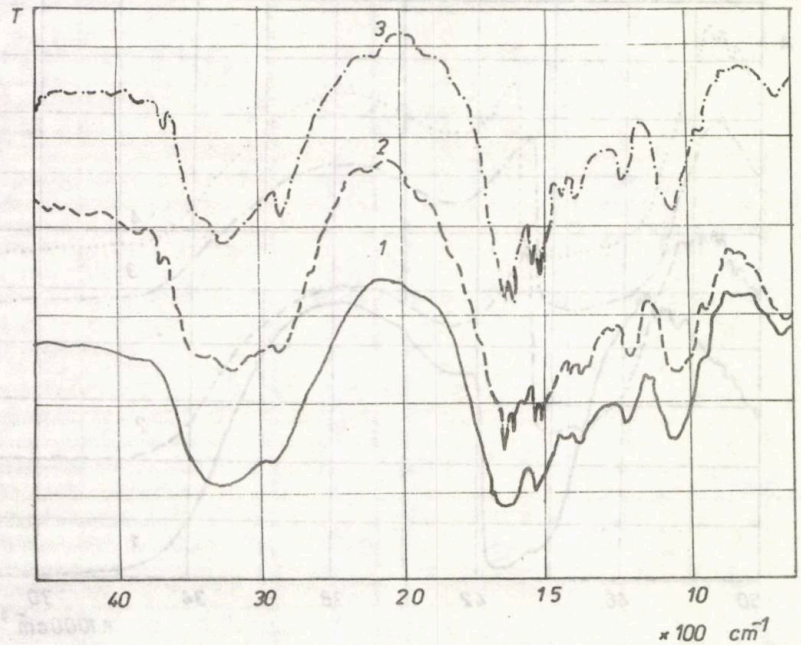

Fig. 2.– IR spectra of enzyme preparations:
—— sample *1*; - - - sample *2*; -·-·- sample *3*.

sorption bands at 3 290, 1 650 and 1 535 cm^{-1} caused by the carbonyl, iminogroups and C–N bond, respectively. The last two bands are named amide *I* and amide *II* [1].

Passing to an ordered structure of the α-helix type the amide *I* frequency turns into two maxima, with $\tilde{\nu} = 1\,650$ cm^{-1} and $\tilde{\nu} = 1\,652$ cm^{-1}, and the amide *II* frequency turns into other two maxima: $\tilde{\nu} = 1\,516$ cm^{-1} and $\tilde{\nu} = 1\,546$ cm^{-1}.

Passing to a pleated sheet structure the amide *I* band splits into the bands $\tilde{\nu} = 1\,645$ cm^{-1} and $\tilde{\nu} = 1\,630$ cm^{-1}, the last being more intense, and the amide *II* bands turns into the bands $\tilde{\nu} = 1\,530$ cm^{-1} and $\tilde{\nu} = 1\,550$ cm^{-1} [1].

As can be seen all recorded spectra show a wide absorption band of $\tilde{\nu} = 3\,200...3\,400$ cm^{-1} with a maximum at $\tilde{\nu} = 3\,290$ cm^{-1}.

The samples *1*, *2* and *3* show amide *I* and amide *II* bands with maxima characteristic of both α-helix and pleated sheet structure.

This type of conformation is similar to that of the standard samples (TR, P, TRIZ) although the frequencies of the amide *II* band are shifter to shorter wavelengths ($\tilde{\nu} = 1\,450$ cm^{-1}).

In our opinion, the molecules of enzymes in sample *1*, *2* and *3* show portions of α-helix and pleated sheet structure alternating with portions of random secondary structure.

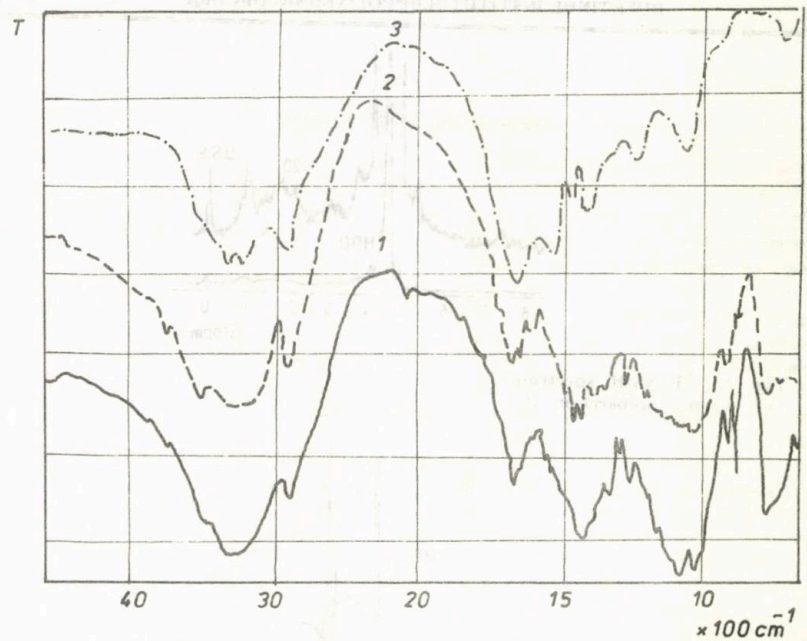

Fig. 3.– IR spectra of standard samples: —— TR; - - - P; ·-·-· TRIZ.

The fact can also be noticed that the samples *1* and TRIZ show similar spectra, with wide absorption bands indicatives of a rather lower purity and a less ordered structure.

Apart from this, the following bands can be noticed: that of frequency $\tilde{\nu} = 2\,900\ cm^{-1}$ in all spectra, which may be attributed to the ν_{S-H} valence vibration, that of $\tilde{\nu} = 1\,240...1\,260\ cm^{-1}$, corresponding to the $\nu_{C-OH\ (phenolic)}$ vibration in tyrosine and that of $\tilde{\nu} = 1\,040...1060\ cm^{-1}$ given probably by the extension vibration $\nu_{C-OH\ (primary)}$ in serine.

Consequently, the catalytic situs of the enzymes in the duodenal enzyme preparations can be assumed to contain the following aminoacids: tyrosine, serine and cysteine.

3.3. Study on ^{1}H-NMR Spectra

The aspect of the ^{1}H-NMR Spectra of the sample *3* (Fig.4) and of the standard samples TR and TRIZ (Fig.5 *a* and 5 *b*) are in a good agreement with literature data [4].

In the spectra of the samples *1, 2, 3* a signal $\delta = 3.5...4.0$ ppm (determined toward DSS), which may be attributed to either serine or cysteine, can be noticed. The signal at $\delta = 0.9...2.5$ ppm could be given by the portion of aliphatic substituents longer than 2...3 carbon atoms, while that at $\delta = 7.2$ ppm is probably

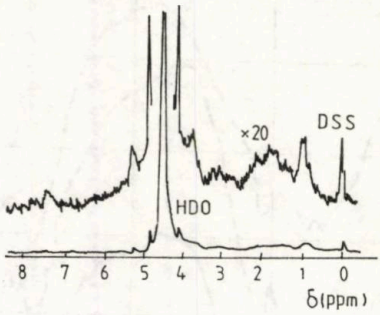

Fig. 4.– ^{1}H-NMR spectrum of enzyme preparation *3*.

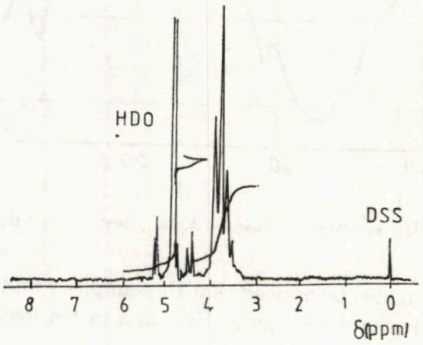

Fig. 5 *a*.– ^{1}H-NMR spectrum of trypsin.

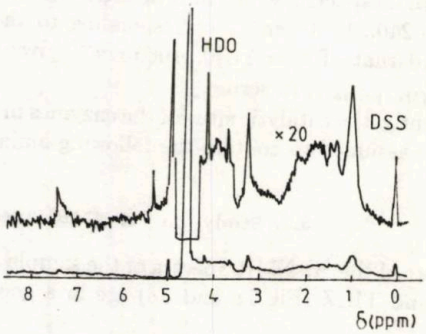

Fig. 5 *b*.– ^{1}H-NMR spectrum of TRIZIM.

due to aryl substituents (in tyrosine, tryptophan). The ^{1}H-NMR Spectra of the standard samples contain either all above mentioned signals (TRIZ) or some of them only (TR: $\delta = 3.5...4.0$ ppm; P: $\delta = 3.5...4.00$ ppm and $\delta = 0.9...2.5$ ppm).

By taking the ^{1}H-NMR signals into account, as well as the fact that the aminoacids of the catalytic situs have a privileged position allowing for their characteristic behaviour in an external magnetic field, the serine, cysteine and tyrosine might be assumed as the potential constituents of the enzyme active centers.

3.4. Particle Shape and Size

By means of the electronical microscopy the samples *1*, *2* and *3* as well as the standard samples TR, P, TRIZ were found to consist predominantly of regular particles of 25...30 μm size. In addition to that P and TRIZ also contain ovoid particles of 100 μm size in agreement to literature data [1].

3.5. Zinc Content of Enzyme Preparations

The estimation of the zinc content was suggested by the possibility of leucine-aminopeptidase presence (a zinc-enzyme) in the enzyme source. The zinc amount in 100 g of dry sample was of 6.3303 mg. The presence of the above mentioned enzyme in the enzyme preparation was thus acertained.

4. Conclusions

By means of spectral methods appreciations can be made on the purity of enzyme preparations. The obtained results indicate the extraction with isotonic saline solution and phosphate buffer solution (pH=7.6) followed by precipitation with acetone to be a suitable method for the extraction and purification of enzymes in the ox duodenal mucous membrane.

The enzyme molecules show a secondary structure predominantly of the α-helix pleated sheet types; the particle shape is regular of 25...30 μm size.

The duodenal enzyme preparations contain a metal-enzyme with zinc (leucine-aminopeptidase), a thiol-enzyme (glycyl-*L*-proline-dipeptidase) and a serine-enzyme.

The enzyme catalytic situs is responsable for the absorption bands in UV and IR Spectra as well as for the ^{1}H-NMR signals, having a privileged position in the molecular chain of the protein enzyme and showing a particular behaviour.

Received, March 3, 1994

Technical University "Gh. Asachi", Jassy,
Department of Analytical Chemistry
and
Macromolecular Chemistry
Institute "P. Poni", Jassy

REFERENCES

1. Dumitru I.F., Iordăchescu D., *Introducere în enzimologie*. Ed. Medicală, Bucureşti, 1981, 155, 161, 192, 204.
2. Străjescu M., Teodor F., *Elemente de chimie bioanorganică*. Ed. Dacia, Cluj-Napoca, 1979, 127.
3. Roman L., Bârzu O., *Implicaţii biomedicale ale combinaţiilor complexe*. Ed. Dacia, Cluj-Napoca, 1973, 112.

4. Cooper A., Houben J.L., Chien L.C., *The Enzyme Catalysis Process: Energetics, Mechanism and Dynamics.* Plenum Press, New York, 1989, 141, 197.
5. Soru E., *Biochimie medicală.* Ed. Medicală, Bucureşti, 1959, 775, 799, 806, 815.
6. Popescu A., Cristea El., Zamfirescu-Ghiorghiu M., *Biochimie medicală.* Ed. Medicală, Bucureşti, 1980, 100.

CARACTERIZAREA PE CALE SPECTROMETRICĂ A UNOR PREPARATE ENZIMATICE CU ACŢIUNE PROTEOLITICĂ

(Rezumat)

Se prezintă unele rezultate stabilite în studiul configuraţiei moleculelor, constituţiei situsului catalitic, dimensiunilor particulelor şi purităţii unor preparate enzimatice proteolitice obţinute din mucoasa duodenală bovină prin diferite procedee.

Studiul s-a efectuat prin spectrometrie de absorbţie moleculară în UV şi IR, spectrometrie ^{1}H-RMN şi microscopie electronică, în comparaţie cu tripsina (pură), pancreatina (pură) şi trizim (preparat enzimatic pancreatic parţial purificat).

BULETINUL INSTITUTULUI POLITEHNIC DIN IAŞI
Tomul XLI (XLV), Fasc. 1-4, 1995
Secţia II
CHIMIE ŞI INGINERIE CHIMICĂ

D.K. 541.128.5; 546.881

PHYSIKALISCH-CHEMISCHES STUDIUM DER AUF DER GRUNDLAGE VON V_2O_5 VERWENDETEN KATALYSATOREN IN DER SCHWEFELSÄUREINDUSTRIE

VON

I. ROŞCA, N. FOCA, DANIEL SUTIMAN und AL. CONSTANTINESCU

1. Vorwort

Wegen seiner besonderen Eigenschaften ist das Vanadium sowohl in reinem Zustand als auch als Verbindung in verschiedenen Oxydationszuständen (V(III), V(IV) und besonders V(V)) eines der am meisten gebrauchten Elemente bei katalytischen Prozessen zur Herstellung von organischen Verbindungen bzw. bei den Oxydationsprozessen des Benzols, seiner homologen Verbindungen (Toluol, Xylol u.a.) und besonders beim Herstellungprozeß von Schwefelsäure.

Eines der am meisten verwendeten Kombinationen ist das Divanadiumpentaoxyd (V_2O_5), das mit dem Katalysatorträgern SiO_3 und Al_2O_3 der einizige Katalysator ist, der im katalytischen Oxydationsprozeß der Schwefelgase, von SO_2 zu SO_3, in der Schwefelindustrie verwendet wird [1].

Die bei der Oxydation von SO_2 zu SO_3 verwendeten Katalysatoren enthalten, je nach dem Hersteller, 4...11% reines V_2O_5. Die katalytische Masse enthält nach Promotoren, am häufigsten K_2O und Zusätze wie Al_2O_3 und Fe_2O_3 auf Silikatbasis [3].

Der verbrauchte Katalysator enthält folgende Komponenten: V_2O_3, $VOSO_4$, $V_2(SO_4)_3$, VO_2 und kleine Mengen von V_2O_5, wodurch bedeutende Mengen von SO_2 uns SO_3 sowohl in physikalischer als auch chemischer Form gebunden werden. Diese Produkte erhält man durch folgende Reaktionen:

$$V_2O_5 + SO_2 \rightleftharpoons V_2O_4 + SO_3, \quad V_2O_4 + 2SO_3 \rightleftharpoons 2VOSO_4,$$

$$2VOSO_4 \rightleftharpoons V_2O_4 + 2SO_3, \quad V_2O_5 + 2SO_2 \longrightarrow V_2O_3 + 2SO_3,$$

$$2VOSO_4 \rightleftharpoons V_2O_5 + SO_2 + SO_3, \quad V_2O_4 + 2SO_3 \longrightarrow 2VOSO_4,$$

$$V_2O_4 + 2SO_2 + O_2 \longrightarrow 2VOSO_4, \quad 2V_2O_5 + 3SO_2 + \frac{1}{2}O_2 \longrightarrow 2V_2O_4 + 3SO_3,$$

$$V_2O_3 + 3SO_2 + \frac{3}{2}O_2 \longrightarrow V_2(SO_4)_3, \quad V_2O_3 + 3SO_3 \longrightarrow V_2(SO_4)_3,$$

$$V_2(SO_4)_3 \overset{410^\circ C}{\longrightarrow} 2VOSO_4 + SO_2, \quad V_2(SO_4)_3 \overset{410^\circ C}{\longrightarrow} V_2O_5 + 2SO_2 + SO_3.$$

Der verbrauchte, fein gemahlene Katalysator liegt als gelb-grünes Pulver vor, schwer löslich in Alkohol oder Äther, aber teilweise löslich in kaltem oder warmem Wasser, wodurch sich grüne Lösungen bilden, die ihre Farbe mit der Zeit ändern [2].

2. Experimenteller Teil

Das physikalisch-chemische Studium der verbrauchten Katalysatoren mit Vanadiumpentaoxyd V_2O_5 verfolgte folgende Aspekte:

a) Verhalten des verbrauchten Katalysators in wässriger, saurer und alkalischer Lösung.

b) Oxydation des Vanadiums V(III) und V(IV) zu V(V), zu seiner Rückgewinnung in Form von NH_4VO_3 oder V_2O_5.

c) Wiedergewinnung des Vanadiums aus dem verbrauchten Katalysator in Form von Ammoniummetavanadat (NH_4VO_3, $(NH_4)_3V_3O_9$) und von Divanadiumpentaoxyd [3].

d) Bestimmung des im verbrauchten Katalysator enthaltenen SO_4^{2-} [4].

e) Bestimmung des Gesamtinhalts von SO_4^{2-} im verbrauchten Katalysator.

f) Zeitabhängige Verlauf der elektrischen Leitfähigkeit des Systems „verbrauchter Katalysator – destilliertes Wasser".

g) Zeitabhängiger Verlauf des pH-Wertes des Systems „verbrauchter Katalysator – destiliertes Wasser".

2.1. Verhalten des verbrauchten Katalysators in wäßriger Lösung

Es wurden Mengen zwischen 50 und 250 g des verbrauchten Katalysators abgemessen, in einen Erlenmeyer-Kolben gegeben und destilliertes Wasser in Abhängigkeit der Katalysatormenge (200...1000 cm^3) zugefüllt. Die Proben wurden 72 h bei Zimmertemperatur in Kontakt gelassen ab und zugeschüttelt, damit sich die löslichen Komponenten SO_2, SO_3, $VOSO_4$, $V_2(SO_4)_2$ und teilweise VO_2 und V_2O_5 so gut wie möglich lösen [5]. Nach dem erwähnten Zeitintervall hat man eine grünliche Lösung erhalten, was auf die Anwesenheit von V(III) in Form von wasserlöslichem $V_2(SO_4)_3$ oder $VOSO_4$ hinweist.

Die obere grüne Lösungsschicht, die V(III) enthält, wechselt mit der Zeit ihre Farbe, wobei sie von grün zu blau übergeht als Folge der langsamen Oxydation von V(III) zu V(IV) [6].

Wenn 5 h bei Wärme (t=80°...90°C) gearbeitet und Luft durch die Probe geblasen wird, dann hat die vom Träger filtrierte Endlösung eine blaue Färbung [7], was auf die Tatsache hinweist, daß in diesem Fall das Vanadium in dem höheren Oxydationszustand V(IV) vorliegt, wahrscheinlich $VOSO_4$, daß in VO^{2+} und SO_4^{2-} ionisiert.

In allen Fällen stellt man einen stark säuren pH-Wert der erhaltenen Lösungen zwischen 1,5 und 2 fest. Der stark saure Charakter der Lösungen, erhalten nach längerem Kontakt des verbrauchten Katalysators (bei 300°C getrocknet) und mit destilliertem Wasser, durch die Luft geblasen wurde, ist auf folgende chemischen Prozesse zurückzuführen:

$$SO_3 + H_2O \longrightarrow H_2SO_4, \quad SO_2 + H_2O \rightleftharpoons H_2SO_3,$$

sowie auf die Ionisierung des Vanadylsulfats:

$$VOSO_4 \rightleftharpoons VO^{2+} + SO_4^{2-}.$$

Das Schwefeldi- und -trioxyd stammt vom Katalyseprozeß her und wurde auf der Oberfläche des Katalysators abgeschieden, aber durch den längeren Kontakt des Katalysators mit Wasser gehen sie in Lösung, in Form von Säuren, über [3].

Wenn in der blauen Lösung, die durch Lösen des verbrauchten Katalysators gewonnen wurde, einige Stunden Luft durchperlt, dann verändert sich nicht mehr die Farbe der Lösung, also findet unter diesen Bedingungen die Oxydation von V(IV) zu V(V) nicht statt, die Reaktion läuft unter diesen Bedingungen sehr schwerfällig ab [3]. V_2O_3 oxydiert langsam zu VO_2 und durch Erwärmung in der Luft geht V_2O_3 in V_2O_5 über.

Die Oxydation von V(III) und V(IV) zu V(V) kann mit starken Oxydationsmitteln erfolgen, wie z.B. Perhydrol (H_2O_2, 30%) konzentrierte Salpetersäure, Kaliumpermanganat [8] oder mit so gewählten Oxydationsmitteln, daß der Übergang von V(III) und V(IV) zu V(V) total ist [3], um V(III) und V(IV) aus dem verbrauchten Katalysator zurückzugewinnen.

2.2. Verhalten des verbrauchten Katalysators im sauren Medium

Wenn man den verbrauchten V_2O_5-Katalysator mit konzentrierter Schwefelsäure behandelt, so löst sich der größte Teil der Vanadiumverbindungen, jedoch erhält man gewöhnlich ein Gemisch von Vanadiumverbindungen in den Oxydationszuständen III, IV, V, die zu V(V) oxydiert werden müssen, um sie unter der Form NH_4VO_3 oder V_2O_5 abzuscheiden. Die Oxydation wurde in diesem Fall mit einem wirksamen und billigen Oxydationsmittel ausgeführt [3].

2.3. Verhalten des verbrauchten Katalysators im basischen Medium

Die Extraktion des Vanadiums in Form von NH_4VO_3 wird auch im basischen Medium durchgeführt, wobei V(III) und V(IV) zu V(V) mit Kaliumpermanganat oxydierte. Als basisches Medium wurde Natriumkarbonat oder ein Gemisch von Natriumkarbonat und Natriumhydroxyd verwendet, das leicht mit V_2O_5 wie folgt reagiert:

$$V_2O_5 + 2NaOH \longrightarrow 2NaVO_3 + H_2O, \quad V_2O_5 + 6NaOH \longrightarrow 2Na_3VO_4 + 3H_2O,$$
$$3V_2O_5 + 6NaOH \longrightarrow 2Na_3V_3O_9 + 3H_2O.$$

Vanadate von alkalischen Metallen sind in Wasser löslich, können durch Filterung abgeschieden werden, und durch die Behandlung mit einem Gemisch von NH_4Cl und NH_4OH werden die in Wasser unlöslichen Ammonium*meta-*, *-ortho-* oder -trivanadate ausgefällt, in deren Form V(V) aus dem verbrauchten Katalysator wiedergewonnen wird [3].

Im Falle der Behandlung des verbrauchten Katalysators mit Natriumkarbonat, Natriumhydroxyd oder einem Gemisch von Karbonat und Hydroxyd erhält man den Nachteil, daß ein Teil des Trägers, besonders das Siliziumdioxyd, sich löst und in lösliches Silikat übergeht. Daß wurde besonders dann festgestellt, wenn im stark basischen Medium und Wärme gearbeitet wird. Die Wiedergewinnung des Vanadiums im basischen Medium setzt die genaue Kenntnis des Vanadiuminhalts des verbrauchten Katalysators voraus. Bei Temperaturen über 60°...70°C löst sich ein großer Teil des Siliziumdioxyds, wodurch das Natriumvanadat verunreinigt wird.

Aus diesem Grunde zieht man vor, im sauren Medium (pH=4) unter Wärme [3] zu arbeiten. Unter diesen Bedingungen löst sich der auf Silizium beruhende Träger nicht mehr.

2.4. Bestimmung der löslichen Komponenten

Der verbrauchte Katalysator enthält neben dem Träger, Siliziumdioxyd und anderen nichtlöslichen Komponenten wie V_2O_5, Fe_2O_3, VO_2 auch eine Reihe von löslichen Komponenten, die sich im Katalyseprozeß bilden als Folge der Reaktion des Divanadiumpentaoxyds mit den Schwefeloxyden SO_2 und SO_3.

Eine Katalysatormenge von 250 g wird in einen Erlenmeyerkolben mit 1,5 l destilliertem Wasser gefüllt und 120 Stunden stehengelassen. Danach wird gefiltert, der Rückstand mehrere Male mit destilliertem Wasser gewaschen, bis alle löslichen Komponenten in das Filtrat übergegangen sind. Der Rückstand wird einige Stunden lang getrocknet, bis sein Gewicht sich nicht mehr verändert. Der verbliebene getrocknete Rückstand weisst eine Verminderung seines Gewichts um 90 g auf. Das Experiment wurde mit zwei Proben auf dieselbe Weise wiederholt: eine Probe enthielt den verbrauchten Katalysator, so wie er aus dem Katalyseprozeß hervorging, und die andere Probe wurde getrocknet (längere Zeit bei 250°C im Trockenschrank erwärmt).

Nachdem wie im vorhergehenden Fall verfahren wurde, stellte man bei beiden Proben eine Gewichtsabnahme von ca. 30% fest. Daraus folgt, daß der lösliche Anteil des verbrauchten Katalysators zwischen 30...35% schwankt.

2.5. Wärmeverhalten des verbrauchten Katalysators

Drei Proben, die je 50 g des vebrauchten Katalysators enthalten, wurden einer Kalzinierung bei 850°C unterworfen. Nach 12 Stunden stellt man fest, daß die Proben dasselbe Gewicht haben. Das wird durch die Tatsache erklärt, daß, obwohl eine Reihe von Komponenten sich zersetzen oder aus dem Katalysator ausscheiden, in derselben Zeit andere Reaktionen stattinden, wie: Oxydation von V(III) und V(IV) zu V(V), die Reaktion zwischen SO_2 und K_2O aus dem Träger oder die Reaktion der Fe(II)- und Fe(III)-Oxyde mit SO_3.

2.6. Bestimmung von SO_4^{2-} des verbrauchten Katalysators

Die Bestimmung von SO_4^{2-} im verbrauchten Katalysator wurde nach zwei Varianten durchgeführt: a) SO_4^{2-}-Dosierung aus der Probe von verbrauchtem Katalysator aus dem Katalyseprozeß; b) SO_4^{2-}-Dosierung aus dem bei 250°C getrockneten, verbrauchten Katalysator.

In beiden Fällen wurde SO_4^{2-} anfangs ohne Oxydierung von SO_2, d.h. SO_4^{2-} bestimmt. Die erhaltenen Daten sind in Tabelle 1 enthalten.

Der Gesamtgehalt von SO_4^{2-} wurde folgendermaßen bestimmt: vier Proben zu je 100 g verbrauchten Katalysator wurden 72 Stunden in Kontakt mit destilliertem Wasser bei 20°C gelassen. Dann wurde zu jeder Probe Perhydrol hinzugefügt, damit SO_3^{2-} zu SO_4^{2-} oxydiert. In jeder Probe wurde gravimetrisch als Bariumsulfat der Gesamtgehalt an SO_4^{2-} bestimmt. Die erhaltenen Daten sint in Tabelle 2 wiedergegeben.

Tabelle 1

SO_4^{2-}-Gehalt in den Proben des verbrauchten Katalysators (Nichtoxydiert: *1* und *2* – Katalysator unkalziniert; *3* und *4* – bei 400°C getrockneter Katalisator)

Proben Nr.	Katalysator	Ausgangsmenge g	Zugefügte Menge H_2O l	Arbeitsprobe cm^3	$BaSO_4$, [g], pro 100 g verbrauchter Katalysator
1.	Unkalziniert	100	2	250	57,56
2.		100	2	250	55,60
3.	Getrocknet bei 300°C	100	2	250	45,92
4.		100	2	250	44,52

Tabelle 2

SO_4^{2-}-Gehalt in den Proben des verbrauchten Katalysators
(getrocknet bei 300°C und Oxydierung der Lösung mit Perhydrol)

Proben Nr.	Unkalzinierter verbrauchter Katalysator	Ausgangsmenge g	Zugefügte Menge H_2O l	Arbeitsprobe cm^3	$BaSO_4$, [g], pro 100 g verbrauchter Katalysator
1.	Unkalziniert Verbrauchter Katalysator	100	2	250	68,94
2.		100	2	250	66,82
3.		100	2	250	67,40
4.		100	2	250	68,56

2.7. Die Veränderung der elektrischen Leitfähigkeit

Es wurde die zeitmäßige Veränderung der elektrischen Leitfähigkeit verfolgt beim Kontakt des verbrauchten Katalysators mit destilliertem Wasser während einer Zeitdauer von 7 Stunden. Die erhaltenen Daten sind in Abb.1 dargestellt.

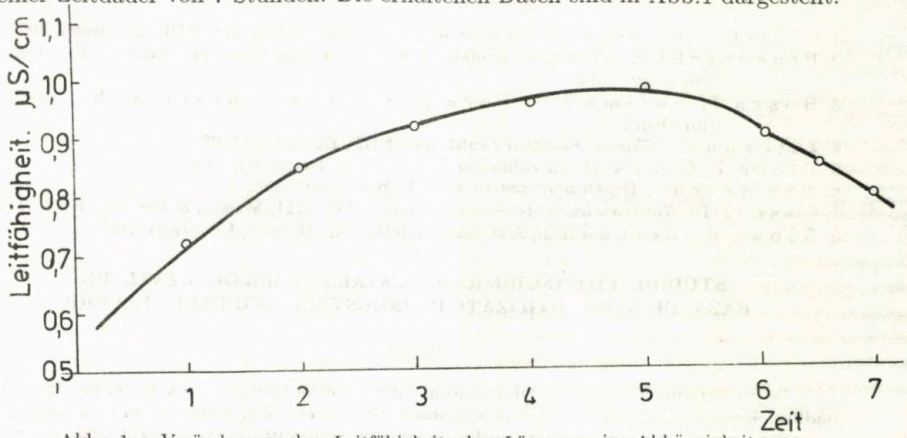

Abb. 1.– Veränderung der Leitfähigkeit der Lösungen in Abhängigkeit von der Zeit bei Kontakt des verbrauchten Katalysators mit destillierten Wasser.

Man verzeichnet ein Anwachsen der elektrischen Leitfähigkeit im Zeitintervall von 5 Stunden, danach fällt sie ab. Das Amwachsen der Leitfähigkeit erklärt sich

aus dem Lösen der löslichen Komponenten, die in der wäßrigen Lösung ionisieren.

Der Abfall der Leitfähigkeit folgt daraus, daß mit dem Abfall des pH-Wertes Polymerisationsprozesse stattfinden, die Bildung von polyvanadischen Verbindungen, was zu einem Abfall der Ionenanzahl, also der elektrischen Leitfähigkeit, führt.

3. Schlußfolgerungen

Es werden einige Aspekte hinsichtlich des Verhaltens der verbrauchten Katalysatoren auf der Grundlage von Vanadiumpentaoxyd behandelt.

Es wurde das chemische Verhalten der verbrauchten Katalysatoren in verschiedenen Reaktionsmedien, wäßrigen, sauren und basischen, verfolgt, sowie ihr Verhalten bei verschieden Temperaturen, hinsichtlich der Oxydation der Vanadiumverbindungen vom niederen Oxydationsstadium (V(III); V(IV) zum höheren Stadium (V(V)).

Gleichzeitig wurde die Gewichtsänderung einiger Proben des verbrauchten Katalysators bei Kalzinierung untersucht, sowie die löslichen Komponenten, die der verbrauchte Katalysator enthält.

Die Prozesse, die bei der Kalzinierung der verbrauchten Katalysatoren auf der Grundlage von V_2O_5 stattfinden sowie als Folge ihrer Wechselwirkungen mit verschiedenen Reaktionsmedien sind komplex und hängen von allen erwähnten Faktoren ab.

Eingegangen am 17. Dezember 1992

Technische Universität „Gh. Asachi", Jassy, Lehrstuhl der Anorganische Chemie

LITERATURVERZEICHNIS

1. Calistru C., Leonte C., *Tehnologia sărurilor anorganice.* EDP, Bucureşti, 1972.
2. Pincovschi E., *Tehnologia acidului sulfuric şi a compuşilor intermediari.* Ed. Tehnică, Bucureşti, 1967.
3. Roşca I., Sutiman D., Foca N., Constantinescu Al., Rev. de chimie (im Druck).
4. Liteanu C., *Chimie analitică cantitativă.* EDP, Bucureşti, 1969.
5. Block I., *Chimie analitică calitativă.* Ed. Tehnică, Bucureşti, 1958.
6. Neniţescu C.D., *Chimie generală.* EDP, Bucureşti, 1972.
7. Pascal P., *Nouveau traité de chimie minérale.* Vol. **XII**, Masson & Cie Ed., Paris, 1958.
8. Ripan R., Ceteanu I., *Chimia metalelor.* Ed. Tehnică, Bucureşti, 1969.

STUDIUL FIZICO-CHIMIC AL CATALIZATORILOR UZAŢI, PE BAZĂ DE V_2O_5, UTILIZAŢI ÎN INDUSTRIA ACIDULUI SULFURIC

(Rezumat)

Se prezintă unele aspecte privind studiul catalizatorilor uzaţi pe bază de pentaoxid de divanadiu, folosiţi în procesele de obţinere a acidului sulfuric, cât şi în industria chimică organică.

S-a urmărit comportarea compuşilor de vanadiu conţinuţi în catalizatorul uzat, în vederea recuperării vanadiului sub formă de diferiţi compuşi, în special V_2O_5 sau NH_4VO_3.

BULETINUL INSTITUTULUI POLITEHNIC DIN IAŞI
Tomul XLI (XLV), Fasc. 1–4, 1995
Secţia II
CHIMIE ŞI INGINERIE CHIMICĂ

D.K. 620.193.4

DIE KORROSION VON UNLEGIERTEM STAHL IN EINEM ÄTHYLENGLYKOL–METHANOL–WASSER-SYSTEM

VON

DANIEL SUTIMAN, ŞT. IVĂŞCAN, I. ROŞCA,
IGOR CREŢESCU und GEORGE GRIGORIU

1. Vorwort

In der Glykolrückgewinnungsanlage der TEROM AG, Jassy, bildet die Glykoldestillationskolonne, die in der Destillierblase das Rohglykol und als Destillat das Methanol und Wasser trennt, eines der größten Korrosionsprobleme. Die korrodiertesten Elemente sind die Glocken der Destillationskolonne, die praktisch einmal oder sogar öfter im Jahr ersetzt werden müssen, wobei ihre Anzahl einige Tausende beträgt. Diese Glocken bestehen aus C-Stahl.

Das reine Äthylenglykol ist bei niedrigen Temperaturen, praktisch inaktiv, was die Korrosion anbelangt. Bei unlegierten Stählen hängt die von ihm verursachte Korrosion besonders vom pH-Wert (wächst bei Absinken seiner Temperatur) und von der Anwesenheit von Wasser ab. Bei größeren Temperaturen, wie es der Fall bei der Destillationskolonne ist, die im Temperaturintervall von 160°...60°C mit einem vertikalen Temperaturgradienten arbeitet, und im Falle des Eindringens von Sauerstoff kann eine Autooxydation des Äthylenglykols stattfinden und es können sich somit korrosive Verbindungen bilden, wie Oxal- und Ameisensäure. Diese Oxydation wird durch die Anwesenheit des Eisens, das die Rolle eines Katalysators spielt, begünstigt [1].

Auch das anwesende Wasser hat einen beträchtlichen Einfluß auf die Korrosionsgeschwindigkeit. So wachst auch bei anfänglich kleinen Prozenten von 1...2% und pH=4 die Korrosionsgeschwindigkeit sehr gegenüber dem reinen Äthylenglykol [2].

Was die Korrosion in Methanol anbelangt, gibt es zahlreiche Untersuchungen hinsichtlich dieser Erscheinung. So korrodiert Fe Annco in wäßrigen Methanollösungen, und es bilden sich $Fe(OH)_3$, Fe_2O_3, FeOOH. Aus diesen Grunde wird die Korrosion in solchen Lösungen eingeschränkt. In nichtwäßrigen Lösungen, also in reinem Methanol, ist die Korrosionsgeschwindigkeit weitens größer als in Lösungen, die verschiedene Wassermengen enthalten, da der Eisenoxyd- oder Eisenhydroxydfilm sich nicht bilden kann [4], [5]. Die Polarisierungskurven weisen auf die Bildung von instabilen Passivierungszonen hin, was zeigt, da die Oxyd-, bzw. Hydroxydfilme instabil und nichtadhärent sind [3]. Die Korrosionsgeschwindigkeit ist doppelt so groß als in reinem Wasser beim Fehlen von Sauerstoff [6].

In diesem Arbeit wird gezeigt die Korrosion von drei Kohlenstoffstählen in Lösungen mit hoher Reinigkeit von Äthylenglykol–Wasser, Äthylenglykol–Metha-

nol, Methanol–Wasser, sowie Rohäthylenglykol, das direkt von der industriellen Anlage übernommen wurde.

Obwohl in dem Rohäthylenglykol durch die IR-Spektren auch andere chemische Verbindungen aufgezeigt wurden, wie Mono- und Dikarbonsäuren, Äthylalkohol, Aldehyde und Ketone, wurde ihr Einfluß nicht weiter untersucht, da dies Gegenstand späterer Studien sein wird.

2. Experimenteller Teil

Unter Berüchsichtigung des vorher Gesagten, wurde also die Korrosion von den drei C-Stählen (OL 37, OLC 45, OLC 60) in Lösungen von Äthylenglykol in Wasser, Methanol in Wasser und Methanol in Äthylenglykol mit verschiedenen Konzentrationen untersucht. Die Zusammensetzung der der Korrosion ausgesetzten Stähle ist in Tabelle 1 wiedergegeben.

Tabelle 1

Die Zusammensetzung der Korrosion aus gesetzten Stähle

	C%	Mn%	S%	P%	Si%	Al%	Cr%	Ni%	Cu%	As%
OL 37	0,22	0,85	0,05	0,05	0,26	0,03	0,3	0,3	0,005	0,05
OLC 45	0,42	0,05	0,04	0,04	0,27	–	0,3	0,3	0,3	0,05
OLC 60	0,61	0,65	0,04	0,04	0,27	–	0,3	0,3	0,3	0,05

Die C-Stahlproben hatten die gleiche Oberfläche und bevor sie in die korrosive Lösung gegeben wurden, wurden sie geschliffen 10 Min. in 3%-iger Salzsäurelösung entfettet und 15 Min. in Benzen gekocht. Zur Zubereitung der korrosiven Lösungen wurde doppeltdestilliertes Wasser mit einer elektrischen Leitfähigkeit von 12 μs/cm, reines Äthylenglykol und Methanol (Merk) sowie Äthylenglykol aus der Destillierblaze verwendet.

Zur Untersuchung der Korrosion wurde die Methode des Gewichtsverlustes im Verhältnis zur Oberfläche gewählt, wofür die Proben alle zehn Tage aus der Lösung genommen, gewaschen und auf der Analysenwaage gewogen wurden. Die Proben wurden in Flaschen mit Schliffstopfen aufbewahrt und täglich geschüttelt, also mit Zutritt von Sauerstoff in das Korrosionsystem.

Aus den Gewichtsverlustkurven wurden die Penetrationskennzahlen P in mm/m^2 und die gravimetrische Kennzahl K in mg/dm^2 Tag berechnet.

Das Korrosionsverhalten der drei Stahltypen in den Äthylenglykollösungen ist bis zu einer Konzentration von 75% der Lösung gleich. Bis zu dieser Konzentration ist das Wasser das Hauptkorrosionsmedium, die Korrosionsverbindungen beeinhalten keinen Kohlenstoff und die chemische Analyse entspricht den Hydrateisenoxyd (Rost). Die Werte der beiden Kennzahlen sinken mit dem Anwachsen der Äthylenglykolkonzentration in der Lösung, also auch die Korrosionsgeschwindigkeit sinkt, was beweist, da in dieser Etappe die Korrosion sich durch den gelösten Sauerstoff abwickelt und dessen Löslichkeit mit dem Anwachsen der

Äthylenglykolkonzentration abnimmt. Ein zusätzlicher Beweis dieser Tatsache ist auch das Anwachsen des Verhältnisses Fe^{2+}/Fe^{3+} Korrosionsprodukt. In 100%-igem Äthylenglykol ist das Korrosionsprodukt von gelber Farbe, haftet an der Metalloberfläche, und die Korrosionskurve hat die form eines „S", was beweist, daß der Korrosionsmechanismus durch die Bildung eines lösbaren Komplexes abläuft [6]. Die Gewichts kennzahlen K fallen bei Anwachsen der Kohlenstoffkonzentration im Stahl. In den Tabellen 2 und 3 sind die Werte der Penetrations- und der gravimetrischen Kennzahlen fur die verschiedenen Änthylenglykol–Wasser-Lösungen dargestellt.

Tabelle 2

Der Penetrationskennzahlen für die verschiedenen Äthylenglykol/Wasser-Lösungen dargestellt

Äthylenglykol, [%]	OL 37	OLC 45	OLC 60
roh/p.a.	Kennzahl P		
25	0,134/0,119	0,059/0,029	0,035/0,032
50	0,077/0,067	0,024/0,021	0,014/0,012
75	0,025/0,015	0,013/0,011	0,009/0,006
100	0,025/0,015	0,007/0,005	0,005/0,003

Tabelle 3

Der Gravimetrischenkennzahlen die verschiedenen Äthylenglykol/Wasser-Lösungen dargestellt

Äthylenglykol, [%]	OL 37	OLC 45	OLC 60
roh/p.a.	Kennzahl K		
25	28,84/25,5	12,63/6,28	7,52/6,15
50	16,28/14,29	5,20/4,64	3,04/2,76
75	8,54/3,37	2,93/2,28	2,85/2,59
100	6,25/3,40	1,50/0,80	1,06/0,71

Was die Korrosion in Methanol betrifft, verläuft diese ebenfalls durch den gelössten Sauerstoff, wobei das Korrosionsprodukt ebenfalls Rost ist. Die Korrosionsgeschwindigkeit fällt mit dem Anwachsen der Methanolkonzentration. Die Werte der Kennzahlen P und K sind in den Tabellen 4 und 5 wiedergegeben.

Tabelle 4

Der Penetrationskennzahlen für die verschiedenen Methanol/Wasser-Lösungen dargestellt

Methanol	OL 37	OLC 45	OLC 60
%	Kennzahl P		
5	0,302	0,250	0,221
10	0,205	0,173	0,143
15	0,174	0,111	0,093
100	0,030	0,023	0,019

Tabelle 5

Der Gravimetrischenkennzahlen die verschiedenen Methanol/Wasser-Lösungen dargestellt

Methanol	OL 37	OLC 45	OLC 60
%	Kennzahl K		
5	50,11	44,63	40,03
10	43,92	35,37	32,84
15	30,24	24,18	20,44
100	6,33	4,30	2,17

Die Korrosion im wasserfreien Äthylenglykol–Methanol-System ist die niedrigste. Die Gewichtsverlustkurven haben den gleichen Verlauf wie die Kurven in reinem Äthylenglykol was beweist, daß das Korrosionsmittel Äthylenglykol mit Hilfe des Sauerstoffs aus der Luft ist. In Tabelle 6 sind die Werte der entsprechenden Kennzahlen P und K dargestellt.

Tabelle 6

Der Penetrationskennzahlen und Gravimetrischenkennzahlen für die verschiedenen Methanol/Äthylenglykol-Lösungen dargestellt

Methanol, [%], in	OL 37	OLC 45	OLC 60
Äthylenglykol	Kennzahl P/K		
5	0,303/3,58	0,287/3,03	0,243/2,47
10	0,224/2,73	0,19/2,03	0,157/1,56
15	0,173/2,12	0,148/1,58	0,101/0,98

Aus der Analyse der Korrosionsprodukte sowie der Lösungen nach der Entfernung der unlöslichen Korrosionsprodukte folgt, daß die elektrochemischen Reaktionen, die zur Korrosion des Eisens in Lösungen mit bis zu 75% Äthylenglykol führen sind die klassischen Korrosionsreaktion in Wasser mit Hilfe des Luftsauerstoffs. Im IR-Spektrum der Lösungen nach der Abscheidung des Wassers durch Vakuumverdampfung erscheint bei 475 nm eine Spitze, die auf die Anwesenheit von kovalenten und koordinativen Fe–O-Verbindungen hinweist [7]. Das Verhalten des Eisens in Äthylenglykol betrachtend [8], [9],

$$Fe^{3+} + 2C_2H_4(OH)_2 \longrightarrow [Fe(CH_2 - O)_4]H + 3H^+$$

ist diese Spitze augenscheinlich. Die Korrosion in Wasser, gerade infolge der Lösung eines Teils des Korrosionsproduktes (Oxyd oder Eisenhydroxyd), wodurch kein Schutzfilm entstehen kann. Was die Korrosion in reinem Äthylenglykol anbelangt, so läuft diese mit Hilfe des Luftsauerstoffs ab, mit Bildung von hexa- oder oktakoordinierten Komplexen. Die chemische Analyse des Korrosionsproduktes zeigt folgendes Ergebnis: Fe=24%; C=26,5%; O_2=44,5%; H_2=5%. Die chemischen Reaktionen sind die folgende:

$$2Fe + O_2 + 4C_2H_6O_2 \longrightarrow [Fe(OH)_2(C_2H_5 - O_2)_4]H_2$$
$$2Fe + O_2 + 6C_2H_6O_2 \longrightarrow [Fe(OH)_2(C_2H_5 - O_2)_6]H_4$$

Die Existenz dieses Verbindungen zeigen auch die IR-Spektren der Lösungen durch die Annwesenheit eines Absorptionsbandes bei 2950 nm, was spezifisch ist für Chelate mit sechs Atomen im Zyklus.

3. Schlußfolgerungen

1°Alle drei Stahltypen korrodieren in den untersuchten Systemen.

2°Das Rohäthylenglykol ist stärker korrodierend als das Äthylenglykol p.a., was beweist, daß es nach andere Korrosionsmittel enthält.

3°Die Korrosion vermindert sich bei Anwachsen der Konzentration von Kohlenstoff des entsprechenden Stahls.

4°Der Korrosionsmechanismus in reinem Äthylenglykol findet unter Bildung eines lösbaren Komplexes, jedoch mit verkleinerter Lösbarkeit, statt.

Eingegangen am 16. März 1994

Technische Universität „Gh.Asachi", Jassy,
Lehrstuhl für Anorganische Chemie
und
Lehrstuhl für Anorganische
Chemische Technologie

LITERATURVERZEICHNIS

1. Thomson P.F., Corrosion, **13**, 531-535 (1957).
2. Lloyd E.G., Ind. Eng. Chem., **46**, 2411-2416 (1954).
3. Belucci F., Corros. Sci., **28**, 371-384 (1988).
4. Caprobianco G., Br. Corros., **25**, 133-137 (1990).
5. Bona J., Metall. Odlow, **16**, 73-83 (1990).
6. Belucci F., Corros. Sci., **27**, 1313-1321 (1987).
7. Pisčik L.M., Zasch. Mat., **22**, 341-342 (1986).
8. Muller D., Arzeimittel. Forsch., **17**, 924-926 (1967).
9. Ivăşcan Şt., *Coroziune şi protecţie anticorozivă*. Inst. polit., Iaşi, 1975.

COROZIUNEA OŢELULUI NEALIAT ÎN SISTEMUL ETILENGLICOL–METANOL–APĂ

(Rezumat)

S-a studiat comportarea a trei tipuri de oţeluri nealiate (OL 37, OLC 45, OLC 60) în soluţii de diverse concentraţii de etilenglicol în apă, metanol în apă şi metanol în etilenglicol. S-au calculat indicii de penetrare şi gravimetrici, s-a propus un mecanism de coroziune şi s-a stabilit că valoarea vitezei de coroziune scade odată cu creşterea concentraţiei în carbon a oţelului respectiv.

BULETINUL INSTITUTULUI POLITEHNIC DIN IAŞI
Tomul XLI (XLV), Fasc. 1–4, 1995
Secţia II
CHIMIE ŞI INGINERIE CHIMICĂ

C.D. 547.29; 542.4

OBSERVATIONS SUR LA DESTRUCTION THERMIQUE DE QUELQUES ACIDES CARBOXYLIQUES

PAR
SAVEL IFRIM et ELENA MIHAI

1. Introduction

Le comportement à la destruction thermique des composés organiques ayant de simples molécules ou bien des structures macromoléculaires, peut être étudié d'une façon satisfaisante par l'utilisation de la méthode thermogravimétrique. Les thermogrammes qui sont enregistrées automatiquement donnent des indications valeureuses sur la stabilité thermique des produits soumis à la destruction, sur la cinétique du processus, aussi bien que sur les phases de la thermodégradation du chaque produit analysé.

On connaît dans la littérature plusieurs études effectuées sur les composés macromoléculaires, en appliquant la méthode thermogravimétrique [1],...,[3]. En utilisant cette méthode, dans quelques recherches antérieures nous avons étudié le comportement à la destruction thermique de certaines fibres protéiques [4], de la fibre de laine traitée dans un alcalin medium [5], de quelques fibres synthétiques par rapport à la fibre de laine [6] et également nous avons effectué des investigations concernant la pointe et la base de la fibre de laine [7].

La méthode thermogravimétrique est également utile pour étudier le comportement à la destruction thermique de plusieurs substances organiques, avec des structures chimiques simples ou ayant un plus grand nombre de groupes fonctionnels, ainsi que les thio-aminoacides [8].

En continuant l'utilisation de la même méthode d'investigation, dans ce qui suit on poursuit le comportement à la destruction thermique de quelques substances organiques, ayant un seul ou deux groupes fonctionnels identiques, comme sont les groupes carboxyliques.

2. Partie expérimentale

On a élu, afin de les étudier, cinq acides organiques, ayant dans leur structure chimique un ou deux groupes carboxyliques à savoir: l'acide benzoïque, l'acide phényl-acétique, et les trois izomères de l'acide benzen-dicarboxylique, c'est-à-dire les acides phtalique, isophtalique et téréphtalique.

Les thermogrammes obtenues pour chaque acide carboxylique ont été enregistrées à l'aide d'un dérivatographe de type Paulik-Erdey M.O.M. – Budapest. Afin d'obtenir des résultats comparables on a soumis à la destruction thermique des échantillons de substances pesant 0,018 g chacun et on a travaillé avec une vitesse

de chauffage de 12°C/min.; pour tous les cas on a utilisé la même sensibilité de 1/15, pour les courbes DTG.

Les thermogrammes obtenues sont représentées dans les Figs.1,...,5.

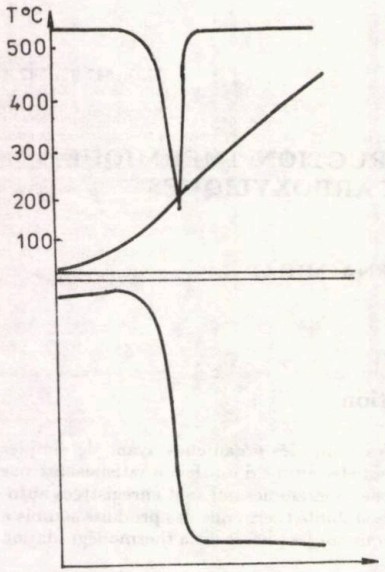

Fig. 1.– Dérivatogramme de l'acide benzoïque.

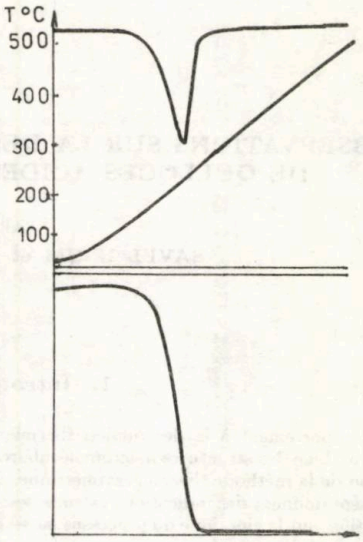

Fig. 2.– Dérivatogramme de l'acide phényl-acétique.

A l'aide des thermogrammes obtenues on a calculé les limites de température du processus, la température initiale du commencement de la décomposition du produit, l'ordre de réaction et l'énergie d'activation. Tous ces données sont indiquées dans le Tableau 1.

L'énergie d'activation a été calculée avec la méthode de F r e e m a n - C a r o l l [9].

Afin d'apprécier le processus cinétique de la décomposition thermique des produits analysés on a calculé les pertes de poids aux différentes températures et dans ce but on a utilisé les courbes TG. Les données obtenues sont enregistrées dans le Tableau 2 et elles peuvent être utilisées pour comparer le comportement à la destruction thermique des acides organiques analysés.

On a introduit dans le Tableau 2, également, les points de fusion pour chaque produit, afin de trouver une relation entre ces caractéristiques et le processus de décomposition thermique. Par T_M, se trouvant de même dans le Tableau 2, on a indiqué la température, en °C, qui correspond à la vitesse maxima de dégradation, calculée à l'aide de la courbe DTG.

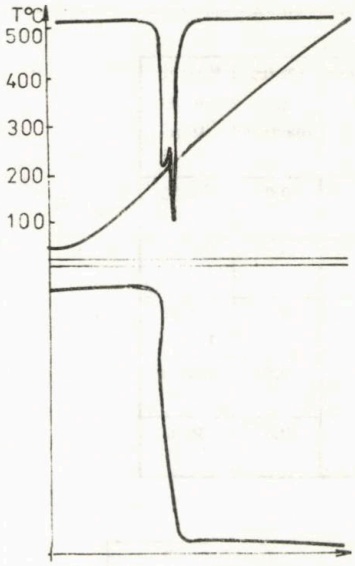

Fig. 3.– Dérivatogramme de l'acide phtalique.

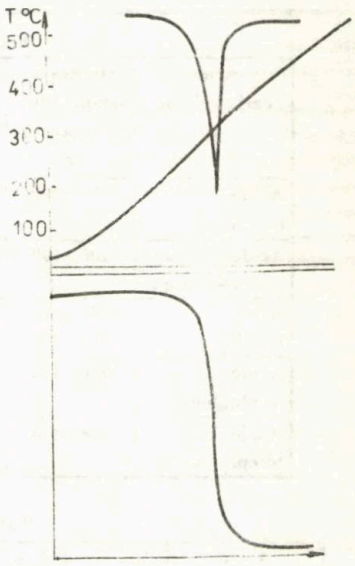

Fig. 4.– Dérivatogramme de l'acide isophtalique.

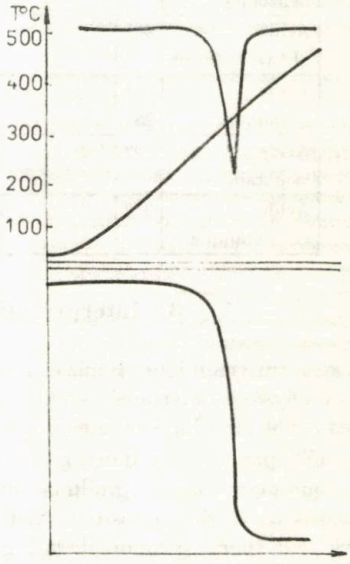

Fig. 5.– Dérivatogramme de l'acide téréphtalique.

Tableau 1

Acide carboxylique	Limites de température du processus °C	Température initiale °C	Ordre de réaction	Energie d'activation
Acide benzoïque	98...384	98	0,6	19,80
Acide phényl-acétique	105...400	105	0,5	20,20
Acide phtalique	143...210 210...470	143 210	0 2	31,57 165,46
Acide isophtalique	200...425	200	0,8	33,90
Acide téréphtalique	208...425	208	0,5	38,22

Tableau 2

Acide carboxylique	T_M °C	Pertes de poids, [%]				Résidu	P.T.
		100°C	200°C	300°C	400°C		
Acide benzoïque	202	0	87,22	99,43	100	0	121
Acide phényl-acétique	231	0	22,11	97,20	100	0	76
Acide phtalique	198 266	0	22,22	97,33	98,2	0	208
Acide isophtalique	308	0	5,55	38,88	99,9	0	345
Acide téréphtalique	342	0	5,55	8,89	99,9	0	très haut

3. Interprétation des résultats

La structure chimique simple et relativement semblable des cinq acides carboxyliques analysés a déterminé, selon ce qu'était à prevoir, l'apparition des thermogrammes ayant les allures de même semblables.

En effet, par un coup d'oeil général des thermogrammes enregistrées on peut observer que pour tous les produits analysés il apparaît une seule étape pendant le processus de la décomposition thermique. Cependant, une observation plus attentive de la thermogramme de la Fig.3, obtenue pour l'acide phtalique, conduit à la conclusion selon laquelle dans le cas de ce produit l'étape de la décomposition thermique renferme deux degrés. L'apparition des ces degrés est parfaitement explicable, compte tenu que les deux groupes carboxyliques, se trouvant dans la position *ortho*, par chauffage, ils donnent la possibilité de l'élimination de l'eau

et l'acide phtalique se transforme tout d'abord dans l'anhydride phtalique. On connaît que l'acide phtalique fond approximativement à 208°C, sans que ce point de fusion soit précis, puisque l'élimination de l'eau et la transformation de l'acide en anhydride commence avant la fusion [10]. Ce comportement de l'acide phtalique est totalement reflété dans la thermogramme de la Fig.3.

Si on analyse les données du Tableau 1 on observe que le premier degré de la décomposition de l'acide phtalique commence à 143°C, donc avant la fusion et il s'élargit jusqu'à 210°C, température à laquelle le produit initial doit être fondu. Donc il apparait une parfaite concordance concernant les propriétés de ce produit et sa thermogramme. Le deuxième degré du processus de la décomposition thermique de l'acide phtalique commence tout-de-suite, à partir de 210°C et il continue jusqu'à 470°C.

Si on observe les limites de température du processus de décomposition thermique il résulte que pour chaque produit ces limites sont beaucoup distancées l'une par rapport à l'autre, avec plus que 200°C; pratiquement ces intervalles sont situés entre 216°et 295°C.

Ainsi qu'il résulte par l'observation des températures initiales de la décomposition, la plus petite thermostabilité correspond à l'acide benzoïque et elle augmente un peu pour l'acide phényl-acétique, ensuite pour l'acide phtalique, l'acide isophtalique et la plus élevée est celle de l'acide téréphtalique. Entre les deux derniers isomères la différence n'est pas très grande; mais si on considère que pour l'acide phtalique le premier degré consiste seulement dans l'élimination de l'eau, ainsi qu'il est naturel, entre tous les trois isomères de l'acide benzen dicarboxylique il n'apparaît pas une grande différence entre les températures initiales du processus de thermodégradation. Ce rapprochement est explicable, compte tenu que l'énergie des liaisons C–C entre les groupes carboxyliques et les atomes de carbone des noyaux aromatiques est toujours la même.

En observant également les paramètres cinétiques, c'est-à-dire l'ordre de réaction et l'énergie d'activation, se trouvant aussi dans le Tableau 1, il en résulte le même ordre de la stabilité thermique, en concordance avec les indications de la température initiale de dégradation. En effet, la plus petite énergie d'activation a résulté pour l'acide benzoïque, suivie par celle de l'acide phényl-acétique, pourtant la plus grande correspond à l'acide téréphtalique. Il est bien connu le fait que au fur et à mesure que l'énergie d'activation d'un processus de décomposition thermique est plus petite, tant le produit est moins stable.

Les valeurs fractionnaires de l'ordre de réaction sont en concordance avec l'apparition d'un mécanisme complexe de la thermodégradation, influencé par des phénomènes physiques, comme la diffusion des produits de la réaction, sans doute gazeux, qui s'éliminent sous l'action de la chaleur.

Les données du Tableau 2 suggèrent une image générale du processus cinétique de la décomposition thermique. En utilisant les données de ce tableau, la première observation évidente est la suivante: jusqu'à la température de 100°C la décomposition ne commence pour aucun produit analysé; d'ailleurs tous ces acides organiques, exceptant l'acide phényl-acétique, fondent au-dessus de 100°ou 200°C.

Les pertes de poids (en %) pour l'intervalle de 100°...200°C sont plus élevées aussi pour l'acide benzoïque, suivi par l'acide phényl-acétique et ensuite par l'acide phtalique. Dans le cas de ce dernier tout d'abord il y a la perte de l'eau résultant l'anhydride phtalique et la décomposition proprement dite commence au-dessus de 210°C. Les pertes de poids (en %) les plus petites sont mises en évidence dans le cas de l'acide téréphtalique et du celui isophtalique. Cette conclusion est en parfaite concordance avec les interprétations proposées plus haut, par l'analyse des données du Tableau 1.

De même, pour la température de 300°C, le plus élevé pourcentage des pertes apparait toujours pour l'acide benzoïque et le plus bas pour l'acide téréphtalique et ensuite pour l'acide isophtalique.

Parmi les trois isomères de l'acide benzen dicarboxylique, d'une façon plus facile se décompose l'acide phtalique et plus difficile l'acide téréphtalique. Probablement, pour l'acide téréphtalique les molécules sont associées par liaisons hydrogène dans un degré très élevé, ce qui explique également sa fusion à une température élevée. Cet aspect présente une importance particulière pour l'acide téréphtalique, puisque celui-ci est utilisé en grande quantité pour obtenir les fibres de polyestère et des téréphtalates, produits auxquels il est capable de transmettre la même thermostabilité.

La valeur de la température qui correspond à la vitesse maxima de dégradation, se trouvant aussi dans le Tableau 2, démontre que le plus petit maximum apparaît, également, pour l'acide benzoïque, tandis que le plus grand – pour l'acide téréphtalique; donc, à son tour ce paramètre prouve le même ordre de la thermodégradation des acides analysés.

On observe aussi que pour tous les produits le residu est nul; ce résultat prouve une très bonne pureté des produits analysés et leur totale dégradation thermique, dans les conditions des expériences effectuées.

4. Conclusions

On étudie la dégradation thermique de quelques acides carboxyliques, ayant des noyaux aromatiques dans leurs structures chimiques; il s'agit des acides: benzoïque, phényl-acétique, phtalique, isophtalique et téréphtalique. Pour tous ces composés on présente les thermogrammes enregistrées à l'aide d'un dérivatographe du type Paulik-Erdey M.O.M. – Budapest.

En utilisant les courbes dérivatographiques, les données obtenues par calcul prouvent que, pour tous les produits analysés, on observe une seule étape pendant le processus de la décomposition thermique; il y a une exception, pour l'acide phtalique, pour qui l'étape de décomposition comprend deux degrés. Il y a une parfaite concordance entre les degrés de la thermodégradation, la structure chimique et les propriétés de l'acide phtalique.

Toutes les données obtenues prouvent, sans doute, que le plus facile est décomposé l'acide benzoïque, ensuite l'acide phényl-acétique et le plus thermostable est

l'acide téréphtalique. La résistance à la thermodégradation de ce produit présente une évidente importance pratique.

Parmi les trois isomères de l'acide benzen dicarboxylique, le plus facile se décompose l'acide phtalique, sa thermodégradation en commençant au-dessus de 200°C.

Reçue le 4 mars 1994

Université Technique „Gh. Asachi", Jassy,
Chaire de Chimie Générale

BIBLIOGRAPHIE

1. Schwenker R.F., Dusenbury J.H., Text. Res. J., **30**, *10*, 800 (1960).
2. Schwenker R.F., Beck L.R., Text. Res. J., **30**, *8*, 624 (1960).
3. Simionescu Cr., Corlăţeanu El., Ind. Textilă, **21**, *12*, 761 (1970).
4. Ifrim S., Mihai El., Bul. Inst. polit., Iaşi, **XVIII (XXII)**, *1-4*, s. VII, 41 (1972).
5. Ifrim S., Mihai El., Bul. Inst. polit., Iaşi, **XVI (XX)**, *3-4*, s. VI, 13 (1970).
6. Ifrim S., Mihai El., Bul. Inst. polit., Iaşi, **XXII (XXVI)**, *1-4*, s. VII, 37 (1976).
7. Ifrim S., Mihai El., Bul. Inst. polit., Iaşi, **XXIV (XXVIII)**, *1-4*, s. VII, 3 (1978).
8. Ifrim S., Mihai El., Bul. Inst. polit., Iaşi, **XXV (XXIX)**, *1-4*, s. VII, 29 (1979).
9. Freeman E.S., Caroll B., J. Phys. Chem., **62**, 394 (1965).
10. Nenitescu C.D., *Chimie Organică*. Vol.**I**, ed. a VII-a, EDP, Bucureşti, 1974, 769.

OBSERVAŢII ASUPRA DESTRUCŢIEI TERMICE A UNOR ACIZI CARBOXILICI

(Rezumat)

Se întreprinde un studiu al comportării la destrucţia termică a unor acizi carboxilici, care au nuclee aromatice în structura lor moleculară. S-au supus cercetării următorii acizi carboxilici: acidul benzoic, acidul fenil-acetic şi cei trei izomeri ai acidului benzen *orto*-dicarboxilic, respectiv acizii ftalic, izoftalic şi tereftalic. Se prezintă derivatogramele obţinute pentru aceşti compuşi, înregistrate cu ajutorul unui derivatograf de tip Paulik-Erdey M.O.M. – Budapesta.

Datele obţinute prin calcul, folosind aceste derivatograme, arată că pentru toţi produşii analizaţi apare o singură etapă în procesul descompunerii termice; pentru acidul ftalic această etapă cuprinde două trepte. Se pune în evidenţă o deplină concordanţă între treptele termodegradării, structura chimică şi proprietăţile acidului ftalic.

Din datele obţinute mai rezultă că cel mai uşor se descompune acidul benzoic, urmat de acidul fenil-acetic, iar cel mai termostabil este acidul tereftalic. Rezistenţa la termodegradare a acidului tereftalic prezintă importanţă practică, ţinând seamă de utilizările tehnice ale acestui produs. Dintre cei trei izomeri ai acidului dicarboxilic, mai termolabil este acidul ftalic.

BULETINUL INSTITUTULUI POLITEHNIC DIN IAŞI
Tomul XLI (XLV), Fasc. 1–4, 1995
Secţia II
CHIMIE ŞI INGINERIE CHIMICĂ

D.C. 66.013.5

MASS TRANSFER IN THIN LIQUID FILMS
III. INFLUENCE OF THE VERTICAL WIRY PROMOTERS OF TURBULENCE ON THE TRANSFER RATE

BY
I. MĂMĂLIGĂ,
RADU Z. TUDOSE
Corresponding Member of the Romanian Academy
and
ECATERINA MERICĂ

1. Introduction

Increasing the rate of transport phenomena is one of the most important research problems. This problem is to be solved by a rational selection of the hydrodynamical conditions, which significantly influence the mass transfer. The creation of certain hydrodynamical conditions which improve the transport can be achieved by introducing an external energy in the fluid, by means of mobile devices (stirrers), or developing inside of fluid an aditional local turbulence, generated by fixed devices-static promoters, with a lower consumption of energy [1]. The gas–liquid, vapour–liquid and liquid–liquid contact is very often used in the mass transfer operations. In most of the cases one of the phases is divided into smaler volumes to increase the interfacial area and the relative rate between the phases, the large values for this variable increasing the transfer rate. These effects can be achieved by flow of the phases in thin films over solid surfaces of different forms. The intensity of transport phenomena that take place in waves or turbulent films is much greater than in flat ones. This is why the intensification methods of transfer operation in films seek to create an advanced turbulence of the liquid film.

There is a relatively small number of studies concerning the increasing the rate of mass transfer processes by using the turbulence promoters in equipments with descending films [2],...,[5]. It was shown [2] that, for the slow soluble gases, the main resistance to the mass transfer is located mainly in the liquid phase and the turbulence increase of the liquid phase results in an important increasing of the mass transfer coefficient. Studies concerning the mass transfer in liquid films that flow on vertical surface, made of different materials [6], evidenced the rate of transport phenomena to be higher for steel than for plastic and cooper pipes. The rate of processes has been increased by cutting grooves perpendicularly to the axis of a steel pipe with a constant width (3 mm) and variable depths (0.47...1.03 mm) and distances (10...400 mm) between the grooves [5]. The experimental studies of D a v i e s and W a r n e r [2] of mass transfer to a film of liquid flowing down a surface with regular roughness, obtained by making a cut perpendicular to the direction of motion, indicate a considerable increase of the value of mass transfer coefficient over those of smooth units under the same process conditions. Such roughness can increase the mass transfer rate up to 3.5 times.

M a k a r o v's researches [4] on the O_2-absorption in water films flowing on flat surfaces or with roughness as a wery spiral at $\Re e$ numbers within 1,600...50,000 range, showed that mass transfer rate goes up faster for rough surfaces. The highest transfer increase was observed for wire diameter between 1.5 and 2.0 mm. The following relation has been derived calculating the dimensionless mass transfer coefficient:

$$Sh = B\Re e^m Sc^{0.5},$$

where B and m are tabulated variables [4].

As previously shown [2] the formation of the surface through the spiral winding of a metal wire determined higher mass transfer coefficient than in the case of smooth surfaces. The maximum increase was obtained when the distance between spirals is equal to wave length.

The purpose of this paper is to show the influence of another type of roughness, which has not been encountered in literature up to now, on the increase of mass transfer rate for pure carbon dioxide absorption in thin distilled water films. It is a matter about longitudinal roughness, disposed evenly, obtained by application on the flow surface metallic wires of 0.4 mm diameter, with a distance of 4.18, 8.35 and 12.5 mm between them.

2. Experimental Part

The absorption of carbon dioxide in water was investigated using the equipment depicted in Fig.1. The absorption column is formed of two concentric pipes. The descending film flows on the external wall of the internal pipe (Ni-Cr alloy steel, length – 2,100 mm, external diameter – 32 mm). In the annular space between the external pipe (polymethyl methacrylate, internal diameter – 60 mm) and the liquid film the carbon dioxide flows against the current. At the top the column

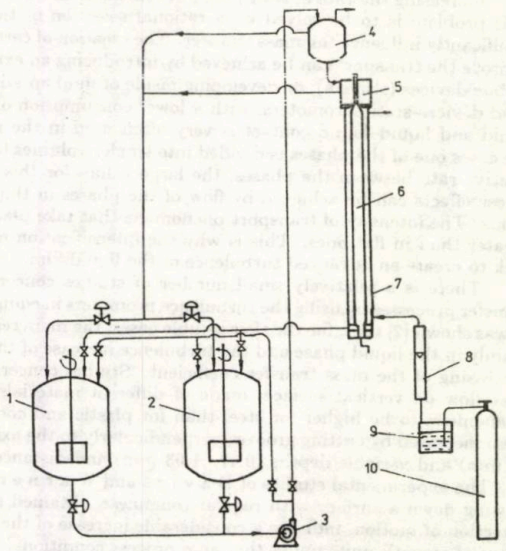

Fig. 1.– Sketch of experimental apparatus: *1, 2* – tanks; *3* – pump; *4* – level vessel; *5* – distribution head; *6* – absorption column; *7* – external tube; *8* – flowmeter; *9* – vessel for CO_2 saturation with water vaporous; *10* – gas tube.

is provided with a distribution head which ensures the formation of a thin film on the internal tube. The liquid is pumped from the supply tank to the level vessel and enters the distribution head of the column. The two tanks work alternatively; while one receives the liquid, from the other the column is fed. The carbon dioxide is fed against the current from a gas tube and its flowrate was adjusted by means of two flowmeters, one for a coarse adjustment, the other for a fine one.

To prevent the diffusion of water in gas the latter was saturated by bubbling it in water (vessel) prior to the admission in the column. The liquid flowrate at the exit was measured by counting the time required for collecting a known volume of liquid. The steel wires used as turbulence promotors were fixed at the ends of the absorption column. The analysis of carbon dioxide in liquid phase has been made by precipitating it as barium carbonate using a mixture of barium chloride and standard natrium hydroxide. The excess natrium hydroxide was then titrated with chloride acid to a phenolphtaleine end point.

Prior to each set of measurements a reference sample was taken, to determine the initial content of carbon dioxide in water. The liquid phase mass transfer coefficient based on mean logarithmic driving force has been calculated for the absorption of pure gas at a pressure of 1 atm. In practical calculations the external surface of the internal pipe was assumed to be the mass transfer surface. Given the high purity of gas the resistance of gaseous phase has been neglected as well as the effect of counter-diffusion, since the gas was previously saturated with liquid. Experimental measurements were taken at temperatures between 20° and 25°C and $\Re e$=500...5,000.

3. Results and Discussion

To elucidate the manner in which the presence of longitudinal roughness influences the mass transfer rate at CO_2 absorption in water thin films a comparative study, in the same conditions of operation, but on the pipes, has been accomplished. It has been obtained, in these conditions, for the dimensionless mass transfer coefficient ($\mathcal{S}h$ number), the following equation:

$$\mathcal{S}h = 1.424 \times 10^{-3} \Re e^{0.593} \mathcal{S}c^{0.5}. \tag{1}$$

The coefficient of determination was $r = 0.9894$ and $\Re e \in [500; 5,000]$. The $\mathcal{S}h$ number values calculated with this equation, compared with literature ones [4], [7], are in a good agreement. Then, the determination in presence of turbulence promoters, has been made. Parallel steel filaments were used of 0.4 mm diameter, disposed longitudinally, at 4.18, 8.35 and 12.5 mm distance between them.

The experimental results obtained with all distances between filaments, plotted as $\mathcal{S}h$ vs. $\Re e$ curves, in logarithmic coordinates, are depicted in Figs.2,...,5. The solid line shows the dependence of $\mathcal{S}h$ number vs. $\Re e$ one for mass transfer on the flat tube. Experimental data processing for three distances between filaments allowed the relationships, between $\mathcal{S}h$, $\Re e$ and $\mathcal{S}c$ numbers, to be setted, presented in Table 1.

The ratio $\mathcal{S}h/\mathcal{S}c^{0.5}$ vs. $\Re e$, obtained with flat and rough tubes, are plotted in logarithmic coordinates, in Fig.5. It can be seen that for the distance between filaments $e = 4.18$ mm an inflexion point has been obtained, for $\Re e = 2,500$. For this point a value of the film thickness of 0.32 mm is found. The film diameter to thickness ratio has been of 1.25. It can be seen that over the value of this ratio,

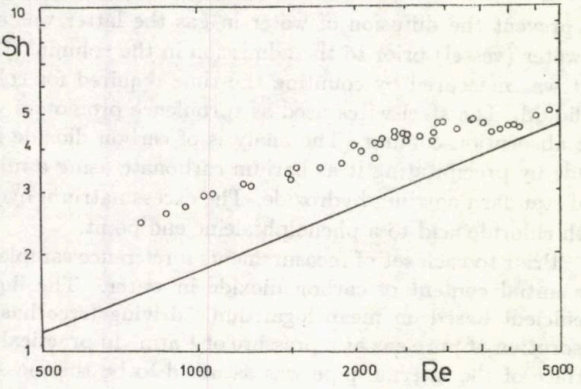

Fig. 2.– Results of experimental investigations for $e = 4.18$ mm.

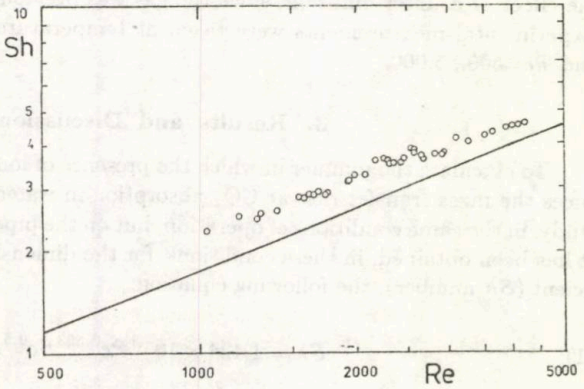

Fig. 3.– Results of experimental investigations for $e = 8.35$ mm.

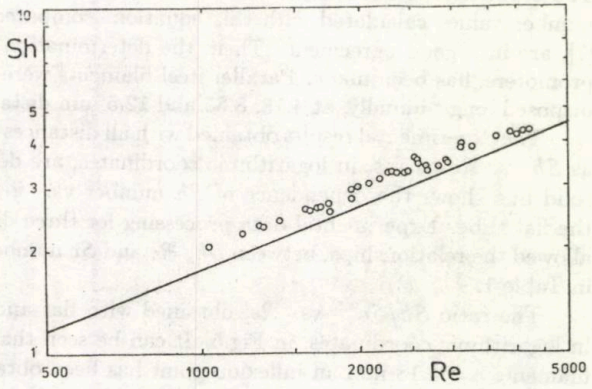

Fig. 4.– Results of experimental investigations for $e = 12.5$ mm.

at the distance between filaments $e = 4.18$ mm, the dependence between Sh, Re

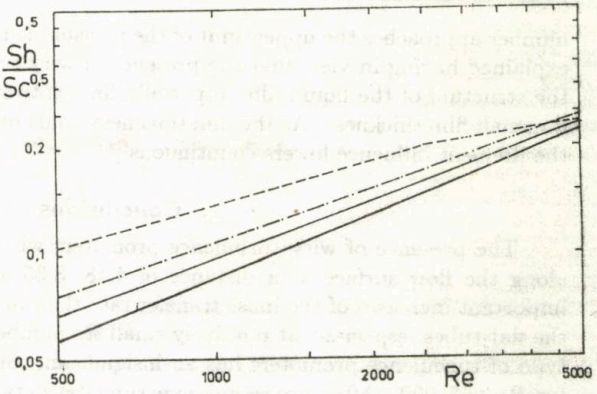

Fig. 5.– Correlation $\mathcal{S}h/\mathcal{S}c^{0.5}$ vs. $\Re e$ for three distances between filaments: — eq. (1); — eq. (2); – · – · – eq. (3); - - - eqs. (4) and (5).

Table 1

No.	Relationship	e, [mm]	Range	r, [%]
1	$\mathcal{S}h = 1.424 \times 10^{-3}\Re e^{0.593}\mathcal{S}c^{0.5}$		$500 < \Re e < 5,000$	99
2	$\mathcal{S}h = 2.3 \times 10^{-3}\Re e^{0.542}\mathcal{S}c^{0.5}$	12.5	$500 < \Re e < 5,000$	98.7
3	$\mathcal{S}h = 3.3 \times 10^{-3}\Re e^{0.5066}\mathcal{S}c^{0.5}$	8.35	$500 < \Re e < 5,000$	97.2
4	$\mathcal{S}h = 8.5 \times 10^{-3}\Re e^{0.4039}\mathcal{S}c^{0.5}$	4.18	$500 < \Re e < 2,500$	97.9
5	$\mathcal{S}h = 3.8 \times 10^{-2}\Re e^{0.2146}\mathcal{S}c^{0.5}$	4.18	$2,500 < \Re e < 5,000$	87.4

and $\mathcal{S}c$ numbers approaches the line obtained for mass transfer on the flat tube. The enhancement of mass transfer rate, I, defined as the ratio between $\mathcal{S}h$ number obtained at mass transfer in the presence of filaments and $\mathcal{S}h$ number obtained at mass transfer on the flat tube, is depicted in Fig.6. One can see that for a distance of 12.5 mm between the filaments there is the lowest increase of mass transfer rate,

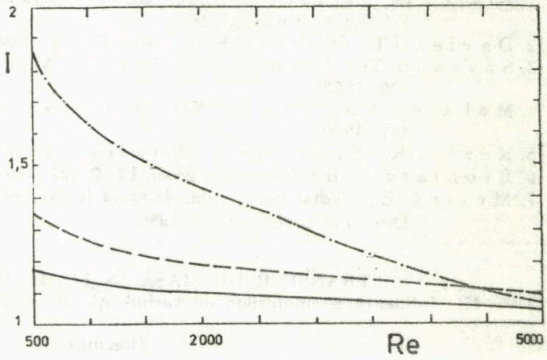

Fig. 6.– Enhancement mass transfer rate vs. $\Re e$: —— $e = 12.5$ mm; - - - $e = 8.35$ mm; – · – · – $e = 4.18$ mm.

from 18% for $\Re e = 500$ to 5% for $\Re e = 5,000$. For a distance of 8.35 mm the increase of mass transfer ranges between 35% and 10% and for 4.18 mm distance the highest increase is obtained, that is between 84% for $\Re e = 500$ and about 7% at $\Re e = 5,000$. The enhancement of mass transfer rate tends towards 1 if the $\Re e$

number approaches the upper limit of the measurement range (5,000). That can be explained having in view that the presence of wiry turbulence promoters modifies the structure of the liquid film, especially for relatively small $\Re e$ numbers, that is for small film thickness. As the film thickness tends towards the filaments diameter the filament influence lowers countinuously.

4. Conclusions

The presence of wiry turbulence promoters with 0.4 mm diameter, disposed along the flow surface at a distance of 4.18, 8.35 and 12.5 mm, leads to more important increases of the mass transfer rate than in the case on mass transfer on the flat tubes, especially at relatively small $\Re e$ numbers ($500 < \Re e < 2,500$). This type of turbulence promoters has an insignificant influence on mass transfer rate for $\Re e > 5,000$. After processing experimental data, obtained with and without turbulence promoters, it has been obtained relationships for the dimensionless mass transfer coefficient and it was shown the intensification of mass transfer rate.

Notations

$\Re e = 4\Gamma/\eta$ – R e y n o l d s number for gravity flow of liquids;
Γ – irrigation rate, [kg $m^{-1}s^{-1}$]; η – dynamic viscosity, [kg $m^{-1}s^{-1}$];
$Sh = k_L \nu_z / D_A$ – S h e r w o o d number; k_L – mass transfer coefficient, [m h^{-1}];
$\nu_z = [\eta^2/(\rho^2 g)]^{0.333}$ – equivalent linear dimension, [m];
D_A – kinematic diffusivity, [m^2h^{-1}]; ρ – liquid density, [kg m^{-3}];
g – gravity, [m s^{-2}]; $Sc = \eta/(\rho D_A)$ – S c h m i d t number;
e – distance between filaments, [mm].

Received, September 27, 1994

Technical University "Gh. Asachi", Jassy, Department of Chemical Engineering

REFERENCES

1. F l o r e a O., J i n e s c u Gh.I., *Intensive Processes in Transfer Operations* (in Romanian). Ed. Tehn., Bucureşti, 1975.
2. D a v i e s J.T., W a r n e r K.V., Chem. Eng. Sci., **24**, 231 (1969).
3. S ă v e a n u Th., I b ă n e s c u I., V a s i l i u M., Bul. Inst. polit., Iaşi, **VIII (XII)**, *3-4*, 129 (1962).
4. M a k a r o v V.A., V o i n o v N.A., N i k o l a e v N.A., Theor. Osn. Khim. Tech., **24**, *4*, 442 (1990).
5. K o z i o l K., B r o n i a r z L., N o w i c k a T., Int. Chem. Eng., **20**, *1*, 136 (1980).
6. B r o n i a r z L., Inz. Chemicz. i proc., **12**, *2*, 227 (1991).
7. M e r i c ă E., *Studiul transferului de masă la curgerea suspensiilor în filme subţiri*. Ph. D. Diss., Polyt. Inst., Jassy, 1986.

TRANSFER DE MASĂ ÎN FILME LICHIDE SUBŢIRI

III. Influenţa promotorilor de turbulenţă filamentari asupra vitezei de transfer

(Rezumat)

Se prezintă rezultatele unui studiu experimental privind influenţa promotorilor de turbulenţă filamentari cu diametrul de 0,4 mm, dispuşi paralel de-a lungul suprafeţei de curgere, la distanţe de 12,5, 8,35 şi 4,18 mm, asupra vitezei de transfer de masă, la absorbţia dioxidului de carbon în filme subţiri de apă distilată, la temperaturi cuprinse între 20° şi 25°C şi numere R e y n o l d s cuprinse între 500 şi 5 000. S-au obţinut intensificări ale transferului cuprinse între 7% şi 84% faţă de cazul în care transferul are loc pe o suprafaţă netedă.

BULETINUL INSTITUTULUI POLITEHNIC DIN IAŞI
Tomul XLI (XLV), Fasc. 1–4, 1995
Secţia II
CHIMIE ŞI INGINERIE CHIMICĂ

D.C. 577.1

MODELLING AND SIMULATION OF ANTIBODY–ANTIGEN BIOSENSORS

BY
OCTAVIAN PETRUŞ and ILIE SIMINICEANU

1. The Mathematical Modelling

The antibody–antigen biosensor may be regarded as a heterogeneous biochemical micro-reactor. The antigen (A) is dissolved in solution and the antibody (B) is immobilized on a side wall of the cell. As a result of the introduction of the solution containing A into the cell, at the time $\tau = 0$, the reaction proceeding at the interface develops a concentration gradient of A. Consequently, A diffuses to the wall until equilibrium results. Let write the reversible chemical reaction by the stoichiometric equation:

$$A + B \underset{k_2}{\overset{k_1}{\rightleftharpoons}} P,$$

whose rate can be described by the kinetic equation:

$$R_A = k_1 C_A C_B - k_2 C_P,$$

where the concentrations of the components, C_A, C_B and C_P, are functions of time (τ) and the space coordinate (X).

The reaction being very fast, the mass transfer of A may be considered the rate determining step. The mass transfer, by an unsteady-state diffusion mechanism, is described by the F i c k's second law:

$$\frac{\partial C_A(X,\tau)}{\partial \tau} = D_A \frac{\partial^2 C_A(X,\tau)}{\partial X^2}, \tag{1}$$

whose solution should satisfy the initial condition:

$$C_A(X,0) = C_A^0 \tag{2}$$

and the boundary conditions:

$$(3)\quad \frac{\partial C_A(0,\tau)}{\partial X}=0,\quad (4)\quad -D_A\frac{\partial C_A(d,\tau)}{\partial X}=k_1C_A(d,\tau)[C_B^0-C_P(\tau)]-k_2C_P(\tau),$$

together with the balance equation:

$$(5)\qquad \int_0^d C_A(X,\tau)\mathrm{d}X+C_P(\tau)=C_A^0d.$$

By substitution of the new independent non-dimensional variables:

$$(6)\qquad x=\frac{X}{d},\quad t=\frac{D_A\tau}{d^2}$$

and scaling the dependent variables:

$$(7)\qquad c_A(x,t)=\frac{C_A(X,\tau)}{C_A^0},\quad c_P(t)=\frac{C_P(\tau)}{C_P^0},$$

the equation (1) becomes:

$$(8)\qquad \frac{\partial c_A}{\partial t}=\frac{\partial^2 c_A}{\partial x^2},$$

with the initial condition:

$$(9)\qquad c_A(x,0)=1$$

and the boundary conditions:

$$(10)\quad \frac{\partial c_A}{\partial x}=0,\qquad (11)\quad -\frac{\partial c_A(1,t)}{\partial x}=\frac{Em}{1+L}\{c_A(1,t)[(1-c_P(t)]-Lc_P(t)\}$$

together with:

$$(12)\qquad mc_P(t)+\int_0^1 c_A(x,t)\mathrm{d}x=1,$$

where:

$$m=\frac{C_B^0}{dC_A^0},\quad L=\frac{k_2}{k_1C_A^0},\quad E=\frac{(k_1C_A^0-k_2)d^2}{D_A}$$

are dimensionless amounts.

The model has been reformulated as an integro-differential V o l t e r r a equation for $c_P(t)$. Analytic and numerical solutions for this V o l t e r r a equation were studied in the literature [1], [2]. The *method of lines* will be applied in this work, for model solving and testing.

2. The Model Solving and Testing

The method of lines is firstly presented in this section. Let u denote the concentration of A and γ the concentration of P, for convenience.

By differentiating (12) with respect to time, we obtain:

$$m\frac{\mathrm{d}\gamma(t)}{\mathrm{d}t} + \int_0^1 \frac{\partial u(x,t)}{\partial t}\mathrm{d}t = 0$$

and using (8) and (10), it results:

$$-m\frac{\mathrm{d}\gamma(t)}{\mathrm{d}t} = \frac{\partial u(1,t)}{\partial x}. \tag{13}$$

The system of differential equations (8) and (13), subject to the conditions (9),... ...,(11), will be solved by the method of lines [3],...,[5].

We choose to discretize the x variable. We define a grid of points x_i by selecting the integer M, and defining:

$$x_i = A + (i-1)x, \quad (i = 1, 2, ..., M+1), \tag{14}$$

where:

$$x = \frac{B-A}{M} \quad \text{and} \quad (16)\quad B = d, \quad A = 0. \tag{15}$$

We now approximate each space derivative of equation (8) by the usual second-order central difference and denote the approximation $u(x_i)$ by u_i. We get:

$$\frac{\mathrm{d}u_i}{\mathrm{d}t} = \frac{u_{i-1} - 2u_i + u_{i+1}}{\Delta x^2}. \tag{17}$$

Eq. (17) is the basic one to determine the unknowns u_i, $(i = 1, 2, ..., M)$. Since the solution is unknown at $x = A$, the index of unknowns u_i begins with $i = 1$. We have the derivative of the solution specified with respect to $x(1, 0)$. We then assume that equation (8) holds in $x = A$ and the unknown u_1 is defined by the equation (17) with $i = 1$:

$$\frac{\mathrm{d}u_1}{\mathrm{d}t} = \frac{u_0 - 2u_1 + u_2}{\Delta x^2}. \tag{18}$$

This assumption requires the introduction of a virtual point x_0 which lies just outside the boundary. The unknown u_0 is eliminated from equation (18) by approximating equation (10) with a second-order central difference formula to get:

$$u_0 = u_2. \tag{19}$$

Combining (18) and (19), we arrive to obtain for u_1 the equation:

$$\frac{\mathrm{d}u_1}{\mathrm{d}t} = \frac{2}{\Delta x^2}(u_2 - u_1). \tag{20}$$

Similarly, we have:

$$\frac{\mathrm{d}u_{M+1}}{\mathrm{d}t} = \frac{u_M - 2u_{M+1} + u_{M+2}}{\Delta x^2}. \tag{21}$$

We have introduced here the virtual point x_{M+2} which lies just outside the boundary. By approximating (11) with a second-order central difference formula, we get:

$$\frac{u_{M+2} - u_M}{2\Delta x} = \frac{Em}{1+L}\{L\gamma(t) - [1 - \gamma(t)u_{M+1}]\}. \tag{22}$$

Combining (22) and (21), we obtain for u_{M+1} the equation:

$$\frac{\mathrm{d}u_{M+1}}{\mathrm{d}t} = \frac{2}{\Delta x^2}(u_M - u_{M+1}) + \frac{Em}{(1+L)\Delta x}\{L\gamma(t) - [1 - \gamma(t)u_{M+1}]\}. \tag{23}$$

If we substitute (11) in (13), it results for the unknown $\gamma(t)$ the differential equation:

$$\frac{\mathrm{d}\gamma(t)}{\mathrm{d}t} = -\frac{E}{1+L}\{L\gamma(t) - [1 - \gamma(t)u_{M+1}]\}. \tag{24}$$

We have obtained, in this way, the system of $M+2$ ordinary differential equations (ODE-s) (17), (18), (21) and (24) subject to initial conditions:

$$u_i(0) = 1, \ (i = 1, 2, ..., M+1); \quad \gamma(0) = 0. \tag{25}$$

The theoretical analysis of this kind of ODE-s obtained by semidiscretization of nonlinear parabolic equations shows that they are stiff [5]. But, when we solve this kind of equations with aid of the computer, it is important to distinguish between theoretical and practical stiffeness. S h a m p i n e [6] asserts that "... stiffeness in a practical sense depends on details of the mathematical problem, the computational

problem, the numerical method and the implementation of the numerical method". Therefore, we can expect that the method of lines could become an efficient one for numerical solution of stated problem if we use a good solver for the initial value problem of ODE-s which satisfies two basic requirements: (i) an automatic step-size control which assures the required accuracy in each point, (ii) an automatic check of stiffeness. To our knowledge, the best solvers which satisfy the above conditions are contained in the mathematical library SLATEC [7]. That is why, we used SLATEC solvers for the computer solution of the system of equations (24) subject to initial conditions (25). From our simulations, using the solvers from SLATEC, it results that from the practical point of view the ODE-s are non-stiff.

The system of $M + 2$ ODE-s with the initial conditions, using two different double precision FORTRAN routines from SLATEC library, was solved. The first one, DDERKF, uses a R u n g e – K u t t a – F e h l b e r g [4], [5] method. The second one, DDEABM, uses the A d a m s – B a s h f o r t s – M o u l t o n method. These codes generally give good results for non-stiff or mild stiff equations. We took $M = 100$, i.e. the space discretization error was of order of 10^{-4}. The absolute and relative error tolerances used by DDERKF and DDEABM for the local error test at each time step were ATOL=1D–8 and RTOL=1D–6. Our numerical experiments showed that both codes work well and the system is non-stiff from practical point of view.

Our results are compared with those from [2] for $E = 10.0$, $L = 0.1$ and $m = 0.5$, in Fig. 1. We can see that our solution is closer to the "highly accurate numerical solution" of V o l t e r r a equation.

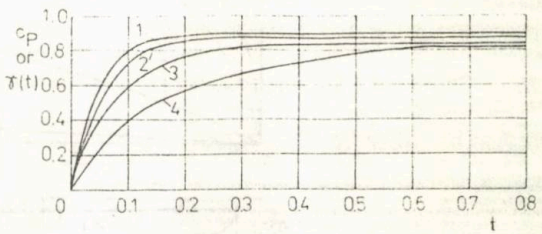

Fig. 1.– Comparison between method of lines and other methods in the literature [2]: *1* – first order approximation; *2* – zero order approximation; *3* – "highly accurate numerical solution" [2]; *4* – method of lines.

We note that the both codes, DDERKF and DDEABM, give the same result (the first 5 exact figures). In order to make more comparisons, we took $E = 0.2$, $L = 0.01$ and $m = 1.0$. The comparison with the results obtained by other methods [2] is given in Table 1. Here we have selected the case from [2] with maximum accuracy which correspond to the step size $h = 1/160$.

From these comparisons results that all the methods of solution for V o l t e r r a equation proposed in the literature [2] give smaller values than the line method. The reason is quite natural because all these methods are based on a truncation procedure. In conclusion, the method of lines, as it is formulated in this paper, appears as a very convenient and simple one for numerical solution of the mathematical model of biosensors based on antigen–antibody technology.

Table 1

Comparison between Our Results (Method of Lines) and those in the Literature [2]

	$\gamma(0.05)$	$\gamma(0.5)$	$u(1, 0.05)$	$u(1, 0.5)$
Our results	0.00953574	0.0857200	0.952240	0.861384
D i x o n scheme	0.009505	0.08560	–	–
Modified D i x o n scheme	0.0095310	0.085677	–	–
Explicit E u l e r scheme	0.0095398	0.085745	0.952211	0.86120
Implicit E u l e r scheme	0.0095315	0.085694	0.952252	0.86156
Trapezoidal product; integration scheme	0.0095356287	0.08571965	0.952234	0.861325

3. Process Simulation. Results

The numerical results presented in the Table 1, as well as in Fig. 1, prove not only the efficiency and the accuracy of the method of lines, but also the capacity of the mathematical model to describe the reaction–diffusion process in a small cell. The validity of the model being tested, a simulation of the process has been performed in this work. The results of this simulation are partly presented in the Figs. 2,...,4.

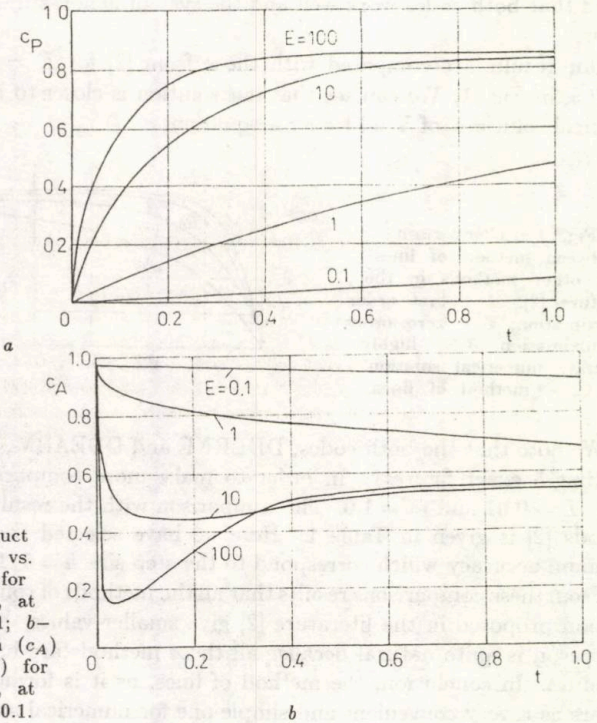

Fig. 2.– *a*– Product concentration (c_P) vs. reduced time (t) for various modules E, at $m = 0.5$ and $L = 0.1$; *b*– reactant concentration (c_A) vs. reduced time (t) for various modules E, at $m = 0.5$ and $L = 0.1$.

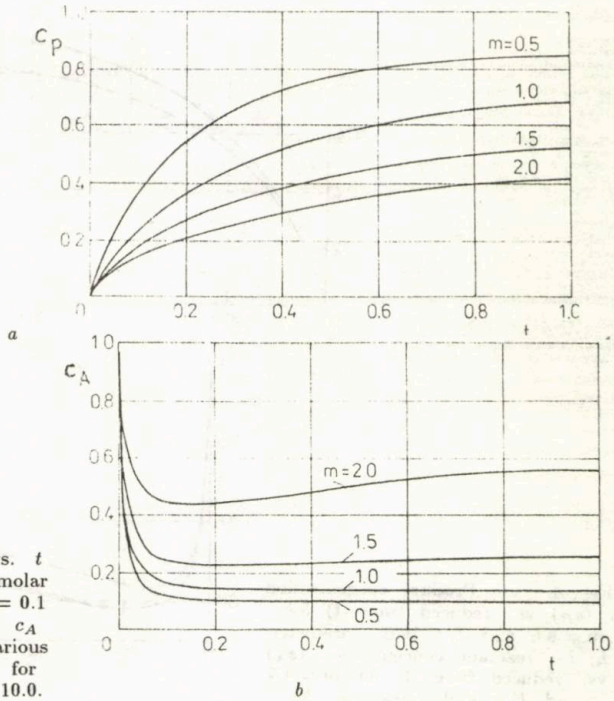

Fig. 3.– a– c_P vs. t curves at various molar ratios (m), for $L = 0.1$ and $E = 10.0$; b– c_A vs. t curves at various molar ratios (m), for $L = 0.1$ and $E = 10.0$.

Fig. 2 a presents the dimensionless concentration of the product (c_P) as a function of reduced time (t) at $m = 0.5$ and $L = 0.1$, for different values of E. In other words, it shows the influence of the modulus E on the conversion–time profiles. Like T h i e l e modulus, E is a measure of the competition between reaction and diffusion. So, the obtained dependence complies with the previous data for solid–fluid reactions.

Fig. 2 b shows the same influence of E on the concentration of the reactant A. The extremal shape of the curve for $E = 100$ may be a result of the complex inner relation of the reaction with the unsteady-state diffusion when the later is rather slow.

Figs. 3 a and 3 b compare the curves c_P vs. t and c_A vs. t, respectively, at $L = 0.1$ and $E = 10.0$, m being the parameter. Fig. 3 a shows that the conversion, at a given time, continuously increases with the excess of the reactant in solution. This is consistent with the law of mass action. The dependence of c_A, in Fig. 3 b, shows an extremal shape again, at molar ratios less than the stoichiometric ones ($m > 1$).

The ratio L is a measure of the chemical equilibrium position. From Fig. 4 a is possible to observe that, at $L < 10^{-3}$, the reaction becomes practically irreversible and the conversion tends to unity. The curves of c_A, in Fig. 4 b, have a minimum

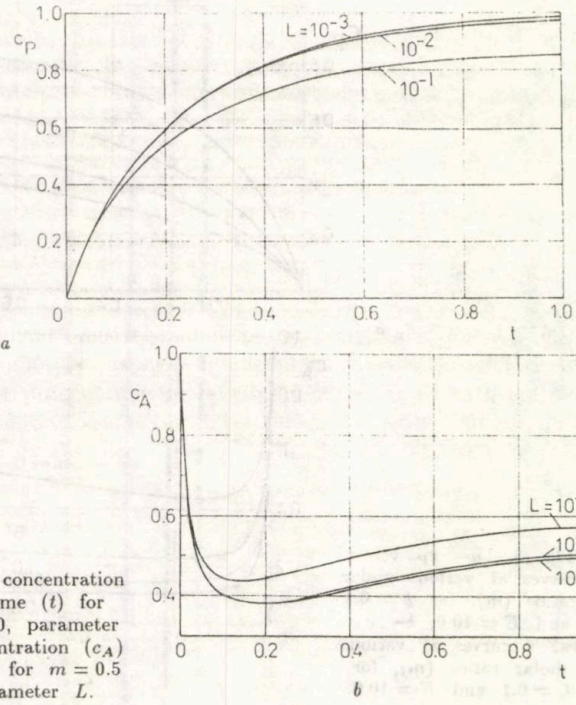

Fig. 4.– a– Product concentration (c_P) vs. reduced time (t) for $m = 0.5$ and $E = 10.0$, parameter L; b– reactant concentration (c_A) vs. reduced time (t) for $m = 0.5$ and $E = 10.0$, parameter L.

in the interval $0.1 < t < 0.2$.

Diagrams like those in Figs. 2,...,4 can be used to set the operating parameters of the process (temperature, initial concentration, d, time) included in the definitions of the dimensionless amounts E, L, and m of the model.

Notations

A – reactant (antigen);
B – reactant (antibody);
C_A^0 – initial concentration of A, [kmol/m^3];
C_B^0 – initial concentration of B, [kmol/m^2];
$C_A(X,\tau)$ – molar concentration of A, [kmol/m^3];
$C_P(\tau)$ – concentration of the product P, [kmol/m^2];
$c_A(x,t) = C_A(X,\tau)/C_A^0$ – concentration of A, dimensionless;
$c_P(t) = C_P(\tau)/C_P^0$ – concentration of P, dimensionless;
D_A – diffusion coefficient of A in solution, [m^2/s];
d – distance from edge of vessel to surface, [m];
$E = (k_1 C_A^0 - k_2)d^2/D_A$ – diffusion/reaction time scale ratio;
k_1 – rate constant for the forward reaction, [m^2/kmol.s];
k_2 – rate constant for the reverse reaction, [m^{-1}.s^{-1}];
$L = k_2/C_A^0 k_1$ – reaction time scale ratio;
M – number of equal intervals for space discretization;
$m = C_B^0/dC_A^0$ – molar ratio;
P – reaction product;

R_A – reaction rate, [kmol/m^3.s];
$t = D_A\tau/d^2$ – reduced time;
$u(x,t)$ – concentration of the reactant A, dimensionless;
X – space coordinate, [m];
$x = X/d$ – space coordinate, dimensionless;
$\gamma(t)$ – concentration of the product P, dimensionless;
τ – clock time, [s].

Received, February 24, 1994

Technical University "Gh.Asachi", Jassy,
Department of Metal Casting
and
Department of Inorganic
Chemical Technology

REFERENCES

1. Radley R.A., Drake R.A.L., Shanks I.A., Smith A.R., Stephenson P.R., Phil. Trans. Roy. Soc., **B316**, 143 (1987).
2. Cones S., Jumarhon B., McKee S., Scott J.A., *A Mathematical Model of a Biosensor.* Reprint RAL-93-073, Chilton DIDCOT, November 1993.
3. Zwillinger D., *Handbook of Differential Equations.* Academic Press, New York, 1992.
4. Schiesser W.E., *The Numerical Method of Lines.* Acad. Press, New York, 1991.
5. Graney I., Richardson A.A., J. Comput. Applic. Math., **7**, 229 (1981).
6. Shampine L.F., J. Comp. Phys., **54**, 74 (1984).
7. * * * The SLATEC Mathematical Program Library, ANL-820, Argonne, 1987 (on line documentation).

MODELAREA ŞI SIMULAREA UNOR BIOSENZORI ANTICORP–ANTIGEN

(Rezumat)

În ultimul timp s-au făcut progrese remarcabile în tehnologia anticorp–antigen, biosenzorii având numeroase aplicaţii medicale. Un biosenzor poate fi considerat un micro-reactor biochimic în care reacţia biochimică $A + B = P$ este însoţită de o difuzie nestaţionară a reactantului A din soluţie către reactantul imobilizat pe peretele celulei (B). Se stabileşte un model matematic al procesului, luând în consideraţie reacţia şi difuzia în regim nestaţionar. Modelul este studiat cu ajutorul unui calculator prin metoda liniilor. Rezultatele concordă satisfăcător cu cele existente în literatură, bazate pe reformularea sistemului ca o ecuaţie integro-diferenţială de tip Volterra. Cu modelul astfel testat se realizează simularea procesului obţinând curbe de profil concentraţie–timp, adimensionale, pe baza cărora se pot stabili condiţiile optimale de operare a unui biosenzor de acest tip.

BULETINUL INSTITUTULUI POLITEHNIC DIN IAŞI
Tomul XLI (XLV), Fasc. 1–4, 1995
Secţia II
CHIMIE ŞI INGINERIE CHIMICĂ

C.D. 621.3.035

GÉNÉRATEURS DES PLASMAS FROIDS POUR L'ÉLECTROCHIMIE ET LA PROTECTION DE L'ENVIRONNEMENT

PAR
ALBIN CZERNICHOWSKI, KHÉLIFA MEGUERNES, EUGEN HNATIUC et P. ONU

1. Introduction

L'électrochimie met en évidence deux préoccupations majeures concernant les décharges dans le gaz, c'est-à-dire l'utilisation du plasma haute température où l'utilisation du plasma basse température.

Les torches à plasma classiques permettent d'obtenir des jets de plasma à des températures élevées (10 000°K) et fonctionnent en régime d'arc électrique, caractérisé par des courants importants et de faibles tensions. L'usure rapide des électrodes dans le milieu oxydant, la haute température des électrodes et la nécessité de les refroidir sont des raisons pour affirmer que les torches à plasma – essentiellement des sources d'enthalpie – sont mal adaptées aux applications de chimie des plasmas et aux opérations de dépollution.

Au contraire les générateurs des plasmas froids de type GLIDARC fonctionnent en régime de décharge avec des tensions relativement élevées (quelques kilovolts) et des courants plus faibles (quelques ampères), que dans le cas d'un arc électrique et permettent d'obtenir à la pression atmosphérique où à des pressions plus élevées des volumes plasmagènes importants à basse température (2 000°K), fortement réactifs, à partir des gaz très différents (oxydants ou réducteurs).

2. Réacteurs électrochimiques de type GLIDARC

Les dispositifs appelés GLIDARC, dont il y a question ci-dessous, sont constitués de plusieurs électrodes profilées en forme de tuyère entre lesquelles des décharges glissantes ont la possibilité de se développer; l'alimentation électrique de ces réacteurs peut être réalisée soit en courant continu soit en courant alternatif (monophasé, triphasé où polyphasé).

Pour une même puissance électrique que pour un arc électrique les décharges de type GLIDARC ont des courants plus faibles et on évite ainsi l'accrochage de celle-ci en un point particulier des électrodes, qui auront donc une meilleure tenue même en atmosphère oxydante. Le dispositif peut fonctionner en: air, vapeur d'eau, CO_2, CH_4, H_2S, N_2, O_2, gaz rares où avec leurs mélanges comme CH_4–CO_2, CO_2–H_2S ou CH_4–air. Les gaz plasmagènes ainsi obtenus sont fortement hors d'équilibre et contiennent de nombreuses espèces excitées qui les rendent très réactifs et intéressants

pour diverses applications de chimie et de dépollution, à savoir: a) production du gaz de synthèse ($CO+H_2$) à partir d'un mélange de méthane et de gaz carbonique avec un rendement énergétique supérieur à 45%; b) décomposition du H_2S contenu dans le gaz naturel; c) destruction des composés organiques volatils; d) réduction du SO_2 vers le soufre pur; e) traitement des gaz contenant SO_x ou NO_x.

La production du gaz de synthèse ($CO+H_2$) à partir du méthane est une étape importante de la valorisation du gaz naturel. Les deux principaux procédés actuellement utilisés, le reformage par la vapeur de l'eau et l'oxydation partielle de CH_4, se heurtent à des difficultés importantes avec l'empoisonnement des catalyseurs. L'oxydation du méthane peut être améliorée en présence d'une décharge de type GLIDARC qui apporte au milieu réactionel une enthalpie facilement contrôlable et des espèces (ions, atomes métastables et excités, radicaux libres) très réactives. Les mesures des puissances effectuées ont indiquées les énergies spécifiques utilisées qui varient de 0,5 à 3 kJ par litre de mélange à traiter.

Les deux réactions chimiques principales qu'interviennent dans le processus d'oxydation de CH_4 par CO_2 sont:

$$(1) \qquad CO_2 + CH_4 \longrightarrow 2CO + 2H_2, \quad 3CO_2 + CH_4 \longrightarrow 4CO + 2H_2O,$$

la première en étant de loin la plus probable.

La décomposition du H_2S, gaz fortement toxique qui se trouve souvent dans le gaz naturel (plus de 30% des réserves mondiales de gaz naturel contiennent plus de 1% de H_2S et plus de 2% de CO_2), peut utiliser, par exemple, le procédé C l a u s, basé sur la mise en oeuvre de deux réactions succesives, pour obtenir d'abord SO_2 en présence d'oxygène où d'air à une température de l'ordre de 900°C:

$$(2) \qquad 2H_2S + 3O_2 \longrightarrow 2SO_2 + H_2O,$$

et après, par la réaction du H_2S restant avec le SO_2 on obtient:

$$(3) \qquad 2H_2S + SO_2 \longrightarrow 3S + 2H_2O.$$

On peut utiliser, également, pour les gaz de géothermie où H_2S se trouve mélangé au gaz carbonique CO_2, une décharge électrique qui favorise la réaction:

$$(4) \qquad H_2S + CO_2 \longrightarrow CO + S + H_2O,$$

et permet d'éliminer H_2S de façon pratiquement complète (à 99,8%), moyennant une dépence énergétique de 0,6...0,8 kWh par Nm^3 de mélange.

La destruction des vapeurs des solvants organiques (et l'industrie automobile est une source de pollution importante de l'atmosphère) n'aime pas du tout la solution d'une simple combustion naturelle. On utilise donc l'élévation de la température des gaz polluants (à 850°C) grâce à un apport thermique, généralement fourni par des brûleurs au méthane, la consommation d'énergie restant relativement élevée quoiqu'on cherche à récupérer une partie de la chaleur des gaz de sortie.

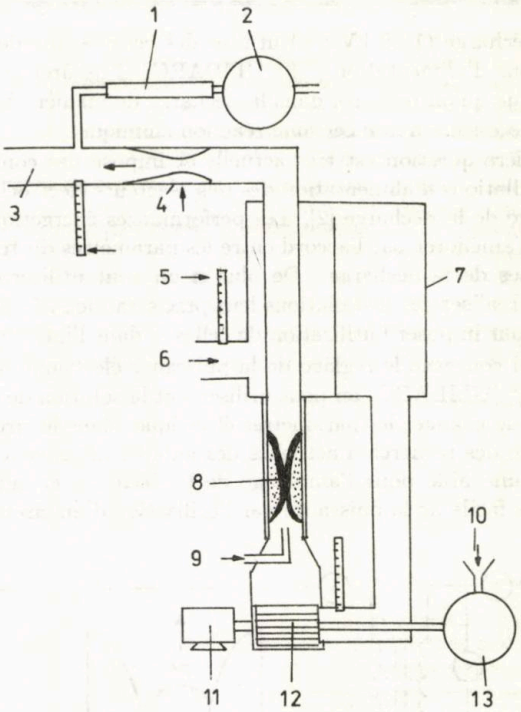

Fig. 1

Le pilot du réacteur électrochimique à arc glissant construit à Gien (France), qui est constitué de deux électrodes disposées dans une conduite en fibrociment, profilée en forme de tuyère (Fig.1), permet de ramener une concentration de xylène dans l'air de 200 ppm à une valeur de 50 ppm avec une dépense énergétique inférieure à 0,1 kWh/Nm^3, soit un gain d'au moins un facteur 2 par rapport au procédé actuellement utilisé. Dans la Fig.1 on a noté par: *1* – tube Draeger, *2* – pompe de prélèvement, *3* – sortie des gaz chauds, *4* – venturi, *5* – thermomètres, *6* – entrée d'air, *7* – échangeur de chaleur, *8* – électrodes, *9* – injection d'air comprimé, *10* – xylène, *11* – moteur, *12* – ventilateur, *13* – pompe doseuse de xylène.

On peut affirmer donc qu'il y a des raisons importantes pour accepter les réacteurs électrochimiques à plasma froid type GLIDARC.

3. Amélioration des performances énergétiques des réacteurs électrochimiques à plasma froid

Pour imposer les réacteurs électrochimiques de dépollution à plasma froid dans l'industrie c'est toujours bien à essayer d'améliorer leurs performances énergétiques, c'est-à-dire de répondre aux questions comme les suivantes: a) avoir des hautes tensions au début, pour l'amorçage (10...20 kV) et des valeurs beaucoup plus petites

pendant la décharge (1...2 kV); b) utiliser des composants de série pour réaliser les installations d'alimentation pour GLIDARC; c) assûrer le réglage de la puissance électrique qu'on retrouve dans la décharge de manière à adapter la dépense énergétique nécessaire à une certaine réaction chimique.

La première question est très actuelle et impose des constructions spéciales pour les installations d'alimentation des tels réacteurs électrochimiques, à fin d'aider l'amorçage de la décharge [2]. Les performances énergétiques de telles installations vont s'améliorer par l'accord entre les paramètres du transformateur et les caractéristiques de la décharge. De plus si on peut utiliser des composants de série à fin de réaliser ces installations leur prix sera bien sûr plus bas, une option importante pour imposer l'utilisation de celles-ci dans l'industrie.

En ce qui concerne le réglage de la puissance électrique qu'on retrouve dans „l'arc glissant" (GLIDARC) on peut utiliser soit la solution de changer le débit du gaz soit celle de changer les paramètres électriques dans le circuit de la décharge. À signaler que des recherches actuelles des auteurs annoncent des solutions pour obtenir tant une aide pour l'amorçage de la décharge et également un réglage électrique très facile de la puissance par l'utilisation d'un circuit de faible courant (Fig.2).

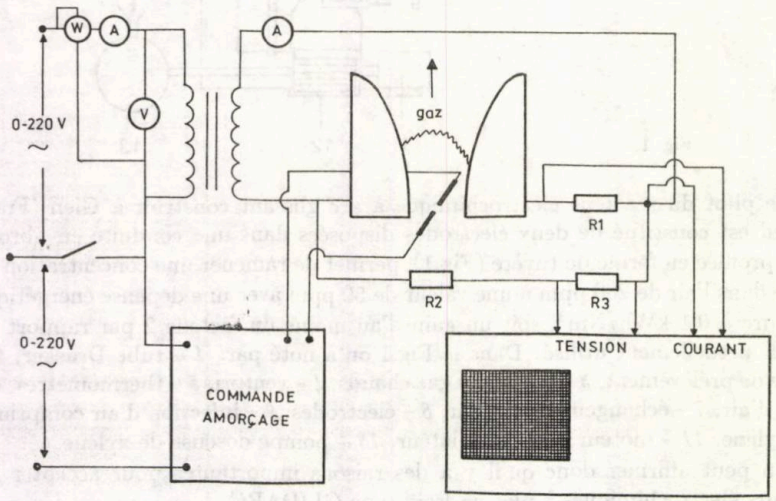

Fig. 2

Les mesures dans le schéma indiqué dans la Fig.2 montrent le fait que la puissance électrique de la décharge, P_a, augmente si le débit du gaz augmente aussi, mais dans les mêmes circonstances l'énergie spécifique du gaz:

$$p^* = \frac{P_a}{Q}, \quad [\mathrm{J/Nm^3}], \tag{5}$$

baisse (Fig.3). Si on dispose d'un réglage facile et efficace de la puissance électrique dans la décharge (Fig.4) on peut poursuivre tant le fonctionnement optimal d'un tel réacteur électrochimique que l'adaptation de l'énergie spécifique du gaz, p^*, à une telle réaction chimique de dépollution.

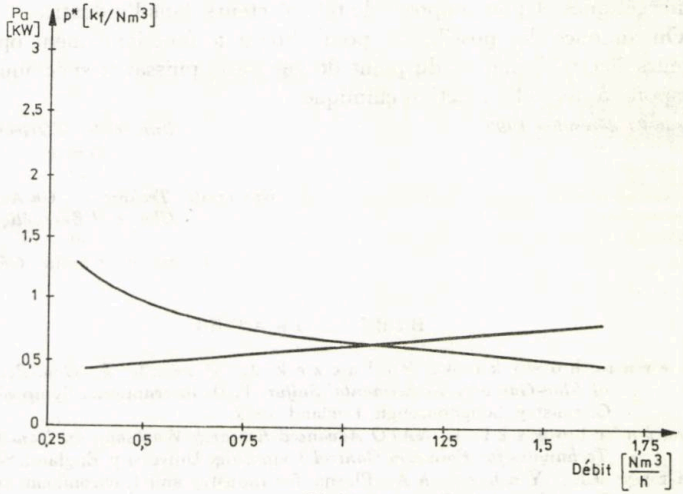

Fig. 3

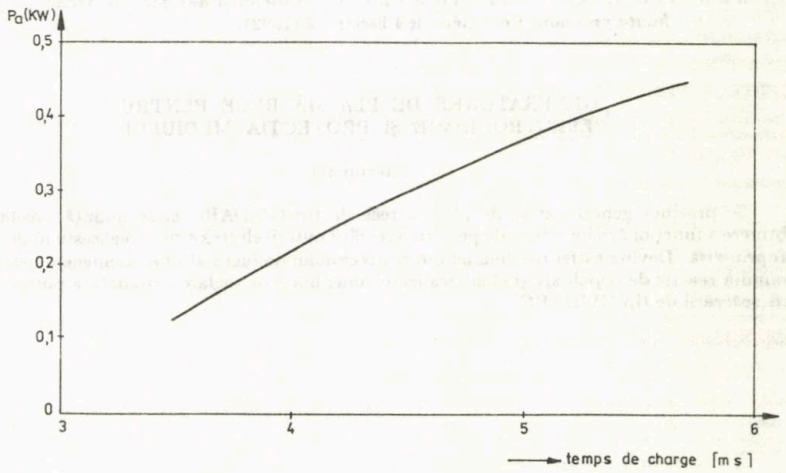

Fig. 4

Pour l'avenir on peut espérer même à une chaîne automatique autonome de réglage de ces réacteurs électrochimiques.

4. Conclusions

On présente les générateurs de plasma froids type GLIDARC et on met en évidence leurs qualités.

On indique également les voies à poursuivre à fin d'ameliorer leurs performances énergétiques et pour imposer de tels réacteurs dans l'industrie.

On annonce des possibilités pour obtenir le fonctionnement optimal de ces réacteurs électrochimiques du point de vue de la puissance spécifique du gaz qui correspond à une telle réaction chimique.

Reçue le 21 décembre 1993

Université d'Orleans,
France
et
Université Technique „Gh. Asachi", Jassy,
Chaire d'Energétique
et
Chaire de Chimie Générale

BIBLIOGRAPHIE

1. Czernichowski A., Polaczek J., Czech T., *Cold-Plasma Reduction of Flue-Gas SO_x to Elemental Sulfur.* 11-th International Symposium on Plasma Chemistry, Loughborough, England, 1993.
2. Czernichowski A., *NATO Advanced Research Workshop on Non-thermal Plasma Techniques for Pollution Control.* Cambridge University, England, September 1992.
3. Harry J.E., Yahya A.A., Plasma for Industry and Environment Technical Conf., September 1990, Oxford, England.
4. Chapelle J., Czernichowski A., *Traitement des gaz par décharges froides à haute pression.* Rev. Gén. de l'Électr., *2* (1992).

GENERATOARE DE PLASMĂ RECE PENTRU ELECTROCHIMIE ŞI PROTECŢIA MEDIULUI

(Rezumat)

Se prezintă generatoarele de plasmă rece de tip GLIDARC şi se anunţă posibilităţi de obţinere a funcţionării lor optimale pe seama reglării puterii electrice ce se regăseşte în descărcarea propriu-zisă. Devine astfel posibilă adaptarea regimului de lucru al unei asemenea instalaţii la o anumită reacţie de depoluare şi chiar realizarea unei bucle de reglare automată a puterii electrice a descărcării de tip GLIDARC.

BULETINUL INSTITUTULUI POLITEHNIC DIN IAŞI
Tomul XLI (XLV), Fasc. 1-4, 1995
Secţia II
CHIMIE ŞI INGINERIE CHIMICĂ

C.D. 661.63

ANALYSE DE L'INSTALLATION NORSK-HYDRO D'OBTENTION DES NITROPHOSPHATES

IV. LE PROCESSUS TECHNOLOGIQUE „OBTENTION DES ENGRAIS N–P ET N–P–K"

PAR
CAROLINA HAGIU et RODICA DIACONESCU

1. Introduction

Dans un travail antérieur [1] on a élaboré des modèles de bilan de masse pour les processus composants (l'ammonisation, la concentration, le dosage KCl et la granulation). Dans le présent travail on élabore et vérifie les modèles de bilan de masse pour le processus technologique „Obtention des engrais N–P et N–P–K" sous une forme adéquate à l'analyse sur ordinateur du processus.

2. Modèles de bilan pour le processus technologique „Obtention des engrais N–P et N–P–K"

Conformément au schéma technologique présenté dans la Fig.1, [1], on introduit dans le processus technologique la solution mère, NH_3, la solution de NH_4NO_3 à la préneutralisation et KCl à la granulation sur la ligne B; en résultent comme produits finis l'engrais N–P (ligne A) et N–P–K (ligne B), de même que les gaz dégagés lors de la neutralisation et de la concentration. C'est en utilisant la méthode générale d'élaboration des modèles de bilan pour un processus technologique [2] et en considérant les matières résultées d'un processus composant comme des matières entrées dans le processus composant suivant, qu'on établit les équations de bilan de masse pour le processus global „Obtention des engrais N–P et N–P–K", présentées dans le Tableau 1.

Les relations de définition et de calcul des rapports phasiques spécifiques sont présentées dans le Tableau 2.

3. Vérification des modèles de bilan de masse

La valabilité des modèles de bilan de masse est prouvée par le calcul du bilan

Tableau 1

Équations de bilan de masse pour le processus technologique d'obtention des engrais N–P et N–P–K

Entrée			Sortie		
Phase	Composant	Équations de bilan	Phase	Composant	Équations de bilan
Solutions mère $[\,]_l^I$	H_3PO_4	$m_{H_3PO_4} = 3,161 m_{[\,]_l}^I \overline{X}_{P[\,]_l}^I$	Engraise N-P $[\,]_{SA}^{II}$	$NH_4H_2PO_4$	$m_{MAP} = YA$
	HNO_3	$m_{HNO_3} = 4,5 m_{[\,]_l}^I (\overline{X}_{N_{[\,]_l}}^I - 0,7\overline{X}_{Ca[\,]_l}^I)$		$(NH_4)_2HPO_4$	$m_{DAP} = YB$
	$Ca(NO_3)_2$	$m_{Ca_3(NO_3)_2} = 4,1 m_{[\,]_l}^I \overline{X}_{Ca[\,]_l}^I$		NH_4NO_3	$m_{NH_4NO_3} = YC$
	HF	$m_{HF} = 1,052 m_{[\,]_l}^I \overline{X}_{F[\,]_l}^I$		H_2O	$m_{H_2O} = YD$
	CO_2	$m_{CO_2} = m_{[\,]_l}^I \overline{X}_{CO_2[\,]_l}^I$		$CaHPO_4$	$m_{CaHPO_4} = YE$
	H_2O	$m_{H_2O} = m_{[\,]_l}^I \overline{X}_{H_2O[\,]_l}^I$		$Ca_3(PO_4)_2$	$m_{Ca_3(PO_4)_2} = YF$
	Inertes	$m_{A''} = m_{[\,]_l}^I \overline{X}_{A''[\,]_l}^I$		CaF_2	$m_{CaF_2} = YG$
	Total	$m_{[\,]_l}^I = 0,4366 m_{[\,]_s}^0 \times$ $\times \overline{X}_{P_2O_5[\,]_s}^0 / \overline{X}_{P[\,]_l}^I = L m_{[\,]_s}^0$		Inertes	$m_{A''} = YH$
				Total	$m_{[\,]_{SA}}^{II} = L_{MA} m_{[\,]_s}^0$
Solutions NH_4NO_3 $[\,]_{l_4}^0$	NH_4NO_3	$m_{NH_4NO_3} = m_{[\,]_{l_4}}^0 \overline{X}_{NH_4NO_3}^0$	Engraise N-P-K $[\,]_{SB}^{II}$	$NH_4H_2PO_4$	$m_{MAP} = (1-Y)A$
	H_2O	$m_{H_2O} = m_{[\,]_{l_4}}^0 (1 - \overline{X}_{NH_4NO_3}^0)$		$(NH_4)_2HPO_4$	$m_{DAP} = (1-Y)B$
	Total	$m_{[\,]_{l_4}}^0 = A_N m_{[\,]_s}^0$		NH_4NO_3	$m_{NH_4NO_3} = (1-Y)C$
NH_3 $[\,]_{g_5}$	NH_3	$m_{NH_3} = m_{[\,]_{g_5}}^0 \overline{X}_{NH_3}^0 = R_A m_{[\,]_s}^0$		H_2O	$m_{H_2O} = (1-Y)D$
KCl $[\,]_{s_2}^0$	K_2O	$m_{K_2O} = m_{[\,]_{s_2}}^0 \overline{X}_{K_2O}^0$		$CaHPO_4$	$m_{CaHPO_4} = (1-Y)E$
	Inertes	$m_{A''} = m_{[\,]_{s_2}}^0 \overline{X}_{A''}^0$		$Ca_3(PO_4)_2$	$m_{Ca_3(PO_4)_2} = (1-Y)F$
	Total	$m_{[\,]_{s_2}}^0 = R_{MB} m_{[\,]_s}^0$		CaF_2; K_2O	$m_{CaF_2} = (1-Y)G$; $m_{K_2O} = m_{[\,]_{s_2}}^0 \overline{X}_{K_2O}^0$
Total		$m_T^0 = m_{[\,]_s}^0 (L + A_N + R_A + R_{MB})$		Inertes	$m_{A''} = (1-Y)H + m_{[\,]_{s_2}}^0 \overline{X}_{A''}^0$
				Total	$m_{[\,]_{SB}}^{II} = (L_{MB} + R_{MB}) m_{[\,]_s}^0$
			Gazes de la neutralisation	NH_3	$m_{NH_3} = I$
				H_2O	$m_{H_2O} = J$
				Total	$m_{[\,]_{g_5}} = G_N m_{[\,]_s}^0$
			Gazes de la concentration	NH_3, CO_2	$m_{NH_3} = K$; $m_{CO_2} = M$
				HNO_3; H_2O	$m_{HNO_3} = N$; $m_{H_2O} = O$
				Total	$m_{[\,]_{g_6}} = G_C m_{[\,]_s}^0$
			Total		$m_T = m_{[\,]_s}^0 (L_{MA} + L_{MB} + R_{MB} + G_N + G_C)$

O b s e r v a t i o n. *A...O* sont donées dans [1].

Tableau 2

Rapports phasiques spécifiques

Notation	Relations de definition	Relations de calcul
Z	$Z = m^{II}_{[\,]_{s_A}} / m^{II}_{[\,]_s}$	$Z = 0,5$
L	$L = m^{I}_{[\,]_l} / m^{0}_{[\,]_s}$	$L = 0,4366 \overline{X}^{0}_{P_2O_5} / \overline{X}^{I}_{P[\,]_l}$
L_A, L_B	$L_A = m^{I}_{[\,]_{l_A}} / m^{0}_{[\,]_s}$; $L_B = m^{I}_{[\,]_{l_B}} / m^{0}_{[\,]_s}$	$L_A = YL$; $L_B = (1-Y)L$
Y	$Y = m^{I}_{[\,]_{l_A}} / m^{I}_{[\,]_l}$	$Y = 0,4366 Z P \overline{X}^{II}_{P_2O_5[\,]_{s_A}} / L \overline{X}^{I}_{P[\,]_l}$
P	$P = m^{II}_{[\,]_s} / m^{0}_{[\,]_s}$	$P = [0,4366 \overline{X}^{0}_{P_2O_5} - Y L_M (\overline{X}^{II}_{P[\,]_{s_A}} - \overline{X}^{II}_{P[\,]_{s_B}})] : \overline{X}^{II}_{P[\,]_{s_B}}$
P_A, P_B	$P_A = m^{II}_{[\,]_{s_A}} / m^{0}_{[\,]_s}$; $P_B = m^{II}_{[\,]_{s_B}} / m^{0}_{[\,]_s}$	$P_A = YP$; $P_B = (1-Y)P$
R_A	$R_A = m^{0}_{NH_3} / m^{0}_{[\,]_s}$	$R_A = 0,8235 G_N \overline{X}_{N[\,]_{g5}} + L(0,5483 \overline{X}^{I}_{P[\,]_l} + 0,4474 \overline{X}^{I}_{F[\,]_l} - 1,2142 \overline{X}^{I}_{N[\,]_l} - 0,425 \overline{X}^{I}_{Ca[\,]_l}) + L_N[1,2142 \overline{X}_{N[\,]_{l_5}} - 0,5483 \overline{X}^{s.a.}_{P[\,]_{l_5}} + 0,2742 \times (\overline{X}_{P[\,]_{l_5}} - \overline{X}^{s.a.c.}_{P[\,]_{l_5}})] - 0,4245 A_N \overline{X}^{0}_{NH_4NO_3}$
R_{AA}, R_{AB}	$R_{AA} = m^{0}_{NH_{3_A}} / m^{0}_{[\,]_s}$; $R_{AB} = m^{0}_{NH_{3_B}} / m^{0}_{[\,]_s}$	$R_{AA} = Y R_A$; $R_{AB} = (1-Y) R_A$
A_N	$A_N = m^{0}_{[\,]_{l_4}} / m^{0}_{[\,]_s}$	$A_N = (L \overline{X}^{I}_{P[\,]_l} \overline{X}_{N[\,]_{l_5}} + G_N \overline{X}_{N[\,]_{g5}} \overline{X}_{P[\,]_{l_5}} - L \overline{X}_{N[\,]_l} \overline{X}_{P[\,]_{l_5}} - 0,8235 R_A \overline{X}^{0}_{NH_3} \overline{X}^{0}_{P[\,]_{l_5}}) : 0,35 \overline{X}_{NH_4NO_3} \overline{X}_{P[\,]_{l_5}}$
A_{NA}, A_{NB}	$A_{NA} = m^{0}_{[\,]_{l_{4_A}}} / m^{0}_{[\,]_s}$; $A_{NB} = m^{0}_{[\,]_{l_{4_B}}} / m^{0}_{[\,]_s}$	$A_{NA} = Y A_N$; $A_{NB} = (1-Y) A_N$
L_N	$L_N = m_{[\,]_{l_5}} / m^{0}_{[\,]_s}$	$L_N = L \overline{X}^{I}_{P[\,]_l} / \overline{X}_{P[\,]_{l_5}}$
L_{NA}, L_{NB}	$L_{NA} = m_{[\,]_{l_{5_A}}} / m^{0}_{[\,]_s}$; $L_{NB} = m_{[\,]_{l_{5_B}}} / m^{0}_{[\,]_s}$;	$L_{NA} = Y L_N$; $L_{NB} = (1-Y) L_N$
G_N	$G_N = m_{[\,]_{g5}} / m^{0}_{[\,]_s}$	$G_N = L + A_N + R_A - L_N$
G_{NA}, G_{NB}	$G_{NA} = m_{[\,]_{g5_A}} / m^{0}_{[\,]_s}$; $G_{NB} = m_{[\,]_{g5_B}} / m^{0}_{[\,]_s}$	$G_{NA} = Y G_N$; $G_{NB} = (1-Y) G_N$
L_M	$L_M = m^{*}_{[\,]_{l_6}} / m^{0}_{[\,]_s}$	$L_M = L \overline{X}^{I}_{P[\,]_l} / \overline{X}^{*}_{P[\,]_{l_6}}$
L_{MA}, L_{MB}	$L_{MA} = m^{*}_{[\,]_{l_{6_A}}} / m_{[\,]_s}$; $L_{MB} = m^{*}_{[\,]_{l_{6_B}}} / m_{[\,]_s}$;	$L_{MA} = Y L_M$; $L_{MB} = (1-Y) L_M$
R_{MB}	$R_{MB} = m^{0}_{[\,]_{s_2}} / m^{0}_{[\,]_s}$	$R_{MB} = (1-Z) P \overline{X}^{II}_{K_2O[\,]_{s_B}} / \overline{X}^{0}_{K_2O[\,]_{s_2}}$
A, S, G, R_S, F, R_L, R_D, R^0_L, N, D_R – v. [3]		

réel de masse, en utilisant les données nécessaires, empruntées à une installation industrielle. Les grandeurs nécessaires sont, outre celles présentées dans [3], [4], les suivantes:

Fig. 1.– Bilan de masse pour le processus technologique d'obtention des engrais N–P et N–P–K.

$\overline{X}^{0}_{NH_4NO_{3[\,]_{l_4}}} = 0,88$; $\overline{X}^{0}_{K_2O_{[\,]_{s_2}}} = 0,60$; $\overline{X}_{N_{[\,]_{l_5}}} = 0,239$; $\overline{X}_{P_{[\,]_{l_5}}} = 0,0510$;

$\overline{X}_{N_{[\,]_{g_5}}} = 0,01138$; $\overline{X}_{N_{[\,]_{g_6}}} = 0,074$; $\overline{X}_{P_{[\,]^{*}_{l_6}}} = 0,06$; $\overline{X}_{N_{[\,]^{*}_{l_6}}} = 0,268$;

$\overline{X}_{H_2O_{[\,]^{*}_{l_6}}} = 0,03$; $\overline{X}^{II}_{P_2O_{5[\,]_{SA}}} = 0,136$; $\overline{X}^{II}_{P_2O_{5[\,]_{SB}}} = 0,111$; $\overline{X}^{II}_{K_2O_{[\,]_{SB}}} = 0,12$.

En outre ils s'avèrent nécessaires les grandeurs calculées à l'aide des équations (1) [1] et les rapports phasiques calculés avec les relations présentées dans le Tableau 2. Les résultats acquis sont présentées sous la forme du schéma de bilan de masse dans la Fig.1.

On constate aisément que la bilan de masse est vérifié avec une suffisante exactitude, tant pour les processus composants que pour le processus global, ce qui démontre que les processus de transformation pris en considération sont capables à décrire quantitativement ceux qui ont lieu dans les réacteurs industriels.

4. Conclusions

On a élaboré des modèles de bilan de masse pour le processus technologique „Obtention des engrais N–P et N–P–K".

Les débits de masse des produits finis et intermédiaire ont été corrélés au débit de la matière première phosphatée et à sa qualité par des rapports phasiques spécifiques, sous une forme accésible à l'utilisation des ordinateurs.

On a vérifié les modèles de bilan de masse par le calcul du bilan pour une installation industrielle, dans les conditions de l'utilisation de la phosphorite de Maroc.

Reçue le 26 octobre 1992

Université Technique „Gh.Asachi", Jassy,
Chaire de Chimie
Technologique Anorganique

BIBLIOGRAPHIE

1. Hagiu C., Diaconescu R., Bul. Inst. polit., Iaşi, **XL(XLIV)**, *1-4*, s.II, 63 (1994).
2. Calistru C., Leonte C., *Tehnologia Substanţelor Anorganice*. EDP, Bucureşti, 1972.
3. Hagiu C., Diaconescu R., Bul. Inst. polit., Iaşi, **XXXVII(XLI)**, *1-4*, s.II, 41-48 (1991).
4. Hagiu C., Diaconescu R., Bul. Inst. polit., Iaşi, **XXXIX(XLIII)**, *1-4*, s.II, 71-78 (1993).

ANALIZA INSTALAŢIEI NORSK-HYDRO DE OBŢINERE A NITROFOSFAŢILOR
IV. Procesul tehnologic „Obţinerea îngrăşămintelor N–P şi N–P–K"

(Rezumat)

Se elaborează şi se verifică modelele de bilanţ de masă pentru procesul tehnologic de obţinere a îngrăşămintelor N–P şi N–P–K, constituit din procesele componente: amonizare, concentrare,

dozare KCl şi granulare. Pentru a evidenţia influenţa calităţii materiei prime, se definesc şi se utilizează rapoarte fazice specifice. Modelele de bilanţ de masă sunt exprimate într-o formă adecvată analizei procesului cu ajutorul calculatoarelor.

BULETINUL INSTITUTULUI POLITEHNIC DIN IAŞI
Tomul XLI (XLV), Fasc. 1–4, 1995
Secţia II
CHIMIE ŞI INGINERIE CHIMICĂ

D.C. 66.065.53

THE CONCENTRATION OF THE BINARY MIX CRYSTALS BY MULTIPLE RECRYSTALLIZATION IN COCURRENT FLOW WITH SALTING-OUT SUBSTANCES

BY
STELIAN PETRESCU, IGOR CREŢESCU and I. MĂMĂLIGĂ

1. Introduction

The crystallization by salting-out represents a method used in the chemical industry, for the separation of a salt in a solution by means of a substance which has the role to diminish the solubility of the salt. This method can be achieved as a recrystallization simple or multiple in cocurrent or back flow.

The literature includes a lot of works which treats the equilibrium or the kinetics of the crystallization process by salting-out [1],...,[10].

Most works refer to the ternary systems [1],...,[8]. Some of them approach the crystallization by salting-out in the quaternary system [8],...,[10].

Some works [11], [12] concern the study of concentration of binary mix crystals by simple or multiple recrystallization, in cocurrent flow or back-flow. In these works, using methods of graphic or analytical calculus, the necessary number of theoretical contact recrystallization unit and the degrees of separation to the equilibrium, are calculated. The calculus are done for the system $K_2SO_4 - (NH_4)_2SO_4 - H_2O$ at the temperature of 25°C and the pressure of 1 atm. which forms by crystallization binary mix crystals $K_2SO_4 - (NH_4)_2SO_4$.

In what follows a graphic-analytical method for the calculus of the multiple recrystallization in cocurrent flow for the binary mix crystals $AM - BM$ by salting-out in the system $AM - BM - S - H_2O$ is proposed. This method allows the calculus of the number of theoretical contact recrystallization unit, the maximum separation degrees of the salt AM and BM for each contact unit and of the water ratio.

Based on this method the system $K_2SO_4 - (NH_4)_2SO_4 - NH_3 - H_2O$ at 25°C and atmospheric pressure, the influence of the mass ratio (R) ammonia/initial mix crystals and of the composition (X_f) of the final mix crystals on the number (n) of theoretical contact recrystallization units, are studied.

It is calculated, too, the separation degrees at the equilibrium for the salts $(NH_4)_2SO_4$ and K_2SO_4, the concentration (X_i) of the mix crystals and the minimum water ratio (r_i) adequate to each contact recrystallization unit.

2. The Method of Calculus

The multiple recrystallization in cocurrent flow by salting-out in order to concentrate the mix crystals formed by the salt AM and BM, supposes the feeding

of each recrystallization unit with water and salting-out substance (S). The initial mix crystals are introduced in the first unit and traverse all units of recrystallization from 1 to n. At the passage of the mix crystals through the n units of recrystallization, the concentration of a salt (BM) increases, the other salt remaining in the solution (AM). In Fig.1 the block schema of the multiple recrystallization in cocurrent flow by salting-out is presented.

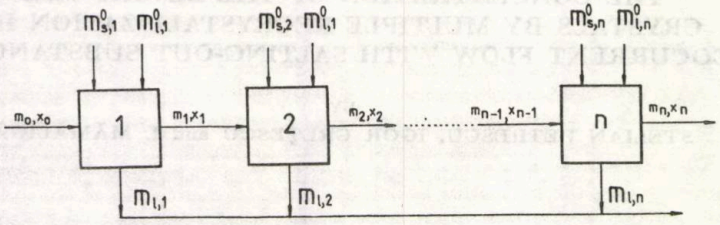

Fig. 1.– Block schema.

Each recrystallization unit implies a stage of dissolving of the mix crystals in a dissolvent (H_2O) followed by a stage of crystallization with salting-out substance (S) of some mix crystals more concentrated in the salt BM.

In accordance with Fig.1, from each recrystallization unit results a liquid phase which includes the salting-out substance. These liquids, after mixture, are sent to the recuperation of salting-out substances which are recirculated in the process.

The graphic-analytical method for the calculus of the multiple recrystallization in cocurrent flow with salting-out substance, supposes the use of a calculus diagram, presented in Fig.2.

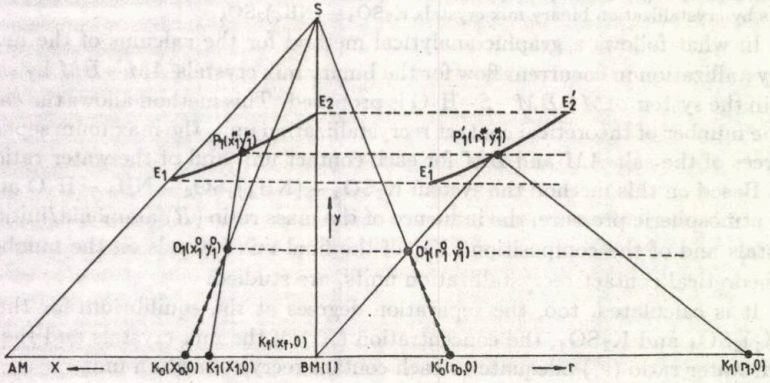

Fig. 2.– Calculus diagram.

The calculus diagram contains two parts: the diagram of the anhydride salts and the diagram of the water. The concentration of the salt AM and of the salting-out substance are expressed in mass fractions (X, Y). The estimate of the initial

and final water quantity of the system is realized by the number of the water (r), which represents the mass ratio water/anhydride salts.

In order to simplify, on the calculus diagram only one blending straight line and only one link line has been represented, corresponding to the first recrystallization unit. The blending straight line for the unit 1 is SK_0 in the anhydride salts diagram, and SK_0' in the water diagram. The link line for unit 1 (P_1K_0) joins the figurative points of the mix crystals resulted after unit 1 (K_1) of the initial system (O_1) and of the liquid phase obtained after unit 1 (P_1). The projection of the link line P_1K_0 in the water diagram is $P_1'K_1'$. The initial mix crystals are represented in the calculus diagram by the point K_0.

The graphic-analytical method for calculus of number of theoretical contact recrystallization units, proposed in this work, supposes the following algorithm:

a) The equilibrium line in the anhydride salts diagram E_1E_2 and her projection in the water diagram $E_1'E_2'$ are represented according to the data given in literature.

b) The figurative point of the initial mix crystals (K_0) and the figurative point of the final mix ones (K_f) are fixed.

c) The concentration of the salt AM from the initial mixture are calculated:

$$X_1^0 = X_0(1-R), \quad R = \frac{m_{s1}^0}{m_0} = Y_1^0. \tag{1}$$

d) On the blending straight line of the unit 1 the figurative point of the initial mixture or of the initial system $O_1(X_1^0, Y_1^0)$ is represented.

e) By graphic interpolation the point P_1 is found and from the diagram the values of the co-ordinates of this point, X_1^* and Y_1^*, are taken and used in the calculation of the concentration of the salt AM from the mix crystals which leave unit 1:

$$X_1 = X_1^* + \frac{Y_1^*(X_1^* - X_1^0)}{R - Y_1^*}. \tag{2}$$

f) The point K_1 on the diagram is fixed and a blending straight line for the unit 2 (SK_1) is drawn, the calculus going on as long as $X_n \leq X_f$. The ratio (R) is maintained constant,

$$X_n = X_n^* + \frac{Y_n^*(X_n^* - X_n^0)}{R - Y_n^*}. \tag{3}$$

The number of the theoretical recrystallization units is given by the index of X_n.

For the calculus of the maximum separation degrees of the salt AM and BM for each recrystallization unit the relations:

$$\alpha_1 = 1 - \frac{RX_1^*}{X_0Y_1^*}, \quad \alpha_2 = 1 - \frac{RX_2^*}{X_1Y_2^*}, \ldots, \alpha_n = 1 - \frac{RX_n^*}{X_{n-1}Y_n^*}, \tag{4}$$

$$\beta_1 = 1 - \frac{R(1 - X_1^* - Y_1^*)}{Y_1^*(1 - X_0)}, \quad \beta_2 = 1 - \frac{R(1 - X_2^* - Y_2^*)}{Y_2^*(1 - X_1)}, \ldots, \tag{5}$$

$$\beta_n = 1 - \frac{R(1 - X_n^* - Y_n^*)}{Y_n^*(1 - X_{n-1})}$$

established by the mass balance sheet are used.

The water quality necessary to obtain a maximum separation degree of the salt BM and respectively of a minimum separation degree of the salt AM is given by the minimum number of the water adequate to the respective recrystallization unit. For the unit i the minimum number of the water (r_i^0) can be calculated with the relation:

$$r_i^0 = \frac{Rr_i^*}{Y_i^*}, \quad (i = 1, 2, \ldots, n). \tag{6}$$

3. Results and Discussions

The proposed graphic-analytical method has been used for the calculus of the number of theoretical contact recrystallization units necessary for the concentration of some mix binary crystals consisting of K_2SO_4 and $(NH_4)_2SO_4$ with the initial concentration in $(NH_4)_2SO_4$, $X_0 = 0.4$. The aim of concentration is to increase the content in K_2SO_4 and therefore to decrease the concentration of $(NH_4)_2SO_4$ until $X_f = 0.04$. Water is used as solvent and ammonia as salting-out substance.

For the ratio (R) ammonia/initial mix crystals the following values have been considered: 0.2, 0.3, 0.4 and 0.5. The equilibrium data for the system $K_2SO_4 - -(NH_4)_2 - NH_3 - H_2O$ at the pressure of 1 atm. and the temperature of 25°C have been taken from literature [13], [14].

In each recrystallization unit the initial mix crystals will be dissolved, therefore a passage of $(NH_4)_2SO_4$ and K_2SO_4 in water and afterwards K_2SO_4 and $(NH_4)_2SO_4$ will crystallize in mix crystals more concentrated in K_2SO_4, by the introduced ammonia.

Using the graphic-analytical method previously presented, the number of theoretical recrystallization units was calculated, the obtained results being illustrated graphically in Fig.3. It can be established that the number n of theoretical recrystallization units decreases with the increase of the final concentration of the $(NH_4)_2SO_4$ (X_f).

As it was to be expected, for obtaining mix crystals with a higher content in K_2SO_4 (therefore with a less concentration X_f) several theoretical recrystallization units are necessary. The ratio R highly influences the number n of theoretical recrystallization units. The larger the quantity of ammonia used, the lesser the necessary number of theoretical recrystallization units is.

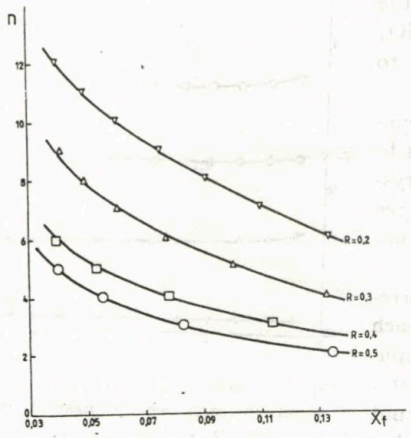

Fig. 3.– Number of theoretical contact recrystallization units for different values X_f and R.

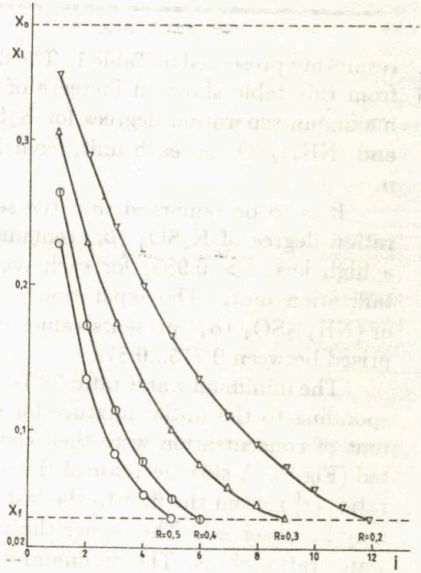

Fig. 4.– Concentration of $(NH_4)_2SO_4$ from the mix crystals at the emergence in each recrystallization unit.

In Fig.4 is illustrated graphically the variation of the concentration of $(NH_4)_2$. $.SO_4$ from the final mix crystals for each recrystallization unit. It can be established that X_i decreases from the first to the last unit. Consequently it achieves a concentration of the mix crystals in K_2SO_4. The higher the values of the ratio R, the better the degree of concentration is.

Based on relations (4) and (5), the maximum separation degrees of $(NH_4)_2SO_4$ (α_i) and K_2SO_4 (β_i) for each recrystallization unit is calculated. The obtained

Table 1

Values of the Separation Degrees at the Equilibrium on each Recrystallization Unit

R	β_i	Recrystallization unit i											
	α_i	1	2	3	4	5	6	7	8	9	10	11	12
0.2	β_i	0.9959	0.9959	0.9964	0.9967	0.9967	0.9972	0.9974	0.9976	0.998	0.9981	0.9977	0.9979
	α_i	0.8258	0.8138	0.8207	0.8268	0.831	0.8301	0.8373	0.845	0.841	0.8364	0.8422	0.8399
0.3	β_i	0.9946	0.9943	0.9956	0.9959	0.9966	0.9962	0.9964	0.9975	0.9967	0.9974	–	–
	α_i	0.7573	0.7539	0.7897	0.8051	0.8136	0.8177	0.8441	0.8495	0.8796	0.8797	–	–
0.4	β_i	0.9913	0.9952	0.9946	0.9956	0.9959	0.9956	–	–	–	–	–	–
	α_i	0.7184	0.746	0.7682	0.7846	0.7958	0.8429	–	–	–	–	–	–
0.5	β_i	0.9865	0.9927	0.9938	0.9951	0.9959	–	–	–	–	–	–	–
	α_i	0.7154	0.7603	0.7861	0.8183	0.8603	–	–	–	–	–	–	–

results are presented in Table 1. The data from this table show an increase of the maximum separation degrees for K_2SO_4 and $(NH_4)_2SO_4$ on each unit, from 1 to n.

It is to be remarked that the separation degree of K_2SO_4 (β_i) remains to a high level (> 0.985) for each recrystallization unit. The separation degree of $(NH_4)_2SO_4$ (α_i) presents values comprised between 0.715...0.87.

The minimum water ratio (r_i^0) corresponding to the initial mixture for each unit of concentration were then computed (Fig.5). A slow decrease of the water ratio (r_i^0) from the first to the last unit may be observed. The higher the value of the ratio R, the higher the minimum water ratio (r_i^0) is. The minimum water ratio allows the calculus of the necessary water quantity, so that the separation degrees have values as high as possible.

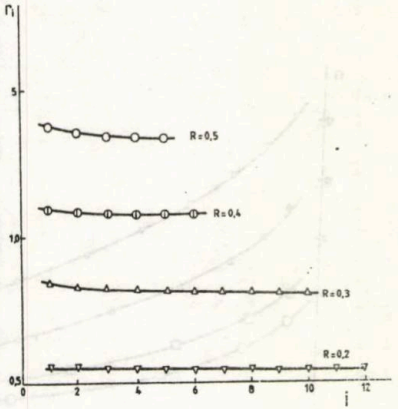

Fig. 5.– Minimum water ratio at the input in each recrystallization unit.

4. Conclusions

A graphic-analytical method for the calculus of the theoretical contact units number at the multiple recrystallization in cocurrent flow of some binary mix crystals $AM - BM$ with salting-out substance was established.

The relations for the calculus of the maximum separation degrees of the salt AM and BM and of the minimum water ratio (r_i^0) for each recrystallization unit are established too.

On the basis of the proposed graphic-analytical method the number of theoretical recrystallization units (n) for the concentration of the mix crystals K_2SO_4–$-(NH_4)_2SO_4$ was determined, using the water as a solvent and the ammonia as salting-out substance. At the same time, the maximum separation degrees of the salts $(NH_4)_2SO_4$ and K_2SO_4, (α_i, β_i), and the minimum water ratio, (r_i^0), on each unit of recrystallization, were calculated.

The obtained results have made evident the influence of the mass ratio R (salting-out substance/initial mix crystals) on n, r_i^0, α_i, β_i.

Notations

$m_{s,i}^0$ – the mass flow of salting-out substance at the input in unit i;
m_0 – the mass flow of initial mix crystals;
X_i – the mass fraction of the salt AM or $(NH_4)_2SO_4$ at unit i;
Y_i – the mass fraction of the salting-out substance (S) or NH_3 at unit i;
R – the mass ratio salting-out substance/initial mix crystals;
r_i – the minimum water ratio at unit i;
α_i – the maximum separation degree of the salt AM or $(NH_4)_2SO_4$ at unit i;

β_i – the maximum separation degree of the salt BM or K_2SO_4 at unit i;
0 – initial;
f – final;
* – equilibrium;
S – salting-out substance.

Received, August 15, 1994

Technical University "Gh. Asachi", Jassy,
Department of Chemical Engineering

REFERENCES

1. Filipescu L., Pincovschi E., *Echilibrul solid–lichid.* Ed. Tehnică, Bucureşti, 1980.
2. Winnacker K., Kuchler L., *Tehnologie chimică anorganică* (transl. form English). Ed. Tehnică, Bucureşti, 1962.
3. Bielopolski A.P., Aleksandrov N.P., Zh. Pr. Khim., **4**, 578 (1931).
4. Verner R.E., Thompson A.R., Ind. Eng. Chem., **41**, 2242 (1949).
5. Verner R.E., Thompson A.R., Ind. Eng. Chem., **42**, 464 (1950).
6. Pozin M.E., *Tekhnologya mineral'nyh solei.* Goskhimizdat, Leningrad, 1970.
7. Viktorov M.M., *Graficeskie rasčioty v tekhnologyi neorganičeskikh vesčestv.* Izd. Khimyia, Leningrad, 1972.
8. Calistru C., Leonte C., *Tehnologia substanţelor anorganice.* Ed. Tehnică, Bucureşti, 1972.
9. Calistru C., Leonte C., Hagiu C., Siminiceanu I., Popa D., *Tehnologia îngrăşămintelor minerale.* Vol. **II**, Ed. Tehnică, Bucureşti, 1985.
10. Calistru C., Petrescu S., Leonte C., Szep A., Rev. Chim., **35**, 7, 613 (1984).
11. Petrescu S., Rev. Chim., **41**, *5-6*, 429 (1990).
12. Petrescu S., Rev. Chim., **44**, *2*, 152 (1993).
13. Zdanovskiy A.B., Leakhovskaia E.J., Shčleinovič R.E., *Spravočnik eksperimental'nyh dannyh po rastvorimosti vodnosolevykh sistem.* T.**II**, Goskhimizdat, Leningrad, 1954.
14. Zdanovskiy A.B., Leakhovskaia E.J., Shčleinovič R.E., *Spravočnik eksperimental'nyh dannyh po rastvorimosti vodnosolevykh sistem.* T.**I**, GNTIKL, Leningrad, 1953.

CONCENTRAREA CRISTALELOR MIXTE BINARE PRIN RECRISTALIZARE MULTIPLĂ ÎN ECHICURENT CU SALEFIANŢI

(Rezumat)

Se stabileşte o metodă grafo-analitică pentru calculul numărului teoretic de trepte teoretice de contact la concentrarea prin recristalizare multiplă în echicurent. Metoda propusă s-a utilizat pentru studiul influenţei raportului (R) amoniac/cristale mixte asupra numărului de trepte teoretice de contact precum şi asupra gradelor de separare maxime a sărurilor $(NH_4)_2SO_4$ (α_i) şi K_2SO_4 (β_i) şi asupra raportului minim al apei pentru fiecare treaptă de concentrare la recristalizarea multiplă în echicurent a cristalelor mixte K_2SO_4–$(NH_4)_2SO_4$.

BULETINUL INSTITUTULUI POLITEHNIC DIN IAŞI
Tomul XLI (XLV), Fasc. 1–4, 1995
Secţia II
CHIMIE ŞI INGINERIE CHIMICĂ

D.C. 542.957; 544.6

NMR STUDY OF SOME ORGANOPHOSPHORUS COMPOUNDS

BY

MOULOUD ATTOU, HIROSHI MORIYAMA and ABDELKRIM AZZOUZ

1. Introduction

Nuclear magnetic resonance (NMR) spectroscopy is one of the most powerful structural and analytical tools available. Structure analysis of compounds becomes significantly easier thanks to the NMR techniques, than with only the classical methods (IR, UV,...). With the event of the Fourier transform technique, the amount of information which can be gained from complexe spectra is considerably increased. However, although the NMR technique has changed greatly (pulse Fourier transform method, multiple pulse, two dimensional NMR), the physical principles of NMR has not changed. Improvement proceeds aimly from the considerable increase in experimental complexity [1] (DEPT/INEPT, INADEQUATE,...) [2], [3] and from instrumental developments, especially with superconducting magnets. These technical and instrumental improvements are required by the need to extract the usual NMR parameters such as chemical shifts and coupling constants from increasingly difficult samples. Although initially, attention of chemists was focussed on ^{1}H and ^{13}C, nowadays, thanks to improvement of NMR techniques and instruments, analysis of nuclei of less sensitivity can be done. Therefore, in the chemistry field, determination of structures and studies of reaction mechanisms can be carried out by using NMR techniques. However, one of the usual tasks in the confirmation of a proposed structure, is the use of NMR data from model compounds.

The present work deals with the analysis and the assignment of some organophosphorus compounds. For this purpose, several NMR techniques are used.

2. Experimental

The experiments were run mostly in a JEOL 90A equipment. A BRUKER equipment, the AC-200P, was also used.

A routine sample consists of about 5...50 mg of the compound [4] in about 0.4 ml of solvent in a 5 mm O.D. glass tube. In some cases, saturated samples are used. When a 10 mm O.D. tube is used, the quantity of the solution is ca. triple than that in case of a 5 mm O.D. glass tube. In the most cases, tetramethyl silane (TMS), mixed with the solvent is used as reference. When TMS is not dissolved into the solvent, it is put in a capillary tube which is plunged coaxially in the tube containing the sample. In all the cases, deuterated solvents were used as lock signals. When non-deuterated solvents are used, the lock is gained by the means

of the external lock (D_2O is already set within the equipment).

3. Results and Discussions

3.1. Triphenylphosphate (TPP)

^1H NMR spectrum of this compound shows one group of resonance in the neighbor of 7.25 ppm. The complicated pattern is due to the all protons A_2B_2C spin systems which are superimposed each other. ^{13}C NMR analysis of triphenylphosphate gave a spectrum with four signals (Fig.1). The group of resonance at lowest field is due to the quaternary carbon atom C-1. The peak (150.4 ppm) is split into two because of the two-bond coupling with ^{31}P, (^2J(COP)=7.33 Hz). The second group of resonance at high field, comprises respectively the peaks of the carbon atom labelled C-3(129.8 ppm), C-4(125.5 ppm) and C-2(120.0 ppm). The latter is split into two due to the coupling with ^{31}P, ^3J(C–P)=4.88 Hz. Generally, ^1H and ^{13}C spectra suffice to elucidate the molecular structure of TPP, however, the ^{31}P spectrum can be taken into account (Fig.2 *a* and *b*). In our case, this spectrum shows only one peak at –18.65 ppm. Splitting due to the interaction between ^{31}P and ^1H cannot be observed: the reason is that the fourbond coupling (^4J(POCCH)) is too weak [5], so that the effect of coupling is not apparent.

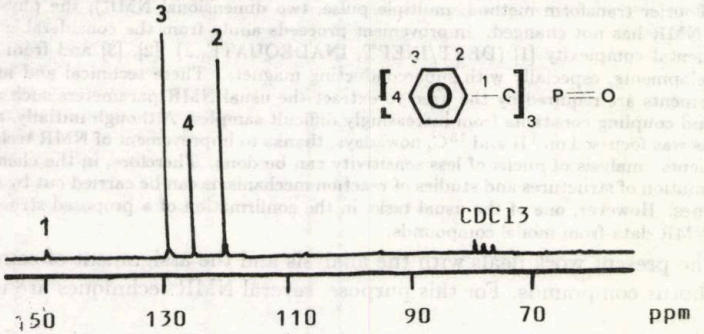

Fig. 1.– ^{13}C spectrum of TPP (JEOL-90A).

3.2. Trimethyl Phosphate

The protons of this compound are chemically and magnetically equivalent, thus the ^1H spectrum of the substance should give rise to one peak. The peak is observed at δ = 3.78 ppm, nevertheless, because of the three bond coupling with ^{31}P, this peak is split into two. The carbon atoms are equivalent. The ^{13}C NMR peak of these atoms appears at δ = 52.85 ppm (Fig.3). Splitting into two of this peak occurs because of the interaction of the two-bond coupling with ^{31}P. The value of the coupling constant is ^2J(COP)=9 Hz. TMP has also been analysed by ^{17}O NMR technique. The spectrum is a pattern of two peaks. Each peak is split into

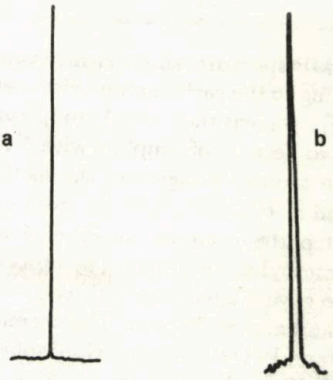

Fig. 2.– ^{13}P NMR spectrum of TPP (JEOL-90A): *a* – with, *b* – without irradiation of ^{1}H.

two by the one-bond coupling with ^{31}P. The pattern corresponding to the oxygene atom bonded with the methyl group, is split into four by the two bond coupling with hydrogene. ^{31}P NMR analysis of the substance gave a pattern of ten peaks (two outer peaks cannot be seen because they are in the noise level). The signal is obtained at $\delta = 0.78$ ppm with the coupling constant $^{3}J(\mathrm{POCH})$=10.5 Hz.

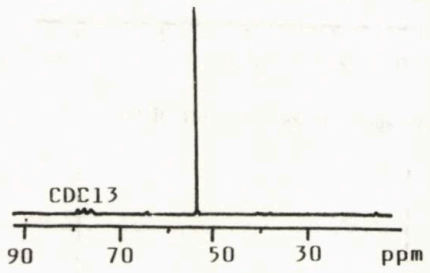

Fig. 3.– ^{13}C NMR spectrum of TMP.

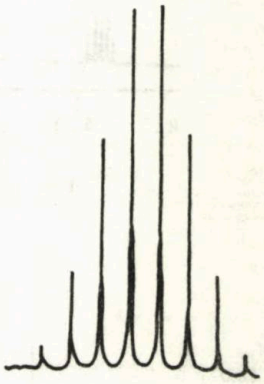

Fig. 4.– ^{31}P NMR of TMP.

3.3. Triethyl Phosphate (TEP)

The ^{1}H NMR spectrum of this substance shows two groups of resonance. The first at 4.11 ppm is due to the methylene group (Fig.5). This methylene group is subject to two interactions: two types of three-bond couplings, $^{3}J(^{1}\mathrm{H}^{1}\mathrm{H})$ and $^{3}J(^{1}\mathrm{H}^{31}\mathrm{P})$. These couplings produce an overlapping of the peaks, as the both couplings are in the similar magnitude, ca. 8 Hz. The second group which appears at $\delta = 1.3$ ppm, is assigned to the methyl group. Thus, the signal shows the coupling pattern as triplet of doublet ($^{3}J(^{1}\mathrm{H}^{1}\mathrm{H})$=7.5 Hz, $^{4}J(^{1}\mathrm{H}^{31}\mathrm{P})$=1.0 Hz). The

^{13}C NMR spectrum shows clearly two peaks of ethyl group. Indeed, the peak corresponding to the carbon atom with methylene protons, is observed at $\delta = 63.23$ ppm (Fig.6), whereas the methyl group appears at $\delta = 15.66$ ppm. These peaks are split into two because of coupling with ^{31}P. The values of the coupling constants for the carbon atoms belonging to the methylene and methyl groups are $^{2}J(COP)=7.33$ Hz and $^{3}J(CCOP)=4.88$ Hz, respectively. ^{31}P NMR spectrum of TEP shows a heptet pattern due to the six equivalent methylene protons. Four-bond coupling with methyl is too small to be observed (ca. 1 Hz). ^{17}O NMR analysis of the substance gave a spectrum with two main peaks whose chemical shifts are at $\delta = 27$ ppm and at $\delta = 74$ ppm. The chemical shift of the two kinds of oxygene in bonds P=O and P–O–C, in trialkylphosphates, are respectively of the same order (Fig.7). ^{17}O NMR analysis, joined to the methods described above, renders the structure analysis of triethyl phosphate easier.

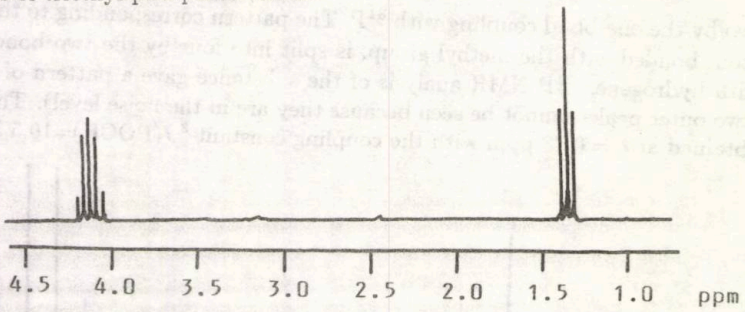

Fig. 5.– ^{1}H NMR spectrum of TEP (JEOL-90A).

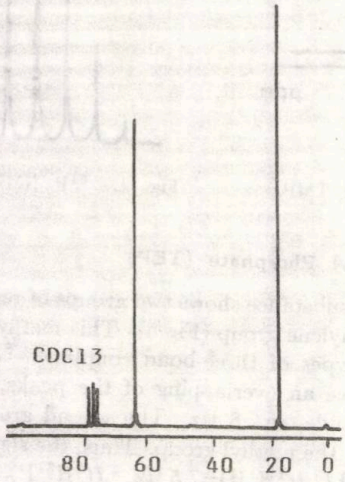

Fig. 6.– ^{13}C NMR spectrum of TEP.

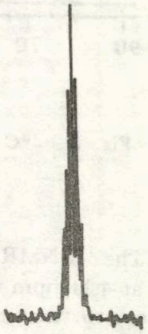

Fig. 7.– ^{31}P NMR spectrum of TEP.

3.4. Tri-n-Butyl Phosphate (TBP)

^{1}H NMR spectrum of TBP is complicated. In the spectrum shown in Fig.8, two groups of resonance can be observed, the first one appears at δ = 4.1 ppm, the second at low field whose chemical shift range is between δ = 0.9 ppm and δ = 1.7 ppm. The group at high field which seems like a quartet, belongs to the methylene group C-4. This group is due to the splitting by protons belonging to the neighboring methylene group C-3. The magnitude of the corresponding coupling constant ($^3J(^1H^1H)$) is ca. 1 Hz. However, this splitting is also due to the interaction with ^{31}P by the means of a coupling of the same order as that of $^3J(^1H^1H)$.

The methylene group labelled C-3 is subject to two conjugated splittings (from ^{1}H and ^{31}P). The result of this splittings is a superimposed pattern, constituted by four peaks (Fig.8). The group of resonance at low field is constituted by signals of two methylene groups labelled C-3 and C-2 which appear respectively at δ = 1.7 ppm and at δ = 1.4 ppm and by a signal of methyl group which appears at δ = 0.9 ppm. For these three groups, only usual spin–spin coupling is involved.

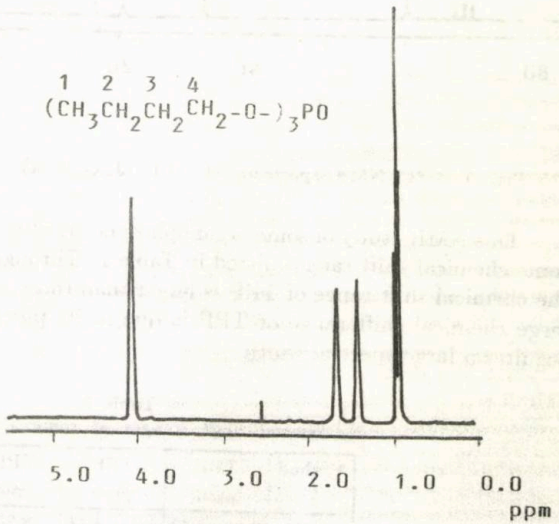

Fig. 8.– ^{1}H NMR spectrum of TBP at 399.650 MHz (JEOL GX-400).

Contrary to the ^{1}H NMR spectrum, the ^{13}C one can easily be assigned. The pattern of the spectrum (Fig.9) comprises three groups of resonance. The first group at low field is represented by a peak which appears at δ = 67.21 ppm and corresponds to the carbon atom labelled C-4. This peak is split into two due to ^{31}P, ^2J(COP)=6.1 Hz. The second peak appears at the middle field (32.29 ppm) and corresponds to the carbon atom labelled C-3. In this case, we also observe a doublet due to the three-bond coupling with ^{31}P, ^3J(COOP)=7.3 Hz. The third group of resonance at high field is constituted by the two peaks at δ = 18.59 ppm

and $\delta = 13.39$ ppm, which are originated from the carbon atoms labelled C-2 and C-1, respectively. One can remark that three-bond coupling constant is larger than that of the two-bond coupling depending on the dihedral angle of the three bonds, this is known as the K a r p l u s effect. ^{31}P NMR spectrum of TBP shows a heptet pattern of broad signals, which is originated from the coupling of long distance four-bound, $^{n}J(^{1}H^{31}P)$, $(n = 4, 5, 6)$. The ^{31}P chemical shift appears at $\delta = 1.87$ ppm, ^{3}J(POCH)=7.1 Hz. These methods described above are enough to clarify the TBP structure.

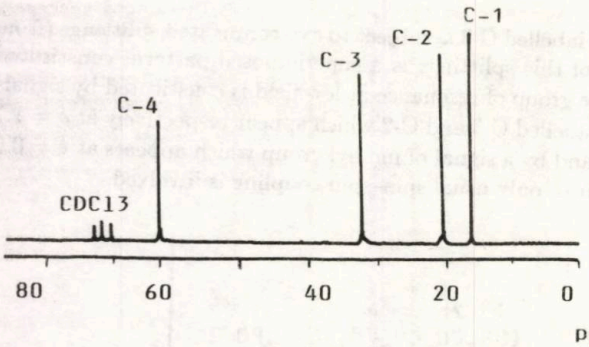

Fig. 9.– ^{13}C NMR spectrum of TBP (JEOL-90A).

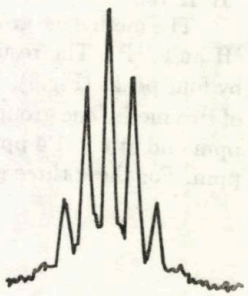

Fig. 10.– ^{31}P NMR spectrum of TBP (JEOL-90A).

This NMR study of some organophosphorus compounds has allowed to collect some chemical shift ranges, listed in Table 1. Through this table, we remark that the chemical shift range of TPP is larger than those of TBP, TEP and TMP. The large chemical shift range of TPP is due to its phenyl group whose observation requires a large spectral width.

Table 1

Chemical Shift Ranges of some Phosphates

Method	TBP ppm	TEP ppm	TPP ppm	TMP ppm
^{1}H	3.92...4.32	1.34...4.11	8.25	3.78
^{13}C	13.4...67.2	15.6...63.1	120...150	52.8
^{31}P	–1.87	–2.27	–18.65	0.7

4. Conclusions

Concerning the substances dealt with here, the following conclusions can be withdrawn:

1. Among the organophosphorus compounds taken into account, triphenyl phosphate has the largest carbon-13 chemical shift range, this is due to the phenyl group.

2. Carbon-13 chemical shift range of TBP, TEP and TMP are of the same order.

3. In some trialkylphosphates, K a r p l u s effect is observed.

4. In case of TBP, three-bond coupling constant is larger than two-bond coupling one.

5. In ^{31}P NMR spectra, some peaks cannot be observed because of the weakness of coupling constants higher than the third order.

Received, March 30, 1994

Haut Commissariat à la Recherche /CDM/LSO, Alger, Algérie
and
National Chemical Laboratory for Industry, Tsukuba Science City, Japan

REFERENCES

1. M o r r i s G.A., Magn. Reson. Chem., **24**, 371 (1986).
2. B e n n R., R u f i n s k a A., Angew. Chem. Int. Ed. Engl., **25**, 861 (1986).
3. B e n n R., G u n t h e r H., Angew. Chem. Int. Ed. Engl., **22**, 350 (1983).
4. S i l v e r s t e i n R.M., B r a s s l e r G.C., M o r i l l T.C., *Spectroscopic Identification of Organic Compounds.* 4th Ed., J.Willey and Sons, New York, 1981.
5. V e r k a d e J.G., Q u i n L.D., *Phosphorus-31 NMR Spectroscopy in Stereochemical Analysis.* VCH, Weinheim, 1987.

STUDIUL PRIN REZONANŢĂ MAGNETICĂ NUCLEARĂ A UNOR COMPUŞI ORGANOFOSFORICI

(Rezumat)

Se efectuează studiul câtorva compuşi organofosforici cu ajutorul diferitelor tehnici RMN şi anume cea a protonului, a carbonului-13 şi a fosforului-31.

Observaţiile făcute în timpul cercetărilor au permis să se ajungă la concluzia că fosfaţii de tributil, de trietil şi de trimetil au, în mod practic, un acelaşi interval de deplasări chimice ale carbonului-13 şi că la unii trialchilfosfaţi se pune în evidenţă efectul K a r p l u s.

BULETINUL INSTITUTULUI POLITEHNIC DIN IAŞI
Tomul XLI (XLV), Fasc. 1–4, 1995
Secţia II
CHIMIE ŞI INGINERIE CHIMICĂ

D.C. 667.15; 621.67

COMPUTER AIDED SIMULATION AND DESIGN OF TWO-ROLL MIXING AND CALENDERING PROCESSES OF POWER-LOW FLUIDS

BY
SIMION S. PETROVAN

1. Introduction

Two-roll mixing and calendering processes play an important role in the polymers processing, the former for the preparation of these in order to be processed on other equipments and the latter for the quality of the obtained products. To know the fundamentals of these processes is also possible to utilize the computer simulation and this may be used for the designing purposes.

This paper presents the theoretical considerations and the algorithm for a computer program which can be used for the simulation of the two roll mixing and calendering of power-law fluids, and also for the designing of the two-roll mixers and calenders.

2. Theoretical Part

The equation of motion for unit volume of fluid is [1], [2]:

$$\rho \frac{\mathrm{D}v}{\mathrm{D}t} = [\nabla \cdot \tau] - \nabla P + \rho g, \tag{1}$$

where ρ, v, τ, P and g are the density, velocity, stress tensor, pressure and gravitation acceleration, respectively. Eq.(1) is the mathematical expression of the N e w t o n's second law, wich may also be written in the form:

$$\rho a = F_1 + F_2 + F_3, \tag{2}$$

where F_1, F_2 and F_3 are the viscous, pressure and gravitational forces and a – the acceleration.

In the conditions of flowing between two rotating rolls, the acceleration term can be ignored due to the laminar character of the flow. Also, by neglecting the gravitational forces, the Eq.(1) simplifies to the following form:

$$[\nabla \cdot \tau] = \nabla P. \tag{3}$$

Additional assumptions can be made in order to simplify the divergence term from Eq.(3), according to Fig.1, as follows: a) the velocities components in the y- and z-directions may be ignored; b) variation of v_x in x-direction is neglected, being much less than that in y-direction; c) the fluid is considered as incompressible; d) due to the fact that the fluid flows in x-direction, pressure variation in the other two directions can be also ignored.

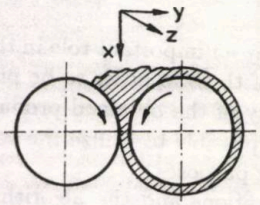

Fig. 1

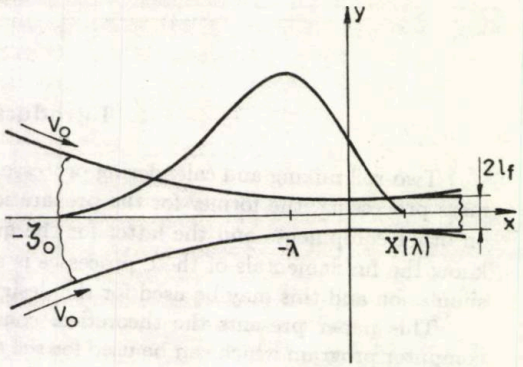

Fig. 2

In these conditions, Eq.(3) reduces to:

$$\frac{\partial \tau_{yx}}{\partial y} = \frac{\partial P}{\partial x}. \tag{4}$$

If new dimensionless variables ζ and ζ_1 are introduced, defined by [2], [3]:

$$\zeta = \frac{x}{(2Rl_0)^{1/2}}, \tag{5_1}$$

$$\zeta_1 = \frac{y}{(2Rl_0)^{1/2}}, \tag{5_2}$$

the Eq.(4) becomes

$$\frac{\partial \tau}{\partial \zeta_1} = \frac{\partial P}{\partial \zeta}, \tag{6}$$

where, for simplicity reasons, the subscripts for stress tensor were dropped and R and l_0 are the rolls radius and half distance at the nip, respectively.

It is considered here that the calender has equal sized rolls rotating at the same speed, or a symetrical calender. In a given section, perpendicular to the x-axis, where the pressure gradient is constant, Eq.(6) can be integrated resulting:

$$\tau = \frac{\partial P}{\partial \zeta}\zeta_1 = \overline{p}\zeta_1. \tag{7}$$

If the processed fluid obeys the power-law, defined by

$$\tau = k\dot{\gamma}^n = k\left(\frac{\mathrm{d}v_x}{\mathrm{d}y}\right)^n \tag{8}$$

and by introducing Eq.(8) in (7), it follows:

$$\frac{\mathrm{d}v_x}{\mathrm{d}\zeta_1} = \left(\frac{\overline{p}}{k}\right)^{\varepsilon}(2Rl_0)^{1/2}\zeta_1^{\varepsilon}, \tag{9}$$

where $\varepsilon = 1/n$ and k and n are the rheological parameters of the fluid, which can be determined from flowing curves. Upon integrating, Eq.(9) becames:

$$v_x = \frac{(2Rl_0)^{1/2}}{\varepsilon+1}\left(\frac{\overline{p}}{k}\right)^{\varepsilon}\zeta_1^{\varepsilon+1} + C, \tag{10}$$

with C – a constant of integration which is determined from the boundary condition

$$y = 1, \quad \left(\zeta_1 = \frac{1}{(2Rl_0)^{1/2}}\right), \quad v_x = v_0, \tag{11}$$

where v_0 is the rolls speed at their surface. It results

$$C = v_0 - \frac{(2Rl_0)^{1/2}}{\varepsilon+1}\left(\frac{\overline{p}}{k}\right)^{\varepsilon}\frac{l^{\varepsilon+1}}{\left[(2Rl_0)^{1/2}\right]^{\varepsilon+1}}. \tag{12}$$

The quantity l is a function of x position coordinate and can be related by the equation:

$$l = l_0 + R - (R^2 - x^2)^{1/2}. \tag{13}$$

By expanding the third term from rightside of Eq.(13) in Taylor's serie and retaining only the first two terms one obtains, by making use of Eq.(5_1), too:

$$l = l_0(1+\zeta^2). \tag{14}$$

If Eq.(14) is introduced into (12) and this one into (10), the following dimensionless speed is obtained

$$\frac{v_x}{v_0} = 1 + \left(\frac{\overline{p}}{k}\right)^{\varepsilon} \frac{1}{v_0(\varepsilon+1)} \left\{ (2Rl_0)^{1/2}\zeta_1^{\varepsilon+1} - \frac{l_0^{\varepsilon+1}(1+\zeta^2)^{\varepsilon+1}}{\left[(2Rl_0)^{1/2}\right]^{\varepsilon}} \right\}. \tag{15}$$

Due to symmetrical condition, the volumetric rate of flow through the rolls, per unit width, is given by the integral

$$M_v = 2\int_0^l v_x \mathrm{d}y = 2(2Rl_0)^{1/2} \int_0^{\zeta_{1w}} v_x \mathrm{d}\zeta_1. \tag{16}$$

If Eq.(15) is introduced into (16) and after integration, the following expression for the volumetric flow rate is obtained:

$$M_v = 2l_0(1+\zeta^2)\left\{ v_0 - \left(\frac{\overline{p}}{k}\right)^{\varepsilon} \frac{l_0^{\varepsilon+1}(1+\zeta^2)^{\varepsilon+1}}{(\varepsilon+2)\left[(2Rl_0)^{1/2}\right]^{\varepsilon}} \right\}. \tag{17}$$

But, according to continuity equation, the volumetric flow rate is equal to that at the exit of the calendering zone (Fig.2) that is:

$$M_v = M_{vf} = 2v_0 l_f = 2v_0 l_0(1+\lambda^2), \tag{18}$$

where λ is the value of the ζ variable at the exit point from the calendering zone.

By introducing the equation (18) into (17), the pressure gradient is obtained finally:

$$\overline{p} = \frac{\partial P}{\partial \zeta} = K \frac{(\zeta^2 - \lambda^2)^{1/\varepsilon}}{(1+\zeta^2)^{1+2/\varepsilon}}, \tag{19}$$

where the constant K is given by the expression:

$$K = k\left[(\varepsilon+2)\frac{v_0}{l_0}\right]^{1/\varepsilon} \left(\frac{2R}{l_0}\right)^{1/2}. \tag{20}$$

To obtain the pressure function $P(\zeta)$ it must to integrate the pressure gradient function given by Eq.(19). This is difficult in an analytical way, so that, in the following, a numerical procedure will be given.

From Eq.(19) one obtains:

$$\int_P^0 \mathrm{d}P = K \int_\zeta^\lambda f(\zeta,\lambda)\mathrm{d}\zeta \quad \text{and consequently} \quad P = K \int_\lambda^\zeta f(\zeta,\lambda)\mathrm{d}\zeta, \tag{21}$$

where

$$f(\zeta,\lambda) = \frac{(\zeta^2-\lambda^2)^{1/\varepsilon}}{(1+\zeta^2)^{1+2/\varepsilon}}. \tag{22}$$

To perform integration of function $f(\zeta,\lambda)$ it is proceeded as follows: a) function $f(\zeta,\lambda)$ is tabulated on a sufficiently large domain, that is from a ζ minimum bound to λ; b) integration is performed step by step, from $\zeta=\lambda$, where $P=0$, to a value of $\zeta=\zeta_0$, where P function is again close to zero, in the limits of a given error, as results from Fig.2.

Values of the pressure function are also tabulated, in order to be used for the determination of the roll-separating force.

The power required to drive the rolls is given by

$$P_u = 2Lv_0(2Rl_0)^{1/2}\int_{\zeta_0}^\lambda \tau_w \mathrm{d}\zeta, \tag{23}$$

where L is the length of the rolls and τ_w – the stress tensor at the walls, which, according to Eq.(7), is

$$\tau_w = \overline{p}\zeta_{1w} = \overline{p}\frac{l}{(2Rl_0)^{1/2}} = \overline{p}\frac{l_0(1+\zeta^2)}{(2Rl_0)^{1/2}}. \tag{24}$$

By introducing Eqs.(24) and (19) into (23) and performing numerical integration, one obtains

$$P_u = 2LKl_0v_0I, \tag{25}$$

where I is the integral

$$I = \int_{\zeta_0}^\lambda \frac{(\zeta^2-\lambda^2)^{1/\varepsilon}}{(1+\zeta^2)^{2/\varepsilon}}\mathrm{d}\zeta. \tag{26}$$

Roll-separating force may be calculated by integrating the pressure on the rolls surface contacting the processed material:

$$F_s = L \int P \mathrm{d}x = L(2Rl_0)^{1/2} \int_{\zeta_0}^{\lambda} P(\zeta)\mathrm{d}\zeta. \tag{27}$$

Integration of the $P(\zeta)$ function is performed numerically, using the tabulated values obtained as explained above.

3. Programming Considerations

3.1. Program Algorithm

The main steps of the program are as follows: a) data input; b) computes the λ parameter from the equation

$$l_f = l_0(1 + \lambda^2), \tag{28}$$

where l_f is the half of the sheet thickness leaving the calender nip; c) determines the coordinate ζ_0, by numerical calculation, according to the procedure described above; d) determines the parameters of the nip geometry; e) calculates the maximum pressure, P_m; f) plots the axes; g) plots the relative pressure distribution given by

$$P_{\mathrm{rel}} = \frac{P}{P_{\max}} \tag{29}$$

versus the ζ variable; h) plots the velocity profile at certain points on the ζ-axis; i) plots the rolls profile; j) copies the screen with the relative pressure and velocity distributions (optionally); k) displays the results; l) computes the mark (optionally); m) copies the screen (optionally).

The user can watch the running of the program by the displayed working step on the uper line of the screen.

The elaborated program presents the following facilities: a) computes the pressure distribution in the material and the maximum pressure; b) plots the relative pressure versus ζ variable in the calendering zone; c) plots the velocity profile at different positions along ζ axis; d) computes the power required to operate the calender; e) computes the roll-separating force; f) computes the volumetric flow rate of the fluid; g) compares the results from a), d), e) and f) with those introduced by the user, optionally, and gives a mark as follows:

- $0 < \mathrm{es} \leq \mathrm{eps}$, mark = 10;
- $\mathrm{eps} < \mathrm{es} \leq 2 \cdot \mathrm{eps}$, mark = 8;
- $2 \cdot \mathrm{eps} < \mathrm{es} \leq 3 \cdot \mathrm{eps}$, mark = 6;
- $\mathrm{es} > 3 \cdot \mathrm{eps}$, mark = 4,

where es is the maximum error determined as:

$$(30) \qquad es = \max\left\{\frac{|P_m - P_{mu}|}{P_m}, \frac{|P_u - P_{uu}|}{P_u}, \frac{|F_s - F_{su}|}{F_s}, \frac{|M_v - M_{vu}|}{M_v}\right\},$$

where P_m, P_u, F_s, M_v are maximum pressure, power, roll-separating force and flow rate, computed by running the program and $P_{mu}, P_{uu}, F_{su}, M_{vu}$ are the corresponding values determined and introduced by the user; h) copies the screen with the pressure and velocities profiles (optionally); i) copies the screen with the main results displayed on it (optionally).

The above facilities are also offered for the Newtonian fluids, when $\varepsilon = 1$ and $k \equiv \mu$. For this case the analytical form of the integral from Eq.(21) is used and defined in the program.

3.2. Data Needed by the Program

The program needs the following data to by introduced:

1° im-index according to which it is decided to compute (im$\neq$ 0) or not (im=0) the mark given to the user. If the user wants to be verified by the computer (for example in case when the program is used for teaching purposes) then he is waited to introduce the following data: a) maximum pressure, [N/m^2]; b) power, [W]; c) roll-separating force, [N]; d) fluid flow rate, [L/s];

2° n – number of the intervals at which function (22) is calculated in order to evaluates numerically the ζ_0 value;

3° k – consistency index of the processed polymeric material, [N.s$^{1/\varepsilon}$/m^2];

4° e – $1/nf$, nf being the fluidity index of the polymer;

5° eps – error used to compute the mark given to the user;

6° er – error used to test the condition when ζ_0 is determined for Newtonian fluids for which the algebraical equation of pressure function is solved numerically. Termination condition is

$$(31) \qquad \Delta\zeta < \text{er},$$

where $\Delta\zeta$ is the increment given by

$$(32) \qquad \Delta\zeta = \frac{\lambda - z_{\min}}{100};$$

7° l_f – half of the sheet thickness, [m];

8° r – rolls radius, [m];

9° l_0 – half of the distance between the rolls at the nip, [m];

10° l – rolls length, [m];

11° v – peripherical speed of the rolls, v_0, [m/s];

12° it – Newtonian fluid viscosity, μ, [Ns/m^2];

13° uv – number of pixels for plotting the speed vector, v_0;

14° ulz – number of the pixels for representing the l_0 segment;

15° z min – lower bound to which the function (22) is evaluated (for power-law fluids) or to which the ζ_0 value is searched for;

16° a – number of the pixels of the left side of the point of coordinates ζ_0.

For a more facile understanding of the manner in which the pressure and velocity distributions are ploted, Fig.3 is given.

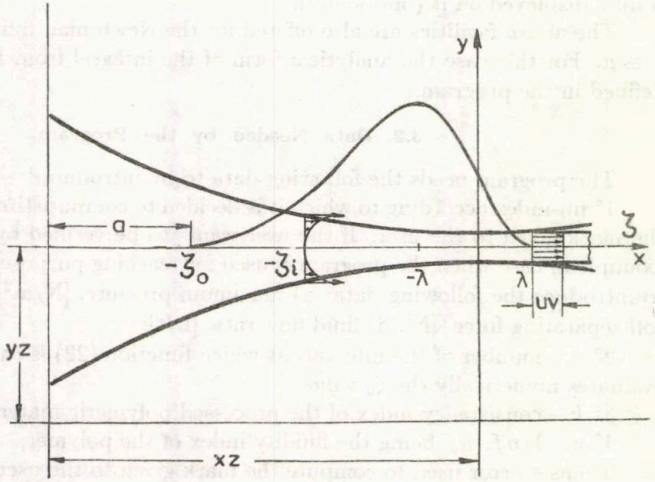

Fig. 3

4. Results and Discussions

In Figs.4...6 the pressure and velocity distributions are given for three polymeric materials of different rheological (k and n) constants. If the three figures are compared, one can notice that the flow index n of the polymer determines the character of the pressure and velocity distributions. So, a rubber (having flow index $n = 0.2$) presents a velocity distribution without backflow zones (Fig.4). Also, the shear rate is about zero in almost all the mixing zones, except two layers near the rolls surfaces and mainly at input region of the nip. This kind of distribution results in a low mixing efficience.

In Fig.5, the pressure and velocity distributions of a Newtonian polymer are given, revealing a stagnation point and a backflow zone contributing to mixing process due to the shearing stresses distributed in the whole space, except the two sections where pressure gradient is zero (i.e. at maximum pressure and exit zones).

The pressure and velocity distributions for a dilatant fluid are given in Fig.6. The velocity varies about linearly from the rolls surface to the midplane of the

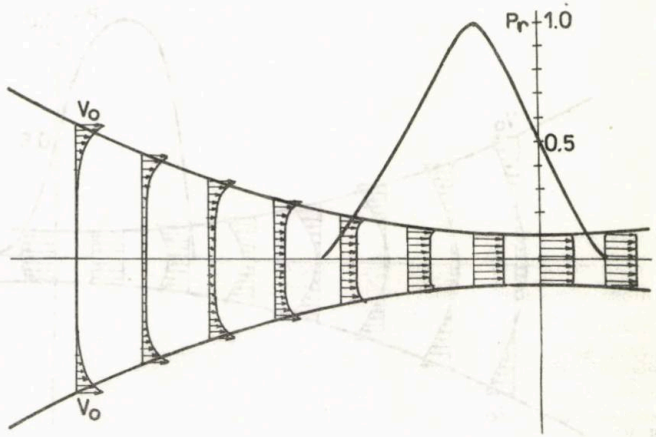

Fig. 4

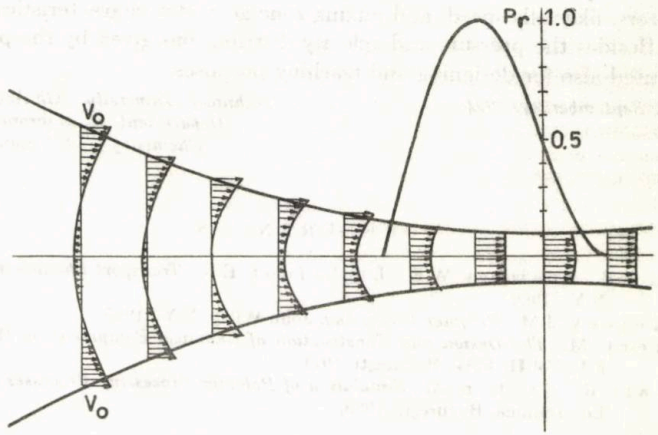

Fig. 5

mixing zone. Backflow occurs, also, in this case, from a stagnation point backward to the entrance zone.

5. Conclusions

1. Based on the theoretical considerations, presented in the paper, the algorithm and main facilities of a computer program are given.

2. The program can be used to simulate the mixing and calendering processes of different polymeric materials, characterized by their rheological parameters k and n from power-law equation.

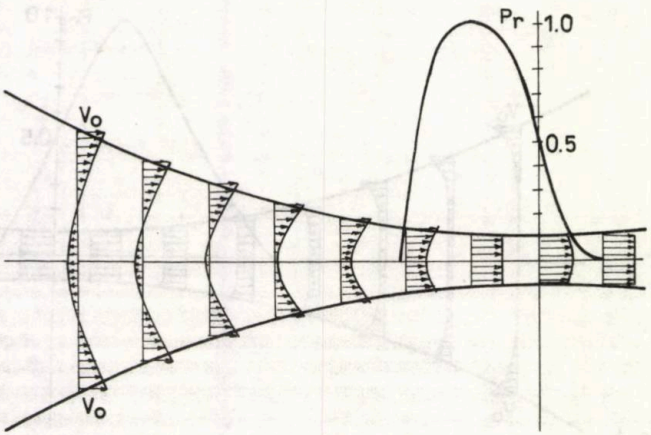

Fig. 6

3. The program allows, also, to study the influence of some technological parameters, like rolls speed, and mixing zone geometry characteristics.

4. Besides the pressure and velocity distributions given by the program, this can be used also for designing and teaching purposes.

Received, September 24, 1994

Technical University "Gh.Asachi", Jassy,
Department of Macromolecular
Chemistry and Technology

REFERENCES

1. Bird R.B., Stewart W.E., Lightfoot E.N., *Transport Phenomena.* John Wiley, N.Y., 1960.
2. McKelvey J.M., *Polymer Processing.* John Wiley, N.Y., 1965.
3. Renert M., *The Design and Construction of Chemical Equipment* (in Romanian). Sec. Ed., Vol.II, EDP, Bucureşti, 1971.
4. Mihail R., Ştefan Al., *Simulation of Polymer Processing Processes* (in Romanian). Ed. Tehnică, Bucureşti, 1989.

SIMULAREA ŞI PROIECTAREA ASISTATĂ DE CALCULATOR A PROCESELOR DE VĂLŢUIRE ŞI CALANDRARE A FLUIDELOR CARE RESPECTĂ LEGEA PUTERII

(Rezumat)

Se prezintă consideraţiile teoretice şi algoritmul pentru un program de calculator care poate fi utilizat pentru simularea proceselor de vălţuire şi calandrare şi pentru proiectarea utilajelor de prelucrare a materialelor polimerice cu cilindri. Este propus un procedeu numeric original pentru integrarea funcţiei gradientului de presiune, în cazul fluidelor ne-newtoniene. Se poate studia influenţa caracteristicilor reologice ale materialului prelucrat şi ale geometriei zonei de amestecare. Programul poate fi utilizat, de asemenea, pentru scopuri didactice.

BULETINUL INSTITUTULUI POLITEHNIC DIN IAŞI
Tomul XLI (XLV), Fasc. 1–4, 1995
Secţia II
CHIMIE ŞI INGINERIE CHIMICĂ

D.C. 54-92; 661.17

POLYMERIC COMPOSITES WITH METALLIC POWDERS
I. PHYSICO-MECHANICAL CHARACTERISTICS

BY

M. RUSU and DANIELA-LORENA RUSU

1. Introduction

In the class of polymeric composite materials, of special interest are those containing powdery filling material, particularly composites with metallic powders [1], [2]. Due to their special, indeed, properties, they are utilized nowadays in several domains of activity, such as: screening of ionizing radiation, screening against the interference of electromagnetic and radiofrequency waves, preventing of electrostatic charges, as materials with magnetic properties, a.s.o.

The present papers aims at characterizing some polyvinyl chloride-based mixtures containing various proportions of copper, aluminium and zinc powders, in order to evidence the influence of their nature, ratio and mode of obtention on the physico-mechanical characteristics of such compounds.

2. Experimental Part

Polyvinyl chloride (PVC) – type S 58 D and copper, aluminium and zinc powders – the particles' maximum dimension being of 70μm – have been employed.

For the obtainement of PVC – based mixtures, the polymer has been mixed with the necessary auxiliaries, according to the following receipt: PVC S 68 D 100 gravimetric parts (p); tin dibutyldimaleate 4 p; epoxidized soybean oil 2.5 p; Kane Ace B 11 A (as impact modifier) 5 p; Loxiol G 40 (as liquid lubricant) 1.2 p and Loxiol G 70 (as solid lubricant) 1.3 p, a Hanschel-type mixer (Germany) with an 140 L warm vat being employed.

The studied compounds have been obtained by adding different amounts of the above-mentioned metallic powders (0; 5; 10; 15; 20 and 25 p metallic powder to 100 p PVC mixture) to the PVC mixture obtained according to the above receipt.

Homogenization of these mixtures was performed in a double-arms mixer.

Half of the mixtures thus obtained were subjected to compounding on a laboratory roller with cylinders heated at 170°C, duration of rolling being of 10 min.

Out of the obtained sheets, plates of 0.5, 1.0 and 4.0 mm in thickness have

been produced; the pressing operation being performed in the following conditions: duration of pre-heating – 10 min., duration of pressing – 10 min., temperature of pressing – 170°C and pressure of pressing – 17 MPa, random compounds being thus obtained [3], [4].

The other half of the mixtures was transformed in 0.5, 1.0 and 4.0 mm thick plates, through direct pressing (without rolling) in the following conditions: duration of pre-heating – 20 min., duration of pressing – 10 min., temperature of pressing – 175°C and pressure of pressing – 18.5 MPa, seggregate compounds being thus obtained.

From the plate thus obtained, test samples have been cut up, for which tensile strength, elongation-at-break and Izod impact notched strength were determined (according to STAS 6642-73 and STAS 7310-87).

3. Results and Discussion

The obtained results are listed in Table 1 and plotted in the following figures, as well.

Table 1

Composition and Physico-Mechanical Characteristics of Compounds

Compounds composition			Physico-mechanical characteristics					
			Statistic compounds			Seggregated compounds		
PVC blend	Nature of metallic powder	Metallic powder	Tensile strength MPa	Elongation-at-break %	Izod impact notched kgf·cm·cm^{-1}	Tensile strength MPa	Elongation-at-break %	Izod impact notched kgf· cm·cm^{-1}
100	–	–	583	1.5	1.25	506	1.3	2.96
100		5	583	1.4	1.50	352	1.2	2.93
100		10	566	1.35	2.72	310	1.15	2.31
100	Copper	15	550	1.30	3.74	301	1.15	2.35
100		20	493	1.2	3.70	358	1.1	2.10
100		25	555	1.0	2.75	416	1.0	1.42
100		5	611	1.35	2.50	362	1.25	1.95
100		10	516	1.2	3.65	308	1.2	1.55
100	Aluminium	15	470	1.1	3.75	297	1.0	1.57
100		20	456	0.9	3.00	298	0.9	1.25
100		25	495	0.8	2.73	334	0.8	1.28
100		5	615	1.4	2.59	405	1.4	1.49
100		10	575	1.2	3.40	358	1.3	1.40
100	Zinc	15	503	1.20	3.75	314	1.2	1.30
100		20	450	1.0	3.10	303	1.0	1.10
100		25	541	0.9	2.35	359	0.9	1.06

Analysis of these results evidences that, regardless of the nature of the metallic powders introduced in the mixture, for statistic compounds the diagrams plotting

the variation of relative tensile strength versus the contents of filling material have an S-shape (Fig.1). The maximum of these diagrams corresponds to a content of 5% metallic powder, while the minimum values are recorded at a content of 16...17% filling material.

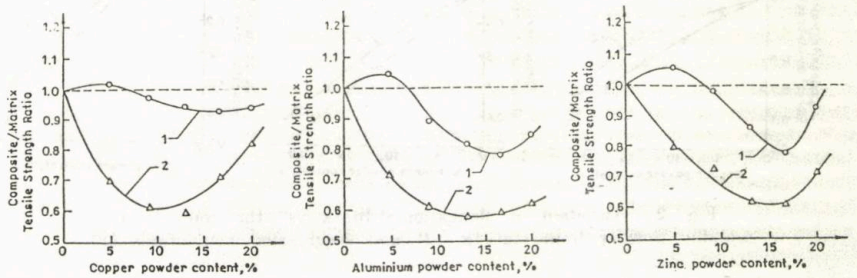

Fig. 1.– Variation of relative tensile strength vs. the content of metallic powder from statistic (*1*) and seggregated compounds (*2*).

In the case of compounds containing copper powder, tensile strength is slightly modified on addition and then increase of the filling material ratio. With compounds containing more than 13% aluminium or zinc powder, decrease of the tensile strength exceeds 15%.

For seggregated compounds, the variation diagrams of tensile strength – as depending on the mixture's composition – evidence the presence of a minimum, the position of which corresponds to filler contents ranging between 10% and 15%. The minimum value of tensile strength represents only 60% of that of the compound taken as reference.

Irrespective of the mode in which they are obtained, elongation-at-break values of the compounds containing metallic powders decrease continuously with the introduction and increase of the filling material ratio in mixtures (Fig.2), the only exception are the compounds containing zinc powder, a case in which introduction of 5% filler induces increase of the elongation-at-break, further increase of the metallic powder content determining a decrease in the values of this characteristic.

For all types and contents of metallic powders, elongation-at-break of the seggregated compounds is higher than in the case of statistic compounds.

The variation curves of the relative Izod impact notched strength, as depending on the content of metallic powder – whichever its nature my be – evidence the presence of a maximum, whose position corresponds to a ratio of about 13% filling material (Fig.3). In the case of seggregate compounds, the value of this characteristic decreases with increasing the content of metallic powder.

For all types and ratios of metallic powder in the mixture, tensile strength, as well as the Izod impact strength of statistic compounds have higher values as compared with the seggregated ones.

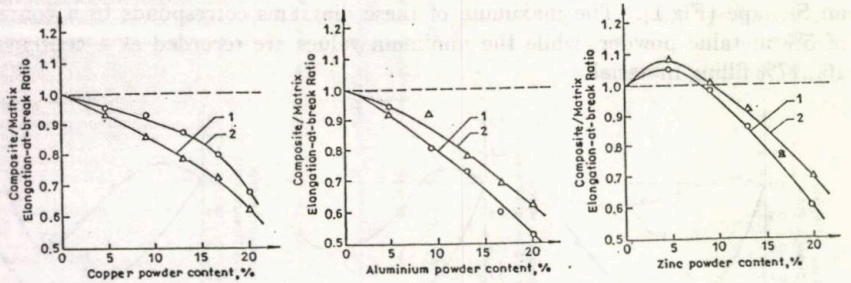

Fig. 2.– Variation of elongation-at-break vs. the content of metallic powder from statistic (*1*) and seggregated compounds (*2*).

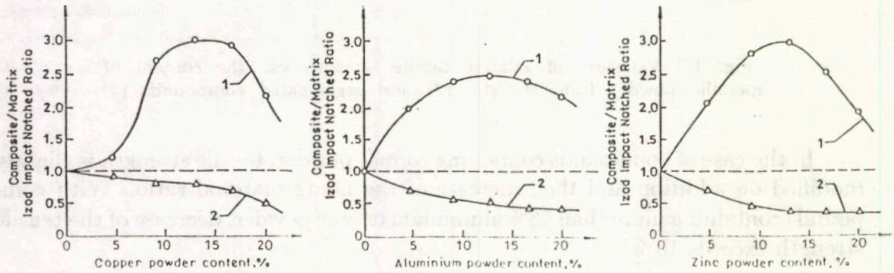

Fig. 3.– Variation of Izod impact notched strength vs. the content of metallic powder from statistic (*1*) and seggregated compounds (*2*).

An unique and absolute interpretation of the above results is quite difficult in this stage, yet some observation are to be made.

The S-shape of the diagrams evidencing the variation of tensile strength with the ratio of metallic powder, observed with statistic compounds, proves that polymer's structuring (i.e., formation of a border layer – the mesophase) occurs around the metallic particles, quite different from that observed with the rest of its matrix. The structuration degree depends on the nature and ratio of metallic powder, being higher for compounds containing copper powder (characterized by increased adhesion to the polymeric matrix) and lower, respectively, for compounds with aluminium and zinc powder. Such assertion is confirmed by the less significant modification of tensile strength when using copper powder as filler, as compared with the other two types of metallic powder.

The polymer's structure around metallic particles is stronger with statistic compounds, as compared with the seggregated ones, which is supported by the fact that both tensile and Izod impact strength values of statistic compounds are higher than those of the seggregated ones.

The positions corresponding to minimum values on the variation diagrams of the tensile strength versus the metallic powder content might correspond to the

critical volume [2], [3]. The fact that this volume is obtained at lower ratios of filler, in the case of statistic compounds, comparatively with the seggregate ones, agrees with the existent literature data [5], [6].

4. Conclusion

The physico-mechanical characteristic of rigid compounds of polyvinyl chloride containing metallic powders depend on both their nature and ratio, and on the mode of mixtures obtainment. The critical volume of filler is reached at metallic powder contents of about 17%, for statistic compounds and of 10% and 15%, respectively, for seggregated ones.

Received, June 15, 1994

Technical University "Gh.Asachi", Jassy,
Department of Macromolecular
Chemistry and Technology

REFERENCES

1. Norman R.H., *Conductive Rubbers and Plastics.* Applied Science, Essex, England, 1970.
2. Bhattacharya S.K. (Ed.), *Metal-Filled Polymers: Properties and Applications.* Marcel Dekker Inc., New York and Basel, 1986.
3. Kusy R.P., J. Appl. Phys., **48**, *12*, 5301 (1977).
4. Bhattacharya S.K., Chaklader A.C.D., Polym.-Plast. Technol. Eng., **19**, *11*, 21 (1982).
5. Gurland J., Trans. Metall. Soc., AIME, *236*, 642 (1966).
6. Kusy R.P., Turner D.T., Nature, **299**, *2*, 58 (1971).

COMPOUNDURI DE POLIMERI CU PULBERI METALICE
I. Caracteristici fizico-mecanice

(Rezumat)

S-a studiat influenţa naturii şi proporţiei de pulberi metalice (cupru, aluminiu, zinc) asupra caracteristicilor fizico-mecanice ale unor compounduri rigide pe bază de policlorură de vinil. În urma analizei rezultatelor obţinute s-a stabilit că, în compoundurile analizate, volumul critic de material de umplutură este atins la conţinuturi de aproximativ 17% pulbere metalică în cazul compoundurilor statistice şi la proporţii cuprinse între 10% şi 15% la compoundurile segregate.

BULETINUL INSTITUTULUI POLITEHNIC DIN IAŞI
Tomul XLI (XLV), Fasc. 1–4, 1995
Secţia II
CHIMIE ŞI INGINERIE CHIMICĂ

D.C. 672.768.2; 54-92

SEMI-INTERPENETRATING POLYMER NETWORK BASED PVC
IV. AGING AND STABILIZATION OF THE FILLED PVC/NBR MIXTURES

BY

CORNELIA VASILE, A. STOLERIU,
LUCIA ODOCHIAN and MĂRIOARA LUCHIAN

1. Introduction

In our previous papers [1]...[5] the compatibility of polyvinyl chloride (PVC) with acrylonitrile (AN) butadiene copolymers (NBR) (PVC/NBR) systems establishing the acrylonitrile content which assures the improvement of certain property such as: impact strength (NBR) must have 28% AN, plasticizer effect (NBR with an AN content higher than 33%), and also processability characteristics of various mixtures have been studied.

It is well-known that most polymer mixtures are incompatible, evolving in time and in service conditions towards thermodynamic equilibrium, commonly, of phases separation [6], [7].

Stabilization against heat, light, oxygen, etc., attack must therefore take into account both this phenomenon and the chemical structure preservation.

There are very few studies in this direction, these being centered either on morphology stabilization or thermoxidative or photostabilization.

In this paper we tray to follow the both aspects on the filled PVC/NBR systems whose both components are very susceptible to the environmental factors.

2. Experimentals

2.1. Materials

Characteristics of polymers used in this study are presented in previous papers [3],...,[5] and, also, crosslinking agents and reaction conditions.

In this paper, the filled 80 p PVC/20 p NBR mixtures have been studied. As fillers: carbon black, ZnO, TiO_2 and chalk have been employed, 10% of these have been mixed with the two polymers in 10% tetrahydrofurane solution. After the solvent evaporation the crosslinking reaction has been carried out. On the basis of previous results as crosslinking agents are selected, three ethylene glycol dimethacrylate ester (10%) (TED), bismalenimide (0.5%...3%) (BM), and phenol-

formaldehyde resins of novolack type (NOV).

Crosslinking reaction with first agent (TED) proceeds in presence of dicumyl peroxide (DCP) (1% in respect with TED), and with the BM, ZnO or diphenylguanidine (DPG) as accelerators (crosslinking agent/accelerator = 3/1) have been used.

2.2. Aging

The aging behaviour has been studied by keeping the samples at room temperature a long period of time and by the employing two ways of accelerated aging: a) thermoxidative aging in air circulating oven at 100°C, various periods of time; b) photooxidative aging at xenotest device 450LF type in the following conditions: a xenon lamp of 1,500 W which simulates solar light, in repeated cycles of dark and light different periods of time of: 100, 200 and 300 h which are equivalent with 42, 84 and 126 days.

2.3. Investigation Methods

Behaviour in the accelerated artificial aging conditions has been established by means of: optical microscopy, IR spectroscopy and thermooptical methods.

Microscopical examination has been effected by a IOR-Microscope MC-1 type, magnitude 600× in phase contrast.

In order to exposure the same portion of films at IR beam the films have been placed in a special support (double ring). The IR spectra have been recorded on a Perkin-Elmer spectrometer in 400...4,000 cm^{-1} wave length range. Their interpretation has been made according to the literature data [9],...,[11].

The device for thermooptical methods has been previously described [8]. The experiments have been conducted from room temperature to 200°C using a heating rate of 3°C/min. The phase transition temperatures on the thermooptical curves have been taken as the beginning of the slope changes in the light transmitted intensity versus temperature curves [12],...,[14].

3. Results and Discussions

The results of the microscopical examination are presented in the Figs.1 and 2.

It is very easy to remark that after crosslinking the homogeneity of mixture is very much improved (Fig.1). The stability is also improved, because the unchanged picture for the crosslinked mixtures is obtained after thermoxidative aging and only a few changes appear after photooxidation (Fig.2 *d*).

Uncrosslinked PVC/NBR mixture becomes after photooxidation more and more heterogeneous (Fig.2 *a*), the longer is exposure period as well as for the uncrosslinked mixtures with various fillers; a tendency of the agglomeration of fillers particles is also to be noticed (Fig.2 *b*).

Phases separation are soon observed in the mixtures photostabilized with a benzophenone type light stabilizer or antioxidant (phenol-styrenate). The un-

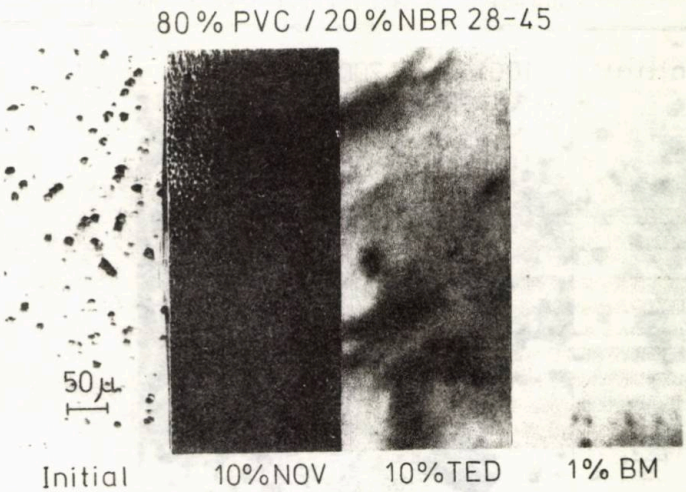

Fig. 1.– Modification of the microscopical aspect of the 80 p PVC/20 p NBR 28-45 mixture after crosslinking with the indicated on figure crosslinking agents.

crosslinked mixtures with TiO_2 are also very deteriorated after 100 h exposure then opacity, yellowishing and failure of films appear (Fig.2 *c*).

Crosslinked films are much stable, keeping the initial distribution of fillers, the best results being obtained in the case of the crosslinking with TED, the semi-interpenetrating polymer network formed has a high photoresistance due to the presence of methacrylic component [9],...,[11].

During accelerated thermoxidative aging, the crosslinked samples remain unchanged or the carbonyl band intensity decreases (Fig.3 *a*) or some modifications appear in 1 100...1 200 and 700...900 cm^{-1} regions by the apparition of ether group or disapparition of bonds corresponding to the antioxidant phenol-styrenate (Fig. 3 *b*).

IR spectra interpretation of photodegradated samples is based on the intensive studies reported in the literature concerning degradation of each component of the mixtures.

It has been established that the double bonds (1 680 cm^{-1}) disappear, appearing many types of oxygen containing groups (wide band with many shoulders in 1 600...1 800 cm^{-1} domain) of aldehyde or ketone type and also hydroxyl and carboxyl groups (3 300...3 500 cm^{-1} domain). The shape of the both bands evolves during degradation, namely oxygenated groups probably are transformed in carbonyl (1 715 cm^{-1}); firstly appear –OH and –OOH groups which are possible to form carboxyl groups (3 300...3 500 cm^{-1}). All these modifications have been observed in the present study, too, only few other pecularities for each system being evidenced (Figs.4 and 5).

It is to mention the important modifications in the uncrosslinked samples in respect to crosslinked ones especially that with TED/DCP system, which prevents

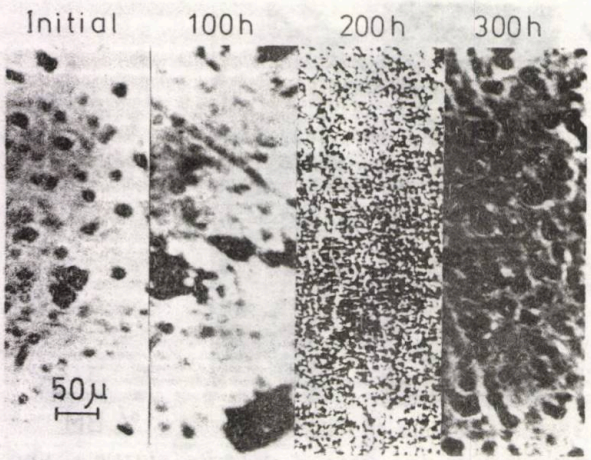

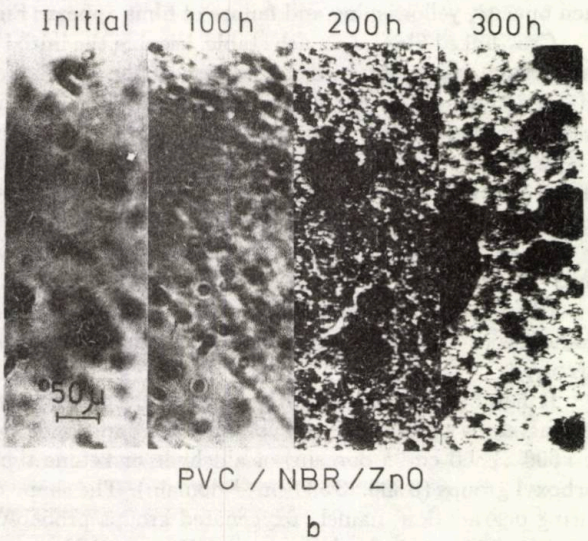

Fig. 2.– Modification of the microscopical aspect of the uncrosslinked and crosslinked 80 p PVC/20 p NBR 28-45 mixtures without (*a*) or with fillers (*b*) during accelerated photodegradation.

also the –OH groups development.

In the unfilled mixture appear many small bands in 2 000...2 600 cm^{-1} region (Fig.4) and in the sample crosslinked with TED after exposure, the peak from 850 cm^{-1} appears more pronounced.

From these spectra the carbonyl (I_{1715}) and hydroxyl index (I_{3400}) have been evaluated considering as reference the 680 cm^{-1} bands because it is almost unaf-

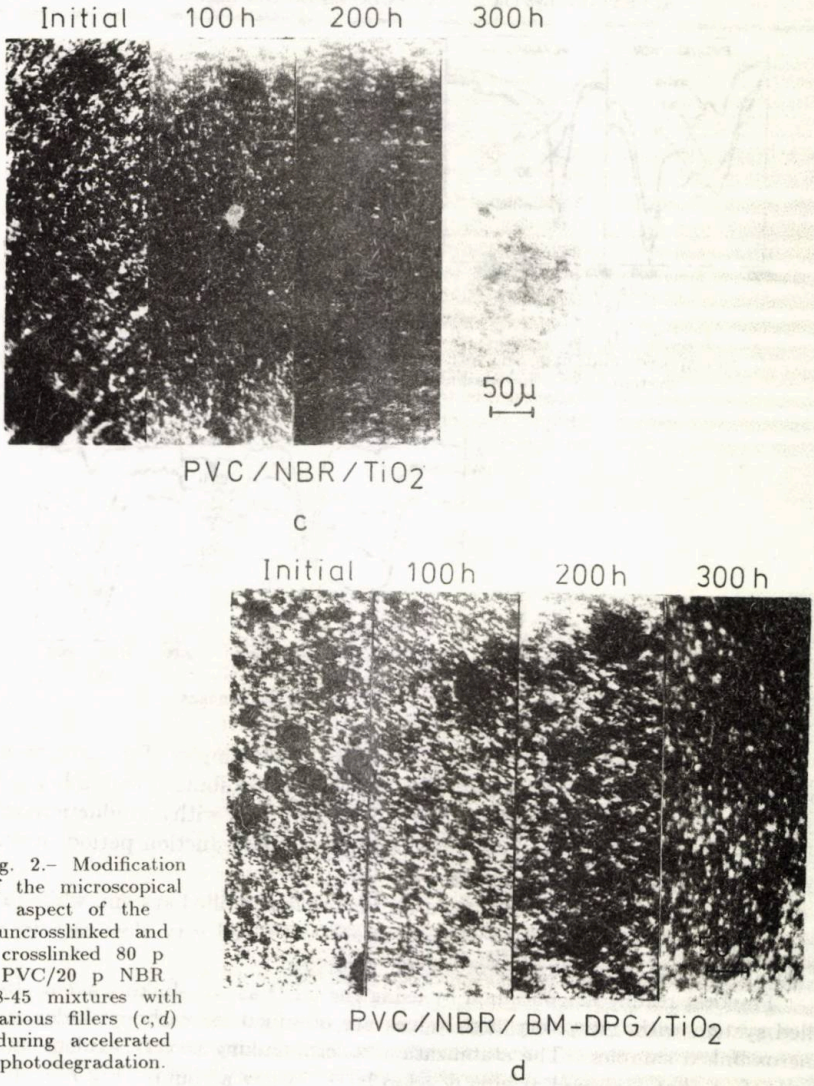

Fig. 2.– Modification of the microscopical aspect of the uncrosslinked and crosslinked 80 p PVC/20 p NBR 28-45 mixtures with various fillers (*c*, *d*) during accelerated photodegradation.

fected (Fig.6) for all samples in all aging conditions used; however it is possible a slight HCl elimination on one hand, probably, due to the very strong absorption of the C-C1 bonds and on other hand due to the fact that the degradation occurs mainly in the elastomeric phase.

From the variation of these values versus exposure time can be made appreciations about stability of the samples in accelerated aging conditions (Fig.7).

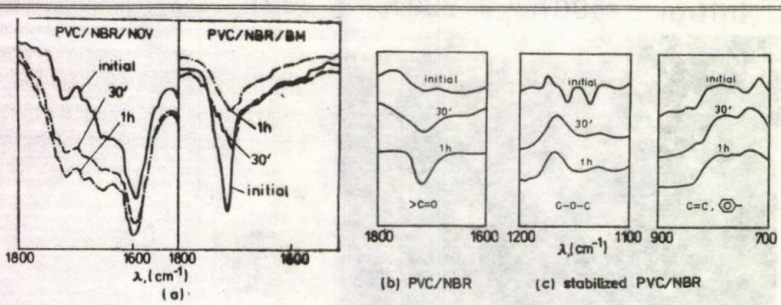

Fig. 3.– IR spectra of 80 p PVC/20 p NBR 28-45 mixture unexposed and exposed various periods of time: *a* – crosslinked systems; *b* – uncrosslinked and *c* – stabilized system.

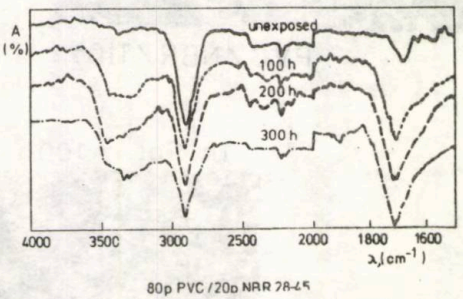

Fig. 4.– IR spectra of the uncrosslinked 80 p PVC/20 p NBR 28-45 system.

Unstabilized and uncrosslinked PVC/NBR 28-45 samples (Fig.7 *a*) present a continuous increase of the both indices, while the photostabilized with a benzophenone type light stabilizer samples present a S-shaped curve with an induction period which is characteristic for all stabilized systems. The induction period increases with the efficiency of light stabilizer.

The same dependence is obtained for uncrosslinked filled system, while for all crosslinked filled samples the both indices are lower and very slow vary in time (Figs.7 *b* and 7 *c*) indicating a more stable structure.

The best results are obtained by using the TED as crosslinking agent. In the filled system with TiO_2 very high values are obtained for carbonyl index in the uncrosslinked samples. The stabilization by crosslinking is very evident as well as the fact that hydroxyl groups develop later, in low amounts (Fig.7 *b*). It can be assumed that TiO_2 has initial a catalytic role for the NBR degradation, being known that this filler (white pigment), sometimes has a sensitizer effect on PVC degradation.

Both indices have small values in the crosslinked samples containing chalk.

Among the sample filled with ZnO a good photostability has the TED crosslinked sample, too (Fig.7 *c*).

Apart from uncrosslinked system which has two transition temperatures (Fig. 8), which shift with the temperature and time of thermoxidative aging the crosslin-

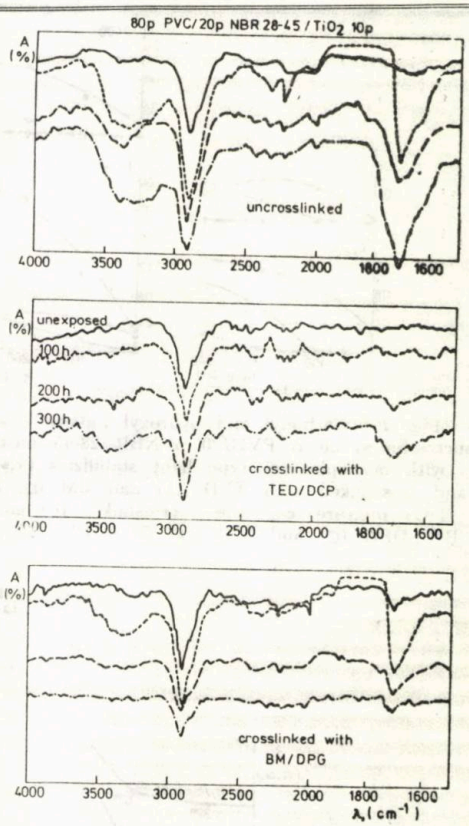

Fig. 5.– IR spectra of 80 p PVC/20 p NBR 28-45/TiO_2 uncrosslinked (*a*) and crosslinked with TED/DCP (*b*) or BM/DPG (*c*) unexposed and exposed various periods of time.

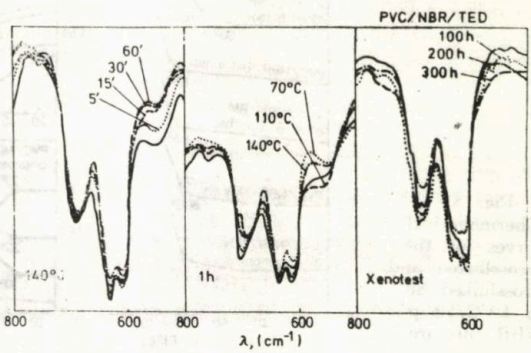

Fig. 6.– 570...750 cm^{-1} region from IR spectra used as reference bands.

ked systems are stable in time, their transition temperatures remain unchanged.

As we have shown, during the aging of PVC/NBR systems occur important chemical modification consisting especially in the apparition of high polar groups

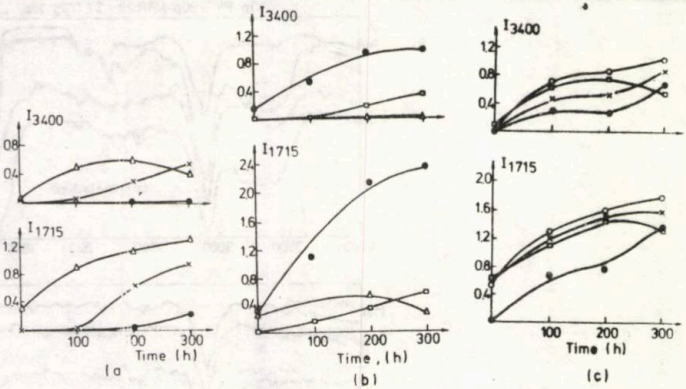

Fig. 7.– Carbonyl and hydroxyl indices versus exposure time for: *a* – the uncrosslinked 80 p PVC/20 p NBR 28-45 unstabilized (Δ) and stabilized samples with benzophenone type light stabilizers (x,•); *b* – on the uncrosslinked (•) and crosslinked with TED (Δ) and BM (□) 80 p PVC/20 p NBR 28-45/10 p TiO_2 mixture; *c* – the uncrosslinked (o) and crosslinked with BM+ZnO (x); BM+DPG (□) and TED (•) 80 p PVC/20 p NBR 28-45/10 p ZnO mixture.

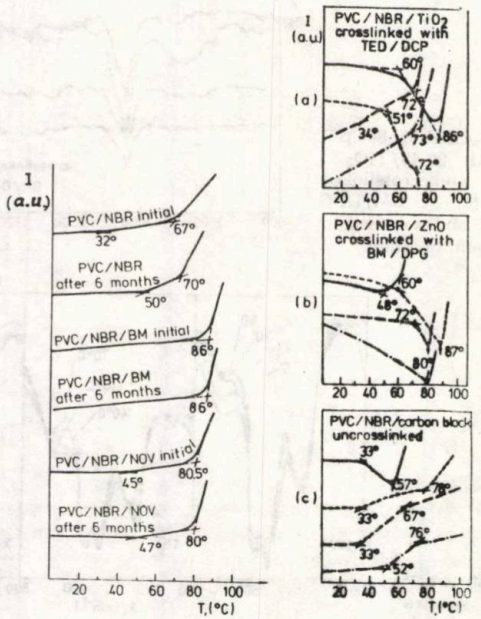

Fig. 8.– Thermooptical curves for the uncrosslinked and crosslinked 80 p PVC/20 p NBR mixture.

Fig. 9.– Thermooptical curves for the uncrosslinked or crosslinked 80 p PVC/20 p NBR 28-45 containing various fillers as TiO_2 (*a*), ZnO (*b*) and carbon black (*c*) unexposed and exposed various periods of aging: —— unexposed; - - - 100 h; — — — 200 h; and ------ 300 h.

(COOH, –OH, C=O) able to form hydrogen bonds. Simultaneously it is very possible (as commonly it happens for most polymers) to develop an other kind of crosslinking reaction as a degradative one.

In the thermooptical curves of all filled systems, very frequently (Fig.9) a

Table 1

Results of the Study by Thermooptical Method of Filled and Crosslinked 80 p PVC/20 p NBR 28-45 Systems

Filler + cross-linking agent	Aging time, [h]											
	0			100			200			300		
O	32	57	–	32	–	77	–	57	91	–	–	92
TiO_2	–	57	–	32	57	82	33	–	77	40	–	82
TiO_2+BM	–	57	–	–	57	82	35	–	82	46	–	82
TiO_2+TED	34	64	77(86)	32	51	72	34	–	72	–	–	73
ZnO	36	50	–	–	52	77	–	60	87	–	70	87
ZnO+BM(DPG)	31(47)	57(60)	–	–	52(60)	77(87)	–	64(72)	86(80)	–	64(80)	84
ZnO+TED	43	–	78	47	61	–	–	60	85	–	60	84
CB	33	57	–	33	–	78	33	67	–	–	52	76
CB+BM	–	64	–	–	–	78	33	67	–	–	–	78
CB+TED	–	67	–	31	–	–	–	50	–	–	50	–
Ch+BM	–	55...69	–	–	70	78	–	77	90	–	–	–
Ch+TED	36	61	–	36	61	–	–	68...77	–	–	62...72	84

BM – bismaleinimide; TED – triethyleneglycol dimethacrylate; DPG – diphenyl guanidine; CB – carbon black; Ch – chalk.

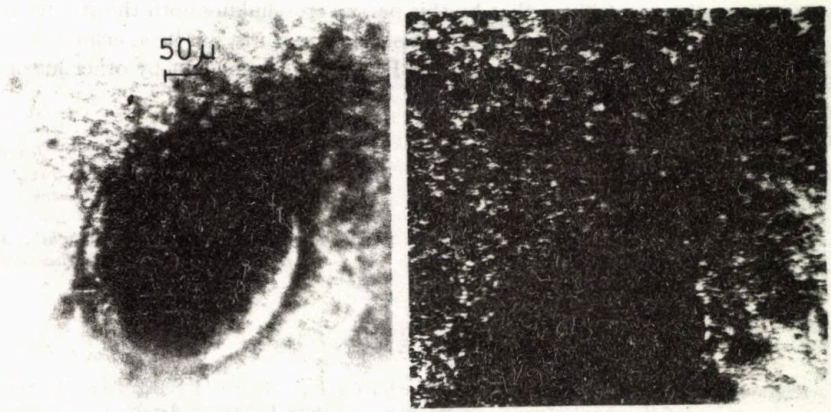

a *b*

Fig. 10.– Microscopical aspects of 80 p PVC/20 p NBR 28-45 filled with TiO_2 (*a*) or carbon black (*b*).

pronounced decrease of the transmitted light intensity, especially for the unexposed samples and exposed 100 h, has been observed. One of the possible explanation of this behaviour should be the existance of an interphasic layer around the filler particles because some filler particles show an halo (Fig.10). The same phenomenon has been especially observed in ternary mixtures containing copolymer [8] and by other autors too [16], [17]. An other explanation is much more probable.

Due to the chemical modifications (by functional groups formation and cross-linking) a rigid phase can appear with higher transition temperatures. Development of this phase can be considered as an aging stability criterion, being well evidenced

by the thermooptical method used.

All results have been hold together in Table 1. It is easily remarked that, in uncrosslinked sample, a high transition temperature appears after 100 h exposure time.

In crosslinked samples this transition appears after longer period of time and has lower values.

The better results are obtained as was expected by the combination carbon black/TED or chalk/TED for which only transition from low temperature are observed and these are almost unchanged in time even that from 36°C (carbon black being an UV absorber, too).

The higher temperatures presented by the systems containing ZnO can be explained by the possibility of C–C bonds formation during the controlled crosslinking, as it is known from the process of rubber vulcanization (curing) with this crosslinking agent.

4. Conclusions

We can be concluded that by this partial crosslinking both the stabilization of morphology and of chemical structure of filled mixtures has been achieved. Similar results for the mixtures containing NBR as main component by other autors have been obtained [18].

Received, August 20, 1992

„P.Poni" Institute of Macromolecular Chemistry, Jassy,
„Al.I.Cuza", University, Jassy, Department of Chemistry
and
Technical University "Gh.Asachi", Jassy, Department of Physical Chemistry

REFERENCES

1. Vasile C., Adamescu G., Odochian L., Chicu L., Badea M., *Semi-IPNs of Polyvinylchloride and Methacrylic Esters.* I. *Kinetic Aspects of the Preparation.* Bul. Inst. polit., Iaşi, **XXXVI (XL)**, *1-2*, s.II, 87-90 (1990).
2. Vasile C., Adamescu G., Chicu L., Ioanid A., Stoleriu A., Durnescu C., Mihăieş M., *Semi-IPNs Based on Polyvinylchloride and Methacrylic Esters.* II. *Morphology and Properties.* Bul. Inst. polit., Iaşi, **XXXVI (XL)**, *3-4*, s.II, 95-98 (1990).
3. Vasile C., Badea M., Costea E., Adamescu G., Ioan S., Cailean A., *Compatibility of PVC/NBR System.* I. *Study in Diluted Solutions,* (in Romanian). Materiale Plastice, **27**, *4*, 181-184 (1991).
4. Vasile C., Stoleriu A., Badea M., Costea E., Durnescu C., Adamescu G., Ioanid A., *Compatibility of PVC/NBR System.* II. *Thermal Behaviour* (in Romanian). Materiale Plastice, **28**, *1-2*, 30-35 (1992).
5a. Vasile C., Costea E., Stoleriu A., *Thermal Studies on Crosslinked Polymeric Systems.* ESTAC'5, Nice, France, August 25-30, 1991, Working Book, P-36.
5b. Vasile C., Costea E., Stoleriu A., Sava M., *Compatibility of PVC/NBR Systems.* III. *Ternary Systems.* Bul. Inst. polit., Iaşi, **XXXVIII (XLII)**, *1-4*, s.II, 75-84 (1992).

6. Vasile C., Schneider I.A., Airinei A., Chiriac A., *On the Compatibility of Binary and Ternary Random Copolymers of Acrylonitrile with Vinyl Acetate and/or α-methylstyrene. II. Influence of the Time Factor.* Europ. Polym. J., **12**, 749-752 (1976).
7. Vasile C., Caşcaval C.N., Odochian L., Schneider I.A., *Temperature and Time Dependence of the Phase Separation in Mixture of Binary Statistic Copolymers of Acrylonitrile.* Preprints Mackro Mainz, Sept. 17-21, 1979.
8. Vasile C., Stoleriu A., Eşanu N., Adamescu G., *Compatibility of Ternary Systems PVC/PVAc/Vinyl Chloride Copolymers,* (in Romanian). Materiale Plastice, **27**, *3*, 117-120 (1990).
9. Field J.E., Woodfard D.E., Gohman S.D., *Analysis of Nitrile Rubbers.* Chem. Technol., **28**, *3*, 770-775 (1955).
10. Amerongen G.J., *IR-Spectra of Rubbers.* Rubber Chem. Technol., **29**, *3*, 856-859 (1956).
11a. Ivan G., Giurgiunca M., *Study by IR Spectroscopy of the Thermoxidative Degradation of some Acrylonitrile-Butadiene Elastomers,* (in Romanian). Ind. Uşoară, **27**, *3*, 115-118 (1980).
11b. Ivan G., Giurgiunca M., *Behavior at Thermoxidative Destruction of NBR/PVC System,* (in Romanian). Ind. Uşoară, **34**, *11*, 490-494 (1987).
12. Faubion B.D., *Study of High Explosives by Optical Thermal Analysis.* Anal. Chem., **40**, *2*, 241-247 (1971).
13. Sun Tong, Bhattacharya S.K., Lenz R.W., Porter R.S., *An Optical Study of Phase Transitions of Poly(ethylene Terephthalate-co-p-Hydroxybenzoic Acid) Liquid Crystal.* J. Polym. Sci., Polym. Phys. Ed., **28**, *10*, 1677-1684 (1990).
14. Mucha M., *Thermo-optical Analysis as a Complementary Method in the Study of Phase Transitions of Thermotropic Liquid Crystalline Polymer and its Blends with Polycarbonate.* Colloid. Polym. Sci., **267**, *10*, 876-880 (1989).
15. Mezhukhin V.B., Guzaev V.V. Sadova S.P., Kotenkov V.Y., Yushikova S.M., Tager A.A., *Influence of Fillers on Polymerization of Oligoesters Acrylates in the Process of Gelation of PVC Plastisols,* (in Russian). Vysokomol. Soedin., **A 26**, *4*, 729-736 (1984).
16a. Berlin A.A., *Hauptsachliche Entwicklungstendenzen der Chemie der polymerizationsfähigen Oligomeren und deren Verwendung zur Modifizierung von Hochpolymeren.* Plaste u. Kautsch., **18**, *8*, 563-571 (1971).
16b. Berlin A.A., *Polymer–Oligomer-Kompositionen und Materialien auf ihrer Grundlagen.* Plaste u. Kautsch., **20**, *10*, 728-737 (1973).
16c. Berlin A.A., Zavodčkova N.N., Yanovskii D.M., *Modification of the Vinylchloride Copolymers with Oligoesters Acrylates,* (in Russian). Plastičeskie Massy, *4*, 47-48 (1975).
17a. Lomonosova N.V., *Physico-mechanical Properties of PVC Modified by Di- and Three-Methacrylate Esters,* (in Russian). Plast. Massy, *3*, 28 (1988).
17b. Lomonosova N.V., Faizi N.H., Čikin Yu.A., *Modification by Radiation of PVC with Dimethacrylate Triethylene Glycol,* (in Russian). Plast. Massy, *4*, 17 (1984).
17c. Lomonosova N., Čikin Yu.A., *Influence of Orientation on the Physico-mechanical Properties of the Composites Based on PVC with TGM-3 Modified by Radiations,* (in Russian). Plast. Massy, *4*, 9-10 (1986).
18. Sain M.M., Oravec J., Lacok J., Beniska J., *Studies on the Modification of Nitrile Rubber Poly(vinyl Chloride) Blends. Effect of Nonconventional Vulcanization Systems.* Acta Polymerica, **40**, *10*, 648-650 (1989).

REŢELE SEMI-INTERPĂTRUNSE PE BAZĂ DE PVC
IV. Îmbătrânirea şi stabilizarea amestecurilor PVC/NBR cu umplutură

(Rezumat)

S-a studiat stabilitatea în timp şi în diferite condiţii de îmbătrânire accelerată a sistemului

incompatibil policlorură de vinil (PVC)/cauciuc nitrilic (NBR)/umpluturi anorganice.

S-a testat şi s-a demonstrat că are loc stabilizarea chimică şi morfologică a sistemului prin reticularea parţială cu diferiţi agenţi. În acelaşi timp se realizează stabilizarea pe termen îndelungat în condiţiile de îmbătrânire sub acţiunea factorilor de mediu.

BULETINUL INSTITUTULUI POLITEHNIC DIN IAŞI
Tomul XLI (XLV), Fasc. 1-4, 1995
Secţia II
CHIMIE ŞI INGINERIE CHIMICĂ

D.C. 678.075

CROSSLINKED POLYURETHANE–POLYSILOXANES

BY
AURELIAN STANCIU, C. CIOBANU,
GH. STOICA and VICTOR BULACOVSCHI

1. Introduction

Many papers are concerned with improvement of the mechanical properties of poly(dimethylsiloxane) (PDMS) elastomers and retaining their valuable physical and chemical characteristics [1],...,[8]. One of the proposed ways refers to synthesis of segmented block-copolymers where hard moieties of polyamides, polycarbonates or polyurethanes are combined with soft segments of PDMS. The hard domains have strong intermolecular forces so that these products exhibit networks behaviour and good mechanical and thermal properties. The physical crosslinks are inoperative in the melt or in the solution state when the network is destroyed due to molecular agitation. In such circumstances more convenient are chemical crosslinks which can be introduced in the hard segment using a polyol (functionality $f > 2$) as a chain extender or in the soft segment using long triols or higher functionality polyols with or without long diols [9].

In this paper we report a successful synthesis of PDMS–polyurethane multiblock copolymers, chemically crosslinked, from poly(diethileneglycoladipate) and PDMS (PDEGA : PDMS = 80:20 wt%) as soft segment and 4,4′-diphenylmethane diisocianate/diglycerinmaleate (DMI/DGMA) as hard segment. The concentration of the two components (soft and hard) was maintained constant at 63 wt% and 37 wt%, respectively. Length of the soft segment was controlled by using PDEGA with $\overline{M}_n = 2,500$ and PDMS having $\overline{M}_n = 10,000$. Chemical crosslinks were introduced by DGMA units and their density adjusted through quantity of diisocianate.

The thermomechanical characteristics of the synthesized polyurethane–polysiloxanes were correlated with the concentration of urethane groups and PDMS in the structure of the soft segment.

2. Experimental

2.1. Materials

PDEGA was obtained from adipic acid and diethylene glycole (1:2 molar ratio) in two steps melt technique (OH number = 56 mg KOH/g and acidity = 0.023%)

[10]. DGMA was obtained from maleic anhydride and glycerine (1:2 molar ratio) in the melt (OH number = 850 mg KOH/g and acidity = 0.02%) [10],...,[12]. PDMS was prepared by anionic polymerization of octamethylcyclotetrasiloxane [13] (OH content = 1.2%, manometrically [14]). DMI (from ICI) was purified by vacuum distillation before use.

2.2. Synthesis of Polyurethane–Polysiloxane Copolymers

The synthesis was carried out by one step polyaddition in the melt state. Tipically, in a reactor equipped with mechanical stirring, nitrogen inlet tube and vacuum line are introduced 80 g (0.0322 mol) PDEGA, 20 g (0.0757 mol) DGMA and 20 g (0.002 mol) PDMS. The mixture was heated for 2 h under stirring to 120°±5°C and 2...3 mm Hg residual pressure to remove traces of water. Subsequently, the temperature was rised to 140°±5°C and maintained for 30 min., then the pressure was rised and 37 g (0.1478 mol) of DMI and 0.002 g *p*-toluene sulfonic acid were introduced under nitrogen stream. The mixture was allowed to react for 5 min. and then poured in a warm mould. The such obtained plates (300×200×1 mm) were heated for additional 6 h at 105°C in order to complete the reaction.

In a similar way were obtained plates that contain 40 g (0.1598 mol) DMI (symbolized as PUS-40), 43 g (0.1718 mol) DMI (PUS-43) and 47 g (0.1878 mol) DMI (PUS-47).

The reference sample was synthesized as above, but PDMS was replaced by PDEGA and the used quantity of DMI was 40 g (PU-40).

2.3. Polymer Characterization

The OH number was measured treating products with acetic anhydride and titration with KOH. The evaluation of OH groups in PDMS was carried out manometrically measuring the H_2 eliberated in reaction with $LiAlH_4$ in toluene.

The X-ray diffraction patterns were obtained on a DRON YM-1 equipment fitted with Ni filter Cu K_α radiation at a power of 35 kW and 20 mA.

The thermal analysis was carried out on Paulik-Paulik-Erdey MOM Budapest apparatus in air, at a heating rate of 9°C/min. in the range of 20°...900°C.

The physical-mechanical properties were evaluated from stress–strain curves, registered on TIRA-test 2161 apparatus, at an elongation rate of 9 mm/min. Measurements were performed at room temperature on samples of 65.3×6×1 mm. The reported data represent the average of six individual tests.

3. Results and Discussion

The synthesis of crosslinked polyurethane–siloxanes was realised following reaction:

$$\mathrm{HO{-}R_1{-}OH + HO{-}R_2{-}OH + \underset{\displaystyle OH}{\underset{|}{HO{-}R_3{-}OH}} + OCN{-}Ar{-}NCO \xrightarrow[cat.]{heat}}$$

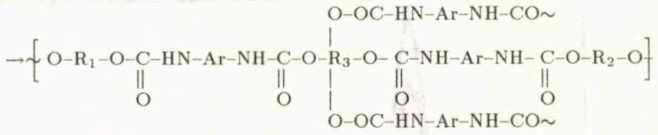

where:

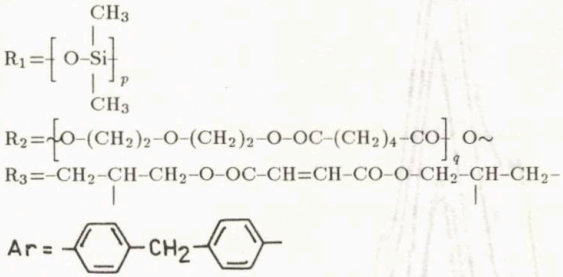

The one step polyaddition technique was adopted as more convenient.

Table 1 contains data refering to molar ratio of the feeded functional groups, also the theoretical composition of the products. One should note that by increasing the MDI content, probability of hydrogen bonding is higher.

Table 1

Theoretical Parameters in Synthesis of Crosslinked Polyurethane-Polysiloxane Elastomers

Polymer code	moles OH/g×10³		moles -NCO/g×10³	Molar ratio OH/NCO
	primar	secundar		
PU-40	1.45	0.95	2.00	1.200
PUS-37	1.40	0.96	1.88	1.255
PUS-40	1.37	0.95	2.00	1.161
PUS-43	1.35	0.93	2.11	1.080
PUS-47	1.31	0.91	2.25	0.998

The elemental analysis of the polyurethanes is summarised in Table 2 and it reflects a good agreement between theoretical and experimental values.

Table 2

Elemental Analysis of Polyurethane-Polysiloxane Elastomers

Polymer code	Theoretical data, [%]				Experimental data, [%]			
	C	H	N	Si	C	H	N	Si
PU-40	58.12	6.49	2.80	–	58.78	6.31	2.91	–
PUS-37	54.96	6.61	2.64	4.82	54.81	6.47	2.67	4.73
PUS-40	55.27	6.56	2.80	4.73	55.75	6.41	2.88	4.64
PUS-43	55.58	6.52	2.95	4.64	55.43	6.37	3.06	4.37
PUS-47	55.95	6.46	3.15	4.53	55.86	6.33	3.18	4.41

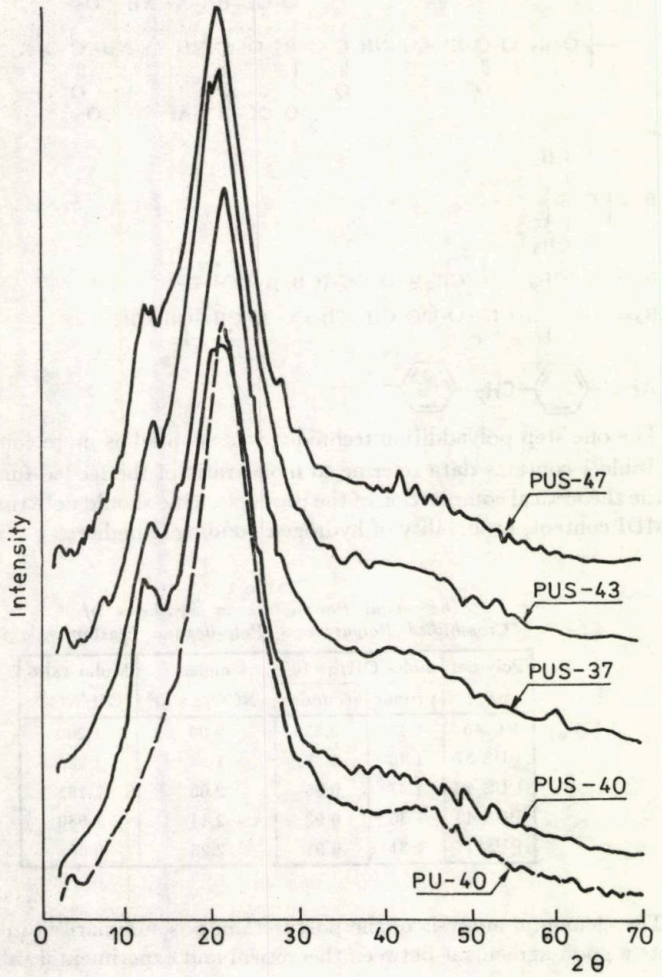

Fig. 1.– X-ray diffractograms of the polyurethane–polysiloxane elastomers (for symbols s. Table 1).

Informations on the supermolecular organization were obtained from X-ray diffractograms of the copolymers (Fig.1). There appear the diffraction patterns at 2θ=12°C in those copolymers containing polydimethyilsiloxane units and do not appear in the reference sample (PU-40). This asserts that the siloxane segments promote a new type of organization in the copolymers. All products reveal an intense diffraction at 2θ=22°C on account of crystalline phase in these products. At wider angles there appear a weak diffraction (2θ=44°) on account of amorphous domains in polyurethane–polysiloxanes. Comparatively, the crystallinity index of reference sample (PU-40) is higher (I_{cr}=81%) than that of PUS-40 product

(I_{cr}=74%). In the last case the flexible segment of PDMS decreases the capacity of macromolecules to organize. Fig.2 is a tentative in representing the modification of I_{cr} and I_{am} as function of urethane groups contained in copolymers. It is obvious that by rising the content of urethanes groups the crystallinity index (I_{cr}) should increase since the density of hydrogen bonds will be higher.

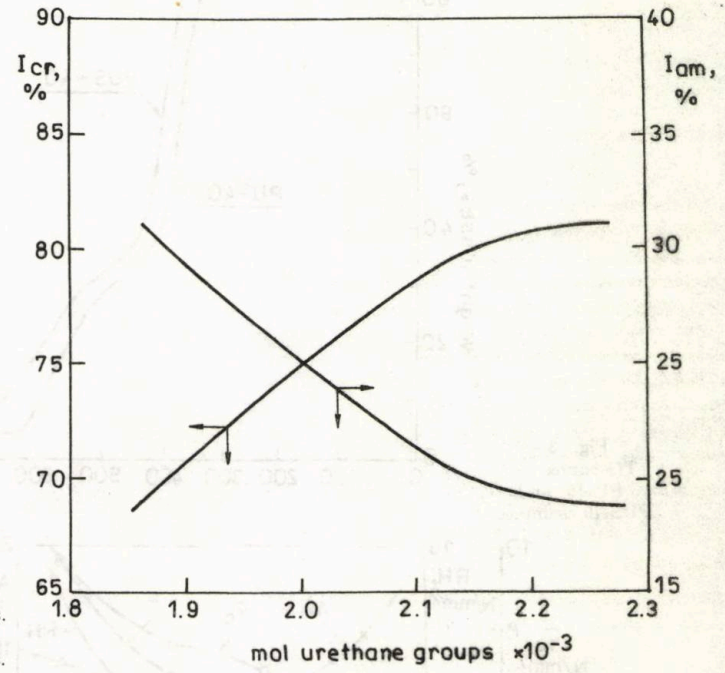

Fig. 2.– Dependence of I_{cr} and I_{am} vs. the content of urethane groups.

The thermogravimetrical analysis of polyurethane–polysiloxane copolymers was realised in air and it results that these products are stable up to 220°...265°C. At higher temperatures they degrade in two steps (220°...450°C and 450°...680°C) with a total weight loss of 88...95% (Fig.3). The PUS-40 sample appears to be more stable than PU-40. The residue (almost 12%) consists in SiO_2 and results from thermal decomposition of PDMS units.

The kinetical parameters of the thermodegradation process (C o a t s–R e d f e r n method [15]) show that it obeys a first order kinetics in both steps (n_I=1.04 and n_{II}=0.87, respectively) with an activation energy of 31.52 kcal/mol and 27.18 kcal/mol, respectively.

One of the remarkable features of these polymers lies in their mechanical properties which determine their performance. The behaviour of the material strongly depends on its chemical structure, also on intermolecular forces occuring between macromolecular chains. From the beginning in synthesis of polyurethane–polysiloxane elastomers there were used special condensing materials that favor

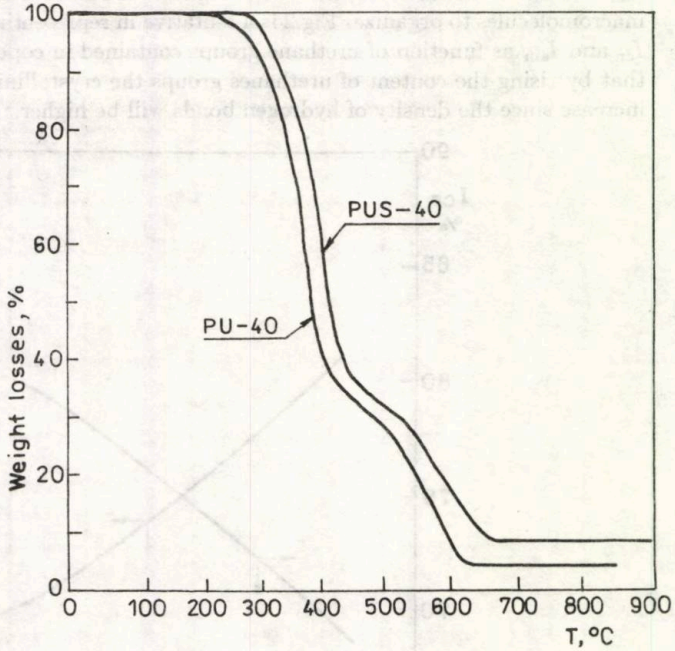

Fig. 3.– TG-curves for PU-40 and PUS-40 samples.

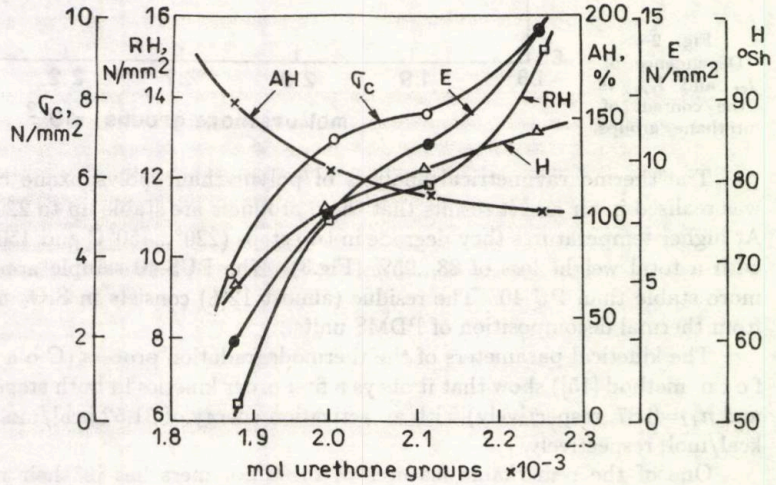

Fig. 4.– Variation of physical-mechanical parameters with concentration of urethane groups in polyurethane–polysiloxane elastomers: RH – tensile strength; E – elastic modulus; σ_c – crystallization stress on deformation; H – hardness; AH – elongation on brake.

physical and chemical crosslinks. They are brought over by hard segments, or urethane groups, respectively.

Fig.4 reflects the influence of urethane groups on main physical-mechanical parameters. Thus, by rising the content of urethane groups in the copolymer, the tensile strength, hardness and the elastic modulus on breaking improve, while the elongation on brake diminishes with almost 100% for an increase of urethane groups by 0.3×10^3.

4. Conclusions

The insertion of the PDEGA/PDMS (80:20) flexible segment in the structure of polyurethane–polysiloxane elastomer lowers the crystalline index by 7% as compared with reference sample. On the other hand, in the synthesized elastomers series, the I_{cr} grows by 10% as the content of urethane groups increases. Their diffraction patterns reveal a diffraction at $2\theta=12°$, which was attributed to PDMS segments.

The polyurethane–polysiloxane elastomers show a better thermal stability than the usual polyurethanes. Their weight losses at 640°C are on 15% lower.

The combined effect of physical and chemical crosslinks is reflected by improvement of physical-mechanical behaviour of such polymers.

Received, January 11, 1995

Institute of Macromolecular Chemistry "P.Poni", Jassy
and
Technical University "Gh.Asachi", Jassy, Department of Macromolecular Chemistry and Technology

REFERENCES

1. Shibayama M., Suetsugu M., Sakurai S., Yamamoto T., Macromolecules, **24**, 6254 (1991).
2. Shibayama M., Inoue M., Yamamoto T., Nomura S., Polymer, **31**, 749 (1990).
3. Hoffman K., Bonarl R., Macromol. Chem., **184**, 1529 (1983).
4. Ishihara H., Kimura I., Yoshihara N., J. Macromol. Sci., Phys., **B22**, 713 (1983-1984).
5. Shibayama M., Ohki Y., Katani T., Nomura S., Polym. J., **19**, 1067 (1987).
6. Bershtein V.A., Lewin V.Yu., Yegorova L.M., Yegorov V.M., Zhdanov A.A., Slovimskii G.L., Makarova L.I., Martirosov V.A., Vysokomol. Soedin., Ser.A, **29**, *12*, 2553 (1987).
7. Askadskii A.A., Surov G.V., Pankatov V.A., Frenkel T.M., Makarova L.I., Zhdanov A.A., Blagodatskii I.V., Pastukhov A.V., Vysokomol. Soedin., Ser.A, **32**, *7*, 1528 (1990).
8. Xiao H., Ping H., Xie Y.W., Yu T.Y., J. Polym. Sci., Part A: Polym. Chem. Ed., **29**, 585 (1990).
9. Petrovic Z.S., Ilavsky M., Dusek K., Vidakovic M., Javni I., Banjanin D., J. Appl. Polym. Sci., **42**, 391 (1991).

10. * * * *Methoden der Organischen Chemie* (Houben-Weyl), Bd.**XIV/2**, *Makromolekulare Stoffe*, II. Teil. Georg Thieme Verlag, Stuttgart, 1963, 16.
11. Ciobanu C., Farcaş A., Bârlădeanu C., Afloarei P., Cioanca C., Rom. Patent, *99,127* (1989).
12. David D.J., Staley H.B., *Analytical Chemistry of the Polyurethanes*. Vol.**XVI**, Wiley, N.Y., 301, 1969.
13. Urban M., Skolova T., C.S. Patent, *262,370* (1989).
14. Smith A.L., *The Analytical Chemistry of Silicones*. Wiley, N.Y., 1991, 189.
15. Coats A.W., Redfern J.P., Nature, **201**, 68 (1964).

POLIURETANI-POLISILOXANI RETICULAŢI

(Rezumat)

Se sintetizează o serie de elastomeri poliuretan-polisiloxanici reticulaţi care se analizează din punct de vedere structural şi al proprietăţilor fizico-mecanice. Introducerea reticulărilor chimice duce la îmbunătăţirea proprietăţilor fizico-mecanice fără a afecta esenţial elasticitatea acestor polimeri. Poliuretan-polisiloxanii sintetizaţi dovedesc, de asemenea, o bună stabilitate termică.

BULETINUL INSTITUTULUI POLITEHNIC DIN IAŞI
Tomul XLI (XLV), Fasc. 1–4, 1995
Secţia II
CHIMIE ŞI INGINERIE CHIMICĂ

D.C. 66.095.2

ALKALINE POLYMERIZATION OF ACRYLAMIDE

BY
LIVIU MITITEANU, AUREL DUŢĂ and VICTOR BULACOVSCHI

1. Introduction

Hydrosoluble polymers based on acrylamide (AAm) are products of large applications in different industrial branches. They are used as dispersive agents, floculants, thickers and their utility depends mainly on molecular weight and/or chemical composition. A particular sort of hydrosoluble polymers is that based on acrylamide/sodium acrylate copolymers which can be prepared in two different ways: a) by copolymerization of the mentioned monomers, starting from a preestablished feed ratio; b) by means of polymer – analogous reactions of the nonionic poly(acrylamide) e.g. by alkaline hydrolysis of the polymer.

More recently a new and convenient method has been proposed for preparation of hydrosoluble polymers. It consists in polymerization of AAm monomer in presence of a hydrolysing agent [1],...,[4]. Following this procedure the composition and molecular weight of the polymer might be controlled. There occur a simultaneous hydrolysis of the monomer and polymer and generates *in situ* the nitrilotrispropionamide (NTPA), which acts as a chain transfer agent.

This paper presents some pecularities of acrylamide/sodium acrylate copolymerization in aqueous solution (17...19%) initiated by $K_2S_2O_8$ in presence of NaOH as hydrolysing agent.

2. Experimental

2.1. Materials

Technical acrylamide 99.8% purity (Cyanamid), sodium hydroxide p.a. (Chemopol) and potassium peroxodisulphate p.a. (Merk), were used as delivered.

2.2. Polymer Preparation

The polymerization was carried out in a 500 ml glass-reactor fitted with mechanical stirring, condenser and thermometer. The reactor was placed in a water bath which heating range was between 15° and 100°C.

In a typical run, the reactor is first charged with AAm and distilled water to obtain a 20...25% solution of the monomer. By maintaining the mixture at room temperature a calculated amount of 30% solution of NaOH is added. Then at fixed periods of time (0, 15, 30 min), preestablished volumes of $K_2S_2O_8$ solution 2.5% are introduced into reactor, so that final concentration of acrylamide reaches 2.7 mol/l (almost 18% wt.). After an induction period which depends on ratio of reactants, the temperature starts to rise due to exothermal character of the process. When

temperature attains 60°C, the mixture is maintained in these conditions for three hours and then cooled down to obtain the polymer as a gel.

2.3. Characterization of Polymers

The unreacted monomer was determined by bromate/bromide method.

The average molecular weight was obtained from viscometric measurements in 1M $NaNO_3$ solution at 30°C with an Ubbelohde viscometer and by using the relation:

$$[\eta] = 1.34 \times 10^{-3} \overline{M}_v^{0.57}.$$

The hydrolysis degree (the anionicity) was determined by pH-metry: an acidic polymer solution (0.15%) was titrated with 0.1N NaOH solution and noted the volumes consumed between pH=3.8 and pH=7.5.

3. Results and Discussion

Reactions accompanying the polymerization of AAm in alkaline solution refer to:

a) Hydrolysis of the monomer:

$$CH_2 = CH - CONH_2 + NaOH \longrightarrow CH = CH - COO^-Na^+ + NH_3$$

b) Generation of nitrilotrispropionamide by addition the ammonia to the double bond of the monomer:

$$3CH_2 = CH - CONH_2 + NH_3 \longrightarrow N(CH_2 - CH_2 - CONH_2)_3$$

c) Copolymerization of acrylamide and resulted sodium acrylate by free-radical mechanism. Since the nitrilotrispropionamide is formed *in situ* and acts as a reducing agent, one should admit that the free radicals are generated in a redox system:

$$x\mathrm{CH_2{=}CH} + y\mathrm{CH{=}CH} \rightarrow \ldots(\mathrm{CH_2{-}CH})_x{-}(\mathrm{CH_2{-}CH})_y{-}\ldots$$
$$\qquad\quad | \qquad\qquad | \qquad\qquad | \qquad\qquad |$$
$$\qquad \mathrm{CONH_2} \qquad \mathrm{COONa} \qquad \mathrm{CONH_2} \qquad \mathrm{COONa}$$

d) As the copolymer is formed it undergoes hydrolysis:

$$\ldots{-}(\mathrm{CH_2{-}CH})_x{-}(\mathrm{CH_2{-}CH})_y \xrightarrow[-\mathrm{NH_3}]{\mathrm{H_2O}} \ldots(\mathrm{CH_2{-}CH})_p{-}(\mathrm{CH_2{-}CH})_q{-}\ldots$$
$$\qquad\quad | \qquad\qquad | \qquad\qquad\qquad | \qquad\qquad |$$
$$\qquad \mathrm{CONH_2} \qquad \mathrm{COONa} \qquad\qquad \mathrm{CONH_2} \qquad \mathrm{COONa}$$

$$(x + y = p + q).$$

One of the important features of this process is that the NTPA acts as a reducing agent in the initiation step affecting the activation energy of the persulphate decomposition. The rate of decomposition increases and, therefore, the induction period shortens. It acts also as a chain transfer agent modifying the molecular

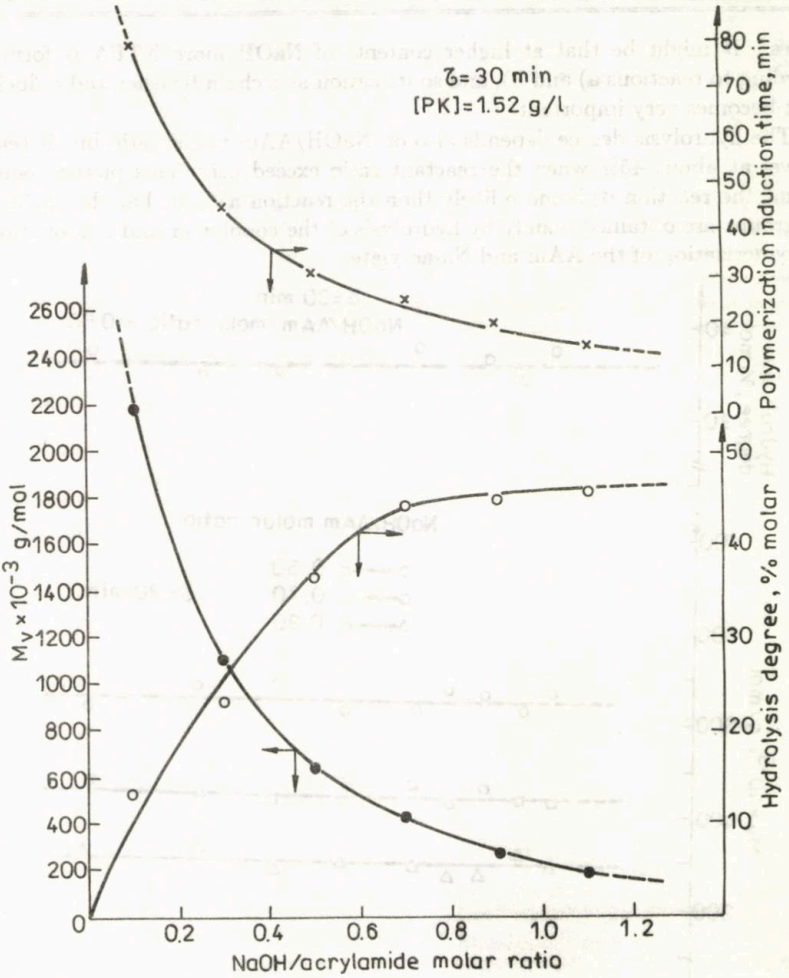

Fig. 1.– Influence of the NaOH/AAm molar ratio on molecular weight, degree of hydrolysis and induction time for a contact time between reactants τ = 30 min. and $[K_2S_2O_8]$=1.52 g/l.

weight of the prepared polymer. In such circumstances it was important to point on the parameters which determine the composition and molecular weight of the copolymer.

Fig.1 presents the dependence of molecular weight and hydrolysis degree on NaOH/AAm molar ratio for a contact time between the two reactants of 30 min. It results that on increasing the quantity of NaOH, the molecular weight of the polymer diminishes, so does, also, the induction period.

This influence is more pronounced at lower values of the NaOH/AAm molar

ratioes. It might be that at higher contents of NaOH more NTPA is formed, according to reactions a) and b), and so its action as a chain transfer and reducing agent becomes very important.

The hydrolysis degree depends also on NaOH/AAm molar ratio but it tends to level at about 45% when the reactant ratio exceed 0.7. This picture points on that the reaction d) is more likely than the reaction a) and that the carboxylate groups are obtained mainly by hydrolysis of the copolymer and less by direct copolymerization of the AAm and Na-acrylate.

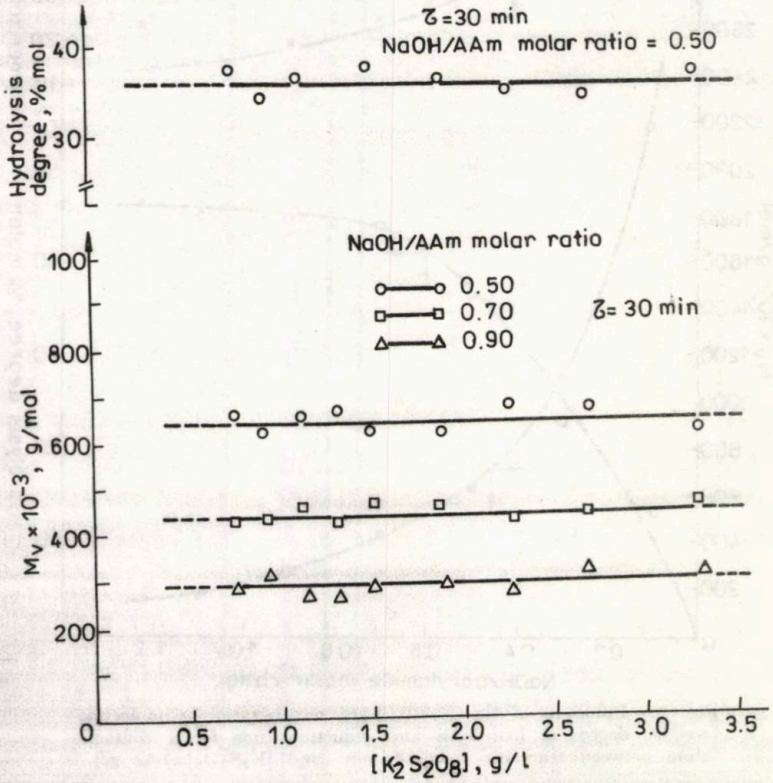

Fig. 2.– Influence of the peroxodisulphate concentration on the molecular weight and hydrolysis degree at constant NaOH/AAm molar ratio and $\tau = 30$ min.

In the alkaline hydrolysis of the polyacrylamide a hydrolysis degree of 35...40% appears to be a limit since there are electrostatic repulsive forces between HO^- and COO^- groups which slow down the process [5], [6]. This might be the reason why the representation of hydrolysis degree versus NaOH/AAm molar ratio levels at 45%. On the other hand, if one admits the hydrolysis of AAm as the main reaction, then by copolymerization of the monomers mixture, a product with almost unlimited hydrolysis degree will result.

A plot of the molecular weight and hydrolysis degree versus the concentration of $K_2S_2O_8$ at constant NaOH/AAm molar ratio, shows that both characteristics do not depend on the oxidant amount (Fig.2). It is obvious that when NaOH/AAm ratio remains constant, the quantity of the NTPA formed will be also constant and from this will be no variations in molecular weight and hydrolysis degree. By rising the NaOH/AAm molar ratio, more NTPA is formed and consequently copolymers of lower molecular weights are obtained.

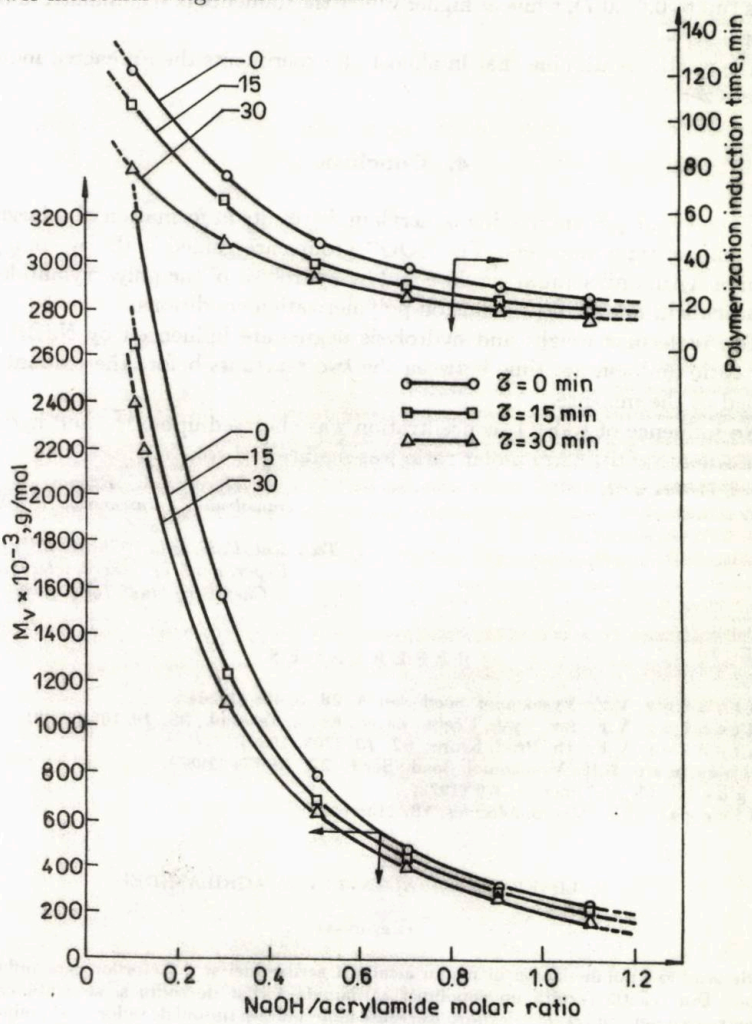

Fig. 3.– Influence of NaOH/AAm molar ratio on the molecular weight and polymerization induction period.

In Fig.3 the variation of molecular weight and induction period are plotted versus NaOH/AAm molar ratio, for different contact times (τ) between the two reactants before introducing the $K_2S_2O_8$. One can see that by rising the contact time, both characteristics – molecular weight and induction period – are decreasing. This behaviour might be due to the increase of the NTPA formed in reactions a) and b) before initiation. The effect is more perceptible at low NaOH/AAm molar ratioes (up to 0.6...0.7), while at higher values the influence is very small and curves overlap.

It is worth mentioning that in almost all experiments the unreacted monomer was near zero.

4. Conclusions

The alkaline polymerization of acrylamide results in formation of a large variety of anionic type polymers. The COO^- groups are gained both, by copolymerization of AAm and sodium acrylate and by hydrolysis of the polyacrylamide. The way which will dominate depends on polymerization conditions.

The molecular weight and hydrolysis degree are influenced by NaOH/AAm molar ratio and contact time between the two reactants before the oxidant agent is added to the mixture.

No influence of $K_2S_2O_8$ concentration was observed upon $\overline{M}_v$ and hydrolysis degree when NaOH/AAm molar ratio was maintained constant.

Received, February 21, 1995

Viaco, S.A., Râşnov,
"Transilvania" University, Brashov
and
Technical University "Gh.Asachi", Jassy,
Department of Macromolecular
Chemistry and Technology

REFERENCES

1. K u r e n k o v V.F., Vysokomol. Soed., Ser.A, **28**, *3*, 488 (1986).
2. K u r e n k o v V.F., Izv. Vysh. Učebn. Zaved. Khim. Tekhnol., **29**, *10*, 105 (1986).
3. K u r e n k o v V.F., Zh. Prikl. Khim., **62**, *10*, 2303 (1989).
4. Z i l b e r m a n E.H., Vysokomol. Soed., Ser.B, **22**, *10*, 774 (1980).
5. H i g u c h i M., Polymer, **3**, 370 (1972).
6. H a l v e r s o n F., Macromolecules, **18**, 1139 (1985).

POLIMERIZAREA ALCALINĂ A ACRILAMIDEI

(Rezumat)

Se studiază polimerizarea în mediu alcalin a acrilamidei şi a factorilor care influenţează reacţia. Din reacţie rezultă un copolimer acrilamidă-acrilat de sodiu şi se arată care sunt parametrii ce determină gradul de hidroliză, masa moleculară şi timpul de inducţie al polimerizării.

Se comentează formarea *in situ* a nitrilotrispropionamidei şi rolul acesteia ca reducător în faza de iniţiere, cât şi cel de agent de transfer de lanţ.

BULETINUL INSTITUTULUI POLITEHNIC DIN IAŞI
Tomul XLI (XLV), Fasc. 1-4, 1995
Secţia II
CHIMIE ŞI INGINERIE CHIMICĂ

RECENZII — BOOK REVIEWS

CHISTI M.Y., *Airlift Bioreactors*. Elsevier Applied Science, London and New York, 1989, X+345 p., ISBN 1-85166-320-7.

Bioprocess design and development include investigations and advances on bioreactors, around which are designed the separation and purification operations, as well as handling of wastes. The importance of bioreactors to successfull design, development and operation of a bioprocess has been stressed in literature. The main objective of this book is to enhance the understanding of the airlift bioreactors by a comprehensive compilation and discussion of existing knowledge together with new research. The book represents the first on the subject. It comprises eight chapters. Chapter I is a brief introduction on bioreactors regarding scope, objectives, present states and future trends. Chapter II provides some fundamental aspects concerning hydrodynamics and mass transfer in disperse systems. Properties of biofluids processed in reactors are also determined. Chapter III is a profound examination of transfer phenomena in airlift reactors: moment, mass and heat transfer. There were made comparisons between bubble columns and airlift systems and were mentioned the areas of particular concern and those in need for further research. Chapter IV reviews some useful experimental techniques, model fluids and reactors used in research of airlift bioreactors. Examples of model reactor configurations and comments on selection of simulation media are provided. Chapter V describes aspects regarding hydrodynamics in airlift reactors. Chapter VI illustrates new findings on mass transfer in airlift reactors. Chapter VII details some possible strategies for overall design of airlift systems. The experimental needs and the methods for solving complex design problems are outlined. Chapter VIII is a unified treatment of the newer research findings and presents some specific conclusions.

The book contains 9 Appendices, 23 Tables and 94 Figures, Nomenclatures, a rich list of References, Author index and Subject index.

The information given in this book is highly informative and it appeared in excellent graphical conditions, representing a valuable contribution in the field of bioreactors design and performance.

The volume provides updaten description in this important and fast-growing field, which will help the researches in this area and serve as a reference for students, engineers and scientists at universities and for specialists in industry to increase their knowledge.

Maria Gavrilescu and Georgeta Andrei

OEHME FR. (Federführend), *Chemische Sensoren heute und morgen*. Expert Verlag, Renningen, 1994, 180 S., ISBN 3-8169-0959-0.

Das Buch: a) geht von Definitionen und Merkmalen von chemischen Sensoren aus; b) beschreibt Funktion und Bauformen; c) bringt eine Zusammenstellung neuartiger Sensoren in Dünn- und Dickschicht-Technik; d) umfaßt alle wichtigen Gruppen marktgängiger und in Entwicklung befindlicher Sensoren und e) bezieht auch die Übertragung und Verarbeitung von Sensorsignalen in die Betrachtungen ein.

Es wendet sich gleichermaßen an Entwickler und Anwender chemischer Sensoren. Das gilt im einzelnen für Chemiker in der analytischen Chemie, für Ingenieure in der Betriebsmeßtechnik und Prozeßkontrolle, für Mitarbeiter in der Forschung und Entwicklung von Sensoren, aber auch für Marketingleiter im Hinblick auf neue Produkte.

I n h a l t: Strategien zur Entwicklung chemischer Sensoren – Definitionen und Merkmale – Herstellungsverfahren – Festkörper Gassensoren – Elektrochemische Sensoren – Faseroptische und piezoelektrische Sensoren – Methoden der Grenzflächenanalytik zur Untersuchung von Sensorfunktionen – Anwendungen handelsüblicher Sensoren für brennbare und toxische Gase – Signalverarbeitung und Gerätesysteme.

SEIDEL P., *Schweres Erdöl – ein alternativer Rohstoff zur Erzeugung von Treibstoffen.* Expert Verlag, Renningen, 1994, 268 S., ISBN 3-8169-0871-3.

Das Fachbuch gibt einen Überblick zum aktuellen Stand der Verarbeitung von schwerem Erdöl und seiner Analytik. Sein besonderer Wert liegt darin, daß wertvolle, in den modernen Industriestaaten weitgehend unbekannte Theorien der Kolloidchemie und der physikalischen Chemie veröffentlicht werden, die eine wesentliche praktische Bedeutung haben.

Der Band ist unentbehrlich für Spezialisten auf dem Gebiet der Chemie und Verarbeitung von Erdöl. Es vermittelt außerdem Studenten und Assistenten an Hochschulen und Universitäten die erforderlichen Grundlagen.

I n h a l t: Aufbau und Eigenschaften von schweren Erdölen – Prozesse der Verarbeitung von schwerem Rohstoff – Katalytisches Kracken und Methoden zur Prozeßpromotierung – Y-Zeolitkatalysatoren des katalytischen Krackens – Methoden zur Oktanzahlerhöhung von Benzin – Chemismus, Reaktionsmechanismus und Kinetik der katalytischen Krackreaktionen.

1996

ISSN 0254-7104